# *The Thickness of the Mantle Lithosphere and Collision-related Volcanism in the Lesser Caucasus*

**Sugden, P. J.[1]*, Savov, I. P.[1], Wilson, M.[1], Meliksetian, K.[2], Navasardyan, G.[2] and Halama, R.[3]**

[1] School of Earth and Environment, University of Leeds, Leeds, LS2 9JT, UK

[2] Institute of Geological Sciences, National Academy of Sciences of Armenia, Marshal Baghramian Avenue, Yerevan 0019, Armenia

[3] School of Geography, Geology and the Environment, Keele University, Newcastle-under-Lyme, ST5 5BG, UK

*Corresponding author. E-mail: eepjs@leeds.ac.uk.



## ABSTRACT

The Lesser Caucasus mountains sit on a transition within the Arabia-Eurasia collision zone between very thin lithosphere (< 100 km) to the west, under Eastern Anatolia, and a very thick lithospheric root (up to 200 km) in the east, under western Iran. A transect of volcanic highlands running from north-west to south-east in the Lesser Caucasus allows us to look at the effects of lithosphere thickness variations on the geochemistry of volcanic rocks in this continental collision zone. Volcanic rocks from across the region show a wide compositional range from basanites to rhyolites, and have arc-like geochemical characteristics, typified by

ubiquitous negative Nb-Ta anomalies. Magmatic rocks from the south-east, where the lithosphere is thought to be thicker, are more enriched in incompatible trace elements, especially the light rare earth elements, Sr and P. They also have more radiogenic $^{87}Sr/^{86}Sr$, and less radiogenic $^{143}Nd/^{144}Nd$. Across the region, there is no correlation between $SiO_2$ content and Sr-Nd isotope ratios, revealing a lack of crustal contamination. Instead, "spiky" mid-ocean-ridge basalt normalised trace element patterns are the result of derivation from a subduction-modified mantle source, which likely inherited its subduction component from subduction of the Tethys Ocean prior to the onset of continent-continent collision in the late Miocene. In addition to the more isotopically enriched mantle source, modelling of non-modal batch melting suggests lower degrees of melting and the involvement of garnet as a residual phase in the south-east. Melt thermobarometry calculations based on bulk-rock major elements confirm that melting in the south-east must occur at greater depths in the mantle. Temperatures of melting below 1200°C, along with the subduction-modified source, suggest that melting occurred within the lithosphere. It is proposed that in the Northern Lesser Caucasus this melting occurs close to the base of the very thin lithosphere (at a depth of ~45 km) as a result of small-scale delamination. A striking similarity between the conditions of melting in north-west Iran and the southern Lesser Caucasus (two regions between which the difference in lithosphere thickness is ~ 100 km) suggests a common mechanism of melt generation in the mid-lithosphere (~ 75 km). The southern Lesser Caucasus magmas result from mixing between partial melts of deep lithosphere (~ 120 km in the south) and mid-lithosphere sources to give a composition intermediate between magmas from the northern Lesser Caucasus and north-west Iran. The mid-lithosphere magma source has a distinct composition compared to the base of the lithosphere, which is argued to be the result of the increased retention of metasomatic components in phases such as apatite and amphibole, which are stabilized by lower temperatures prior to magma generation.

**Key words:** collision setting; Lesser Caucasus; magma petrogenesis; mantle lithosphere thickness; Sr-Nd isotopes



## INTRODUCTION

The Arabia-Eurasia collision zone is one of the very few places on Earth where it is possible to study active volcanism associated with a continent-continent collision event. The geodynamic processes which drive volcanism remain unresolved, with numerous and sometimes conflicting models for its origin (Pearce *et al*., 1990; Keskin, 2003; Göğüş & Pysklywec, 2008; Faccenna *et al*., 2013). Most of the volcanism in the region is located on the Anatolian-Armenian-Iranian Plateau, a broad uplifted region to the north and east of the Arabian foreland, with an average elevation of over 2 km (Şengör *et al*., 2008; Priestley & McKenzie, 2013). The lithospheric structure of this plateau is considered to show a strong contrast between very thin mantle lithosphere in the west (below Eastern Anatolia), and very thick mantle lithosphere in the Zagros Core to the SE (Fig. 1), below western Iran (Priestley *et al*., 2012).

The Lesser Caucasus mountains sit close to the edge of the Zagros Core region, and therefore close to a transition from thick to thin lithosphere. The region thus provides an opportunity to look at the influence of lithospheric thickness on the geochemistry of collision-related magmas. Figure 1 shows the four volcanic highlands considered in this study, which form a NW-SE transect almost orthogonal to contours of lithospheric thickness from Priestley *et al*. (2012), which increase from NW to SE. It should be noted that the resolution on these lithospheric thickness estimates is limited by the 30-50 km vertical resolution of the seismic tomography data (McKenzie & Priestley, 2008). The Priestley *et al*. (2012) model is used

because it is likely to give better local resolution in the Lesser Caucasus region than other global lithospheric thickness studies (Priestley & McKenzie, 2006, 2013).

Volcanic rocks from the SE of this transect, where the lithosphere is thought to be thicker, are known to be more potassic than volcanic rocks from the NW (Meliksetian, 2013). This study provides the first complete geochemical dataset for volcanic rocks from the SE of the Lesser Caucasus. This dataset includes a complete range of compositions from basanite to rhyolite, which are used to evaluate the extent to which crustal contamination is an important component of magma petrogenesis. We then compare the geochemistry of the more primitive mafic volcanic rocks between the NW and SE of the Lesser Caucasus, and the mechanisms by which thicker lithosphere in the SE might influence the geochemistry of volcanic rocks found there. In order to indicate how thicker mantle lithosphere might influence the composition of magmas, volcanic rocks from a region of very thick lithosphere (> 200 km) in NW Iran (Fig. 1; Allen *et al*., 2013) are used as an end-member comparison of melting in a thick lithosphere regime.

## GEOLOGICAL BACKGROUND

### Pre-collision geological history

The evolution of the Arabia-Eurasia collision zone, as a part of the Alpine-Himalayan orogenic belt, is a consequence of the closure of the Neotethys Ocean (Rolland, 2017 and references therein). The pre-Miocene geology of the territory of Armenia and the Lesser Caucasus (Fig. 2), like much of the interior of the Anatolian-Armenian-Iranian Plateau, is a complex amalgamation of a series of terranes (microplates), which accreted to the Eurasian continental margin during the closure of the Tethys Ocean (Hosseinpour *et al*., 2016; Rolland, 2017). The north and east of Armenia include rocks associated with the Mesozoic to early

Cenozoic volcanic arc of the Lesser Caucasus (Mederer *et al.*, 2013), an eastern continuation of the Pontides of Anatolia. The Pontide and Lesser Caucasus arcs together formed the active southern margin of the Eurasian Plate (Yilmaz *et al.*, 2000). Figure 3 illustrates the various stages of closure of the Neotethys Ocean. During the Mesozoic there were likely several subduction zones which contributed to the closure of the northern and southern Neotethys basins (Fig. 3 panels 1 and 2; Galoyan *et al.*, 2009; Rolland *et al*., 2010, 2012; Sosson *et al.,* 2010; Mederer *et al.*, 2013; Karaoğlan *et al*., 2013, 2016; Topuz *et al*., 2013a, 2013b, 2014; Hässig *et al.,* 2015).

The Sevan-Akera suture zone is defined by several (likely N. Neotethys-derived) ophiolite complexes (Fig. 2). The ophiolites were obducted onto the South Armenian block (SAB) at 88-83 Ma (Galoyan *et al.,* 2007; Rolland *et al.,* 2010; Sosson *et al.,* 2010). The SAB (Fig. 2) is a micro-continental fragment composed of Proterozoic metamorphic basement and its sedimentary cover (Şengör, 1984; Rolland *et al.,* 2009), which rifted from the Arabian margin in the early Mesozoic (Şengör, 1984; Jrbashian *et al*., 1996) and is likely continuous with the Taurides-Anatolides of Anatolia (Rolland *et* al., 2016) and the Cimmerian terrane of Iran (Stampfli *et al*., 2013). Ophiolite obduction was followed by accretion of the SAB to the Pontide-Lesser Caucasus arc at 50-80 Ma (Rolland *et al*., 2009; Sosson *et al*., 2010), marking the closure of the N. Neotethys. Northward subduction of the S. Neotethys continued until 'soft' collision of Arabia with the Bitlis-Poturge terrane and SAB in the late Eocene- early Oligocene (Fig. 3 panel 3; Rolland *et al*., 2012; Karaoğlan *et al*., 2013). Hard collision was delayed until the Pliocene, following the Kura Basin closure to the north (Fig. 3 panel 4, Rolland, 2017).

The numerous subduction zones illustrated in Fig. 3 would have added slab-derived material to large parts of the mantle wedge beneath the present day collision zone. It has been suggested that this signature of a subduction-modified mantle has been widely inherited by

the post-collisional volcanic rocks in the Arabia-Eurasia collision zone (Pearce *et al*., 1990; Keskin *et al*., 1998; Keskin, 2003; Allen *et al*., 2013; Oyan *et al*., 2017).



**Post-Miocene volcanism and tectonics**

The widespread volcanism occupies a wide zone across the collision zone (Fig. 1), arguing against any single subducting slab driving magma generation. Elevated topography of 1-2 km is observed across the collision zone, however the deep lithospheric structure which might isostatically support this elevated topography shows strong contrasts between the east and west. In the west, a low seismic velocity anomaly in the uppermost mantle below the East Anatolian Plateau (Al-Lazki, 2003; Angus *et al*., 2006; Zor, 2008; Gök *et al*., 2011; Koulakov *et* al., 2012; Skolbeltsyn *et al*., 2014), has been used to suggest that the mantle lithosphere is very thin under eastern Anatolia, such that the high topography is not isostatically supported. Based on the fairly uniform crustal thickness (~ 40 km; Angus *et al*., 2006), and the very thin lithospheric mantle, both the current structure of this western part of the Plateau and the associated volcanism have been attributed to a slab break-off event (Keskin, 2003, 2007; Şengör *et al.,* 2003, 2008). Given the later onset of eruptions, and the more alkaline nature of magmas in the south (Pearce *et al*., 1990; Keskin *et al.,* 1998), it has been postulated that the slab which broke off and thereby fuelled recent volcanism was a north dipping S. Neotethys slab below the Bitlis Suture (Keskin, 2003).

In contrast, relatively fast seismic velocities in the upper mantle under western Iran suggest that a thick lithospheric root isostatically compensates the high topography in the south-eastern part of the collision zone, termed the "Zagros Core" (Priestley & McKenzie, 2006, 2013; Priestley *et al*., 2012). There is no evidence in NW Iran of the coupled spatio-temporal variability in volcanism seen in Eastern Anatolia, such that instead of slab break-off,

it has been postulated that the volcanism is driven by small-scale lithospheric dripping or amphibole break-down melting (Allen *et al*., 2013; Kaislaniemi *et al*., 2014; Lechmann *et al*., 2018).

As can be seen in Fig. 1, the Lesser Caucasus is located close to the boundary between these two tectonic regimes. The transect of volcanic highlands thus provides a key opportunity to understand the effect of lithospheric thickness on the composition of mantle derived magmas in a continental collision zone.

**Geology and geochronology of collision-related volcanism in the Lesser Caucasus**

Three major styles of volcanic activity can be observed in the Lesser Caucasus. The first of these are relatively low volume eruptions from mostly small eruptive centres in monogenetic volcanic fields. In both the north and south of the Lesser Caucasus, this style of volcanism becomes increasingly dominant in the most recent eruptive products (Fig. 4, Connor *et al.,* 2011; Neill *et al*., 2013). Secondly, large composite volcanoes are also found throughout the Lesser Caucasus. In the central Lesser Caucasus, such a volcano is Aragats (Connor *et al*., 2011), while in the south the smaller stratovolcanoes Tskhouk and Ishkhanasar (Fig. 4) dominate the landscape. Such large volcanoes (4090 m altitude, ~70 km diameter in the case of Aragats), capable of generating many caldera collapse eruptions, are required to produce the ignimbrites that are widespread throughout the Lesser Caucasus. Finally, large fissure-fed 'flood basalt' style lava flows are found predominantly in some of the older (~3-2.05 Ma) volcanic successions (Sheth *et al.,* 2015).

Previous geochronological studies have constrained the ages of the volcanic deposits upon which this study focuses as being late Pliocene or younger. All of the samples analysed for geochemistry from the north-west of the transect are 2.5 Ma or younger, based on

correlations of the oldest "valley series" lavas of Neill *et al*., (2015) with sediments containing mammalian fossils (Kharazyan, 1983), and a K-Ar age of 2.5 Ma for one such "valley series" lava in the Shirak province of NW Armenia in the northern Lesser Caucasus (Chernyshev *et al*., 2002). Volcanic rocks from further south were all collected from Quaternary volcanic highlands, which form monogenetic volcanic fields and so have an even more restricted age range. A limited number of ages from the Syunik volcanic highland (number 4 in Figs 1 and 2) suggest volcanism ranges from 1.3 to 0.11 Ma, based on two Ar-Ar ages of pumice layers in diatomaceous sediments (Joannin *et al*., 2010), along with K-Ar ages of local lava flows which overlie the sediments (Ollivier *et al*., 2010). Archaeological evidence from $^{14}C$ dating of petroglyphs and burial places around the youngest lavas in Syunik suggest volcanism may extend to within the last 5 ka (Karakhanian *et al*., 2002). These ages are very similar to the estimated age span of the Gegham volcanic highland (highland 2 in Figs 1 and 2) of 1.2-0.02 Ma (Lebedev *et al*., 2013). In summary the complete age span of the volcanic rocks studied for geochemistry in this study is < 3 Ma, and it is likely that the present-day structure of the lithosphere can be used as an interpretive framework for all samples.

## SAMPLING

While recent work (Neill *et al*., 2013, 2015) has provided important new geochemical data for collision-related volcanism in the northern Lesser Caucasus, our study presents the first comprehensive dataset for mafic volcanic rocks from the southern part of the Lesser Caucasus (Table 1). All samples are from the Vardenis and Syunik volcanic highlands (highlands 3 and 4 in Figs 1 and 2). Table 1 gives the co-ordinates for all the mafic samples in the Vardenis and Syunik volcanic highlands. Figure 4 shows the newly completed geological map of the Syunik volcanic highland; a PDF version is provided as Supplementary Data C. The map

shows that even in this small area there is a wide range of volcanic structures and rock compositions, including large andesite-dacite stratovolcanoes, small basaltic scoria cones and rhyolitic monogenetic domes, often with obsidian flows. Sampling in the region covers the complete stratigraphic range of the map, but there was a bias towards the younger eruptive centres in order to collect the least altered samples for geochemical analysis. There is as yet no such similar geological map of Vardenis available, however the sampling was similarly comprehensive in terms of rock compositions and stratigraphic range. The studied rock types range from basanite to rhyolite, although Table 1 only includes data for the most mafic samples, which form the main focus of this study. The complete dataset (including the more felsic samples) can be found in Supplementary Data A.

## METHODS

### Major and trace elements

Sample preparation was done at the University of Leeds. 60-100g of rock was crushed in a TEMA agate mill. The agate was cleaned extensively between the crushing of each sample, including pre-contamination of the agate by the crushing of 50g of sample, which was then discarded. Bulk-rock major and trace element analysis of samples from this study was done at ACME Labs by Bureau Veritas minerals, in Vancouver, Canada, and at Royal Holloway University, London.

For analysis at ACME Labs, samples were heated to 1000°C to determine loss on ignition (LOI), and then fused in a platinum-gold crucible with a lithium tetraborate flux. The resulting fusion beads were then analysed by XRF for major elements. Two internal ACME standards reproduced expected values to better than 3 % (for all oxides > 1 wt %). Trace element concentrations were determined by ICP-MS on the fused beads after digestion in

nitric acid. Analysis of Ni concentrations involved digestion in aqua regia at 95°C. Two internal ACME standards reproduced expected values to better than 10% for trace elements. Values for internal and external standard data are shown in Supplementary Data A.

Analysis at Royal Holloway was by inductively coupled plasma optical emission spectroscopy (ICP-OES) for major elements and some high abundance trace elements (Sr, Zr, Ni) and ICP-MS for low abundance trace elements. Major element analyses followed the methods described by Walsh *et al*. (1981) and Garbe-Schönberg (1993). The relative standard deviation on the external standards NIM-G, NIM-L, BHVO-1, RGM-1 and STM-1, as well as internal standards, was better than 5% (for all oxides > 1 wt %). Trace elements were analysed after $HNO_3$-HF-$HClO_4$ digestions. Prior to analysis, samples were spiked with 5 ng per ml of indium (In) and rhenium (Re) for internal standardization. For analytical quality control, five international reference materials were analysed: NIM-G, NIM-L, BHVO-1, RGM-1 and STM-1. The standards analysed as unknowns generally gave trace element concentrations that deviated by < 15% from literature values; the results of these measurements are reported in Supplementary Data A.

**Sr-Nd isotopes**

Thermal Ionization Mass Spectrometry (TIMS) was used for the analysis of $^{87}Sr/^{86}Sr$ and $^{143}Nd/^{144}Nd$. Strontium (Sr) and Neodymium (Nd) were extracted from unspiked rock powders that were dissolved in an $HNO_3$: HF acid mixture (1:4), followed by conventional ion-exchange chromatographic techniques at the University of Leeds. Sr and Nd isotope ratios were measured on a *ThermoScientific* Triton multi-collector mass spectrometer running in static mode. The normalization value for fractionation of $^{87}Sr/^{86}Sr$ was $^{86}Sr/^{88}Sr = 0.1194$; that of $^{143}Nd/^{144}Nd$ was $^{146}Nd/^{144}Nd = 0.7219$. Instrument errors for determinations of $^{87}Sr/^{86}Sr$

and $^{143}Nd/^{144}Nd$ are reported as the standard error, 2σ, (i.e. 2 standard deviations about the mean using 200-240 measurements). External precision (2σ) for Sr and Nd isotopic ratios from successive replicate measurements of primary standards was better than 35 ppm for the NIST SRM-987 International Reference Standard ($^{87}Sr/^{86}Sr$ = 0.710260 for 9 runs averaged, with a standard deviation of 1.1 $x10^{-5}$) and better than 25 ppm for the La Jolla Nd International Reference Standard ($^{143}Nd/^{144}Nd$ = 0.511842 for 11 runs averaged, with a standard deviation of 2.5 $x10^{-5}$). USGS standard BHVO-1 was also run as a validation material throughout the run period for both $^{87}Sr/^{86}Sr$ and $^{143}Nd/^{144}Nd$. Once corrected to an NIST SRM 987 preferred value of 0.710246 using the accompanying primary standard measurement, all measurements of $^{87}Sr/^{86}Sr$ for BHVO-1 reproduce a literature value of 0.703475 to within 2σ (Weis *et al*., 2006). All measured $^{87}Sr/^{86}Sr$ ratios were corrected to the literature NIST SRM 987 only. For Nd isotopes, all samples were corrected to the literature value of BHVO-1 (0.512986) giving an average correction of 0.00002. The total chemistry blanks for Sr and Nd were negligible during the period of measurements (0.4 ng for Sr and 0.3 ng for Nd).

## PETROGRAPHY

Southern Lesser Caucasus volcanic rocks are generally very fresh, with generally low loss on ignition (LOI) values (usually <1%) for the majority of mafic samples (Table 1). The groundmass can sometimes contain minor amounts of clay minerals, but in many cases it is very fresh, with small pockets of volcanic glass present in a minority of samples (Table 2).

Tephrites, trachybasalts and trachybasaltic andesites from Syunik always contain phenocrysts (>0.3mm) of clinopyroxene, and may have olivine, amphibole and apatite

phenocrysts. Clinopyroxene is ubiquitous and normally occurs as glomerocrysts (Fig. 5f). Some samples have abundant olivine microphenocrysts (Fig. 5d) and phenocrysts (up to 600μm), although olivine is generally restricted to the most mafic samples (low silica trachybasaltic andesite or more mafic). Amphibole phenocrysts are common (up to 2cm), and occur across the compositional range (Fig. 5a). In several samples amphibole is absent, or partially resorbed (Fig. 5c), due to disequilibrium conditions prior to eruption. The apatite phenocrysts can reach up to 2mm in size in some cases (Fig. 5b). The common occurrence of hydrous minerals, such as amphibole and apatite, is noteworthy in comparison to the volcanic rocks from the northern and central Lesser Caucasus, where such mineral phases are less common, certainly in the most mafic samples (Connor *et al*., 2011; Neill *et al*., 2013). Typical groundmass in mafic volcanic rocks from Syunik is composed of plagioclase, clinopyroxene, and Fe-Ti oxides, with volcanic glass in some scoria samples. Note that plagioclase is only present in the groundmass and is not a phenocryst phase.

More evolved high-silica trachybasaltic andesites, trachyandesites and trachytes from Syunik show the appearance of abundant plagioclase phenocrysts. In some cases, these plagioclase crystals (up to 2mm) show evidence of multiple stages of crystallisation with distinct core to rim zonation (Fig. 5e). Amphibole also becomes a more common phenocryst phase, whereas clinopyroxene is less dominant. The groundmass is increasingly dominated by plagioclase. Rhyolites are common in the northern part of Syunik, where they commonly form obsidian flows.

In Vardenis all samples are trachybasaltic andesites or more evolved, and plagioclase is always a phenocryst phase. In one trachybasaltic andesite (Table 2- sample 6.3.15), biotite is also a phenocryst phase. Rhyolites from Vardenis commonly have biotite, plagioclase, quartz and potassium feldspar as phenocrysts, and a groundmass composed of quartz and potassium feldspar.

From the occurrence of different minerals in the range of rock types we sampled across the Syunik and Vardenis volcanic highlands (34 samples, Table 2), it is possible to suggest a general order of crystallisation for both areas, which would likely have been: olivine + Fe-Ti oxides ± apatite; clinopyroxene + Fe-Ti oxides ± olivine ± amphibole; clinopyroxene + plagioclase + Fe-Ti oxides ± amphibole ± phlogopite; plagioclase + potassium feldspar + Fe-Ti oxides ± phlogopite. The predominant focus of this study is on the mechanism of mantle melting, which requires the effect of fractional crystallisation to be minimised. Only primitive samples with < 54 wt % $SiO_2$ and > 4 wt % MgO are used to investigate questions of magma petrogenesis. These samples will likely all have only fractionated mafic minerals, with no significant feldspar fractionation.

## RESULTS

### Major element characteristics

Across the Lesser Caucasus there is a great diversity in the compositions of the volcanic rocks within each volcanic highland, with most showing a complete compositional range from basalt to rhyolite (Fig. 6). Rhyolites are also present in the northern Lesser Caucasus (Karapetian *et al*., 2001), although they were not sampled for the Neill *et al*. (2013) study. Southern Lesser Caucasus samples, with Syunik being the most extreme, have more alkaline compositions compared to those from the north, with the largest $Na_2O$ and $K_2O$ variations between north and south in the most mafic samples (Fig. 6). Southern Lesser Caucasus samples are also more potassic when compared to their northern counterparts (shoshonitic *versus* calc-alkaline series; Fig. 7a). As well as being more alkaline, mafic southern Lesser Caucasus samples extend to lower $SiO_2$ contents.

On some major element variation diagrams, such as MgO *versus* $SiO_2$ (Fig. 7b) the trends are fairly similar for northern and southern Lesser Caucasus samples. However other elements, notably P, display a significant geographic gradient in concentration for the most mafic samples, from 0.4 wt % $P_2O_5$ in the north to as high as 1.6 wt % in the south (Fig. 7c).

**Trace element characteristics**

MORB-normalised trace element patterns all show profiles typical of subduction-related volcanic rocks, with positive anomalies for Ba, K, Pb and Sr and negative anomalies for the high field strength elements (HFSE) Nb, Ta and Ti (Fig. 8). Superimposed on this is an additional enrichment in incompatible trace elements, in particular the light rare earth elements (LREE; Fig. 9), Sr, Ba and P, which becomes increasingly pronounced to the south of the transect. Due to the LREE enrichment, as well as a more moderate depletion in heavy rare earth elements (HREE), REE profiles become increasingly steep towards the south (Fig. 9), with CI- normalised La/Yb ratios of 5 in the northern Lesser Caucasus compared to values as high as 40 in the south.

These additional enrichments do not resemble those of typical intra-plate ocean island basalts (OIB), which show uniform enrichments in all the most incompatible trace elements, rather than the larger enrichments seen in the LREE relative to the HFSE (Fig. 8e), as exemplified by Ta and La in Figs 7e and f, respectively. These additional enrichments are seen most clearly in volcanic rocks from NW Iran (Fig. 8e), a region of very thick lithosphere- up to 220 km (Priestley *et al*., 2012). On Figs 8a-d we show that the variations in the composition of basalts within individual volcanic highlands are small, relative to the variations in composition between the highlands. Both the ubiquitous subduction ("arc") signatures, and additional enrichment are highlighted in Fig. 10. All samples plot above the

mantle array, typical for rocks from volcanic arcs. However, the samples from the southern Lesser Caucasus have higher Th/Yb and Ta/Yb relative to their northern counterparts (Fig. 10). Volcanic rocks from the thick lithosphere Zagros Core region of NW Iran again plot as a compositional end-member.

Given that amphiboles are relatively common in the southern Lesser Caucasus rocks, it should be noted that low Y (amphibole fractionation) trends dominate the Y *versus* $SiO_2$ plot for these rocks (Fig. 7d). Samples from further north, in which anhydrous mineral assemblages are more common, show both high Y (anhydrous assemblage) and low Y (hydrous) fractionation trends.

**Sr-Nd isotope systematics**

The Sr-Nd isotope compositions of the southern Lesser Caucasus samples are shown in Table 3. $^{87}Sr/^{86}Sr$ varies from 0.7043 to 0.7047, whereas εNd varies from +2.2 to +4.2. All mafic volcanic rocks from the Lesser Caucasus plot along the mantle array, with compositions more enriched than N-MORB but more depleted than Bulk Earth (Fig. 11). In general, those samples from the south-east have higher (more radiogenic) $^{87}Sr/^{86}Sr$, and less radiogenic εNd than those samples from the north-west, defining a steep gradient on the Sr-Nd isotope diagram (Fig. 11). A few samples plot away from this trend to higher $^{87}Sr/^{86}Sr$ (see Crustal contamination section of Discussion). Lesser Caucasus volcanic rocks are isotopically more depleted than volcanic rocks formed above very thick lithosphere in NW Iran (> 200 km; Priestley *et al*., 2012). They are also more depleted than volcanic rocks from the Lake Van area, which commonly display significantly more variable Sr-Nd isotope compositions (not shown), probably because those magmas interacted extensively with continental crust during ascent (Pearce *et al*., 1990; Sen *et al*., 2004; Özdemir *et al.*, 2006; Oyan *et al*., 2017).

## DISCUSSION

### Crustal contamination

Volcanic rocks produced within the thicker lithosphere of the southern Lesser Caucasus have higher concentrations of incompatible trace elements, more radiogenic $^{87}Sr/^{86}Sr$, and lower $^{143}Nd/^{144}Nd$ ratios. All of these features could be produced by crustal contamination during magmatic evolution, as has been suggested for various parts of Eastern Anatolia, where assimilation of radiogenic ancient continental crust gives $^{87}Sr/^{86}Sr$ ratios of up to 0.7065 and marked variation of these ratios with $SiO_2$ (Pearce *et al*., 1990; Keskin *et al*., 2006). All Sr-Nd isotope ratios for the Lesser Caucasus volcanic rocks show small variations compared to what would be expected if the magmas had been contaminated by continental crust. The crust in the Lesser Caucasus is composed of a mixture of felsic metamorphic basement (South Armenian Block), arc volcanic rocks and Mesozoic-Cenozoic sediments (Fig. 2). Only the arc-related volcanic rocks would have similar isotope compositions to the collision-related magmas, such that assimilation of any of the other lithologies would alter, often dramatically, the isotope composition of the host magma. The majority of samples show insignificant variability in $^{87}Sr/^{86}Sr$ and $^{143}Nd/^{144}Nd$ with $SiO_2$ within individual volcanic highlands (Fig. 12), suggesting that isotope ratios are not being modified significantly during magma evolution and storage in the crust prior to eruption. The lack of isotopic variability with $SiO_2$ content suggests that assimilation of South Armenian Block crust (Fig. 2), which with a basement $^{87}Sr/^{86}Sr$ ratio of ~0.7303 (Baghdasaryan & Ghukasyan, 1985) should be easily identified, is unlikely. Similarly, assimilation of sedimentary material is also unlikely, given typical Tethyan (Mesozoic) flysch $^{87}Sr/^{86}Sr$ of 0.7112 (Prelević *et al*., 2008).

One sample from the Syunik volcanic highland (1-4A-08), which was sampled from a scoria cone containing large (cm-sized) felsic xenoliths entrained within the trachybasaltic andesite scoria, has trace element and isotopic characteristics indistinguishable from the other mafic samples. The Sr-Nd isotope composition of one of the xenoliths (sample 1-4B-08, Table 3) is also shown in Fig. 12, and is only slightly elevated in $^{87}Sr/^{86}Sr$ (0.7049) above that of the Quaternary basalts, suggesting that an unrealistically high degree of assimilation would have to occur for the composition of the magma to be significantly affected. The $^{143}Nd/^{144}Nd$ (0.5128) is indistinguishable from Syunik basalts. It is likely the felsic xenolith is cogenetic with the trachybasaltic andesite scoria host. It provides evidence that basaltic magmas in the southern Lesser Caucasus are interacting with felsic igneous rocks in the crust, which have a similar origin, rather than interacting with ancient crust which would have strongly impacted the Sr-Nd isotope ratios.

The curved patterns for major element variations *versus* $SiO_2$, including MgO (Fig. 7b), $P_2O_5$ (Fig. 7c) and $Al_2O_3$ (not shown), suggest the rhyolites are derived from extreme degrees of magmatic differentiation, rather than being crustal melts. These rhyolites also do not appear to be mixtures between primitive magmas and continental crust (Rudnick & Gao, 2003). The Rb and Sr contents of a rhyolite from Syunik are actually more extreme relative to the basalts than average continental crust (Rb more strongly enriched, Sr more strongly depleted in the rhyolite; Fig. 8d). $K_2O$ is more enriched in the rhyolite than in the basalts, whereas continental crust has lower $K_2O$ than continental crust (Fig. 8d). The lack of evidence for extensive assimilation of continental crust in the petrogenesis of the rhyolites suggests that these processes are likely to be unimportant in the petrogenesis of the more primitive magmas.

It is also possible that the magmas may have been contaminated by Mesozoic-Paleogene arc crust (Fig. 2) on their ascent, as has been suggested for the northern Lesser

Caucasus in some isolated cases (Neill *et al*., 2015). The similar Sr-Nd isotope compositions of these arc rocks (Mederer *et al*., 2013) to the collision-related magmas, means that assimilation could be "cryptic", without obvious modification of Sr-Nd isotope ratios. Given the arc-like incompatible trace element geochemistry of Lesser Caucasus volcanic rocks, arc-crust assimilation is unlikely to significantly alter trace element compositions, although it is possible that such assimilation could explain some of the spread in the southern Lesser Caucasus data. The average composition of Mesozoic arc rocks from the southern Lesser Caucasus (Kapan Zone) is shown in Fig. 10 (Mederer *et al*., 2013). The Th/Yb ratio of the arc rocks is elevated above the mantle array similar to the post-collisional Lesser Caucasus samples. However, the low Ta/Yb ratios of these arc rocks make them unlikely candidates to explain the more enriched composition of southern Lesser Caucasus magmas.

There are a few examples of elevated $^{87}Sr/^{86}Sr$ ratios in evolved samples above the background range. In most cases, it seems that the Nd isotopes are unaffected. Some ancient arc samples from the Kapan zone, southern Lesser Caucasus have very high initial $^{87}Sr/^{86}Sr$, but $^{143}Nd/^{144}Nd$ does not vary significantly in the same samples (Mederer *et al*., 2013). Extensive assimilation of such material would be required to explain the elevated $^{87}Sr/^{86}Sr$ of these samples. Worthy of note however, are the very high Rb/Sr ratios (7-23) in these rhyolites- sometimes 1000x greater than typical basalts (Table 1). While decay of $^{87}Rb$ over the relatively short timeframe (< 2 Myr) since cooling and crystallisation of lavas will have negligible effects on the $^{87}Sr/^{86}Sr$ of basaltic rocks, such high Rb/Sr ratios mean that post-crystallisation decay will have a significant effect for rhyolites (Fig. 12a). Indeed, minimum ages for the rhyolites of between 0.6 and 1.4 Myr are sufficient to give initial $^{87}Sr/^{86}Sr$ within the range observed for basalts. As such, even in these rhyolites, crustal contamination may have played an unimportant role in magma evolution. It should be noted that the lower Rb/Sr

ratio of the felsic xenolith (0.12) means that its elevated $^{87}Sr/^{86}Sr$ ratio was likely present during emplacement of the host Quaternary mafic magma.

In summary, assimilation of crustal rocks with markedly distinct geochemistry is unlikely, and although assimilation of igneous rocks with similar petrogenetic origins cannot be precluded, such processes would be incapable of driving the enrichment in incompatible trace element concentrations and Sr-Nd isotope ratios observed from north to south in the volcanic rocks of the Lesser Caucasus. The lack of evidence for crustal contamination, along with the gradient in Sr-Nd isotope ratios in Fig. 11, requires that there must be variation in the composition of the mantle source.

**Subduction modification of the mantle source in the Lesser Caucasus**

All mafic samples show distinct negative Nb-Ta and Ti anomalies (Fig. 8), and positive spikes in Ba, K, Pb and Sr in normalised trace element patterns, such that the overall patterns, if not the absolute concentrations, are typical of arc magmas. In the absence of evidence for widespread crustal contamination, it is likely that these features are inherited from the mantle source. Collision between Arabia and Eurasia was preceded by subduction of various Tethyan ocean basins along several convergent margins (Fig. 3). These subducting slabs would likely have contributed slab material to the mantle below the collision zone.

Following the approaches of Turner *et al*. (2017) and Hofmann (2003), Fig. 13 illustrates how the ratios Ba/La, Ce/Pb, Sr/Nd and Nb/U in mafic samples (< 54 wt % $SiO_2$, > 4 wt % MgO) vary with latitude. These ratios show little variation within all MORB and OIB, but are much more variable in volcanic arc rocks due to the subducted slab contribution, such that they can be used here as proxies. In all of the plots in Fig. 13 these ratios deviate from those of MORB/OIB, demonstrating the presence of a slab component in their mantle source.

These ratios do not show consistent variability between the volcanic highlands (Fig. 13), although Sr/Nd ratios are slightly elevated to the south (Fig. 13c) and the Nb/U ratio reaches a minimum (highest slab contribution) in the central Lesser Caucasus. The lack of a consistent trend in these ratios between volcanic highlands means the slab contribution is likely to be fairly uniform.

Although mixing between a depleted mantle source and the likely composition of subducted sediment, e.g. Tethyan flysch (Prelević *et al*., 2008), comes close to explaining the Sr and Nd isotopic composition of the least enriched samples in Fig. 11, such mixing is unable to explain the trend towards the higher $^{87}Sr/^{86}Sr$ and lower $^{143}Nd/^{144}Nd$ seen in the SE. This enrichment in the southern Lesser Caucasus must therefore be driven by some other process. Pre-collision subduction events have likely imparted a subduction signature on the mantle source across the Lesser Caucasus. However, the geochemical gradient between volcanic rocks of the northern and southern Lesser Caucasus cannot be explained by differences in the composition, or size of the slab contribution to the mantle source.

**Modelling the conditions of mantle melting**

It is possible to investigate how a thicker lithosphere affects the conditions of melting by using the approach of Shaw (2005) to forward model the composition of the samples using a non-modal batch melting model (Table 4), with the equation:

$$\frac{C_l}{C_0} = \frac{1}{D + F(1 - P)} \qquad (1)$$

where $C_l$ is the concentration of an element in the liquid, $C_0$ is the concentration of that element in the source, D is the element's bulk partition coefficient, F is the fraction of melting, and P represents the partitioning of the element into the melt according to the

proportion in which each mineral enters the melt. None of the samples in the region are in equilibrium with mantle olivine, so all must have undergone some fractional crystallisation between last equilibration with the mantle and eruption. This is accounted for by assuming 8% fractional crystallisation of an assemblage composed of 90% olivine and 10% spinel (following the approach of Shaw, 2005). From equation 1 we can see there are three parameters, each of which can be varied to generate the trace element concentration of the most primitive southern Lesser Caucasus samples. Firstly, the fraction of melting (F) could vary, impacting the concentration of all incompatible trace elements. Secondly, if the modal mineralogy is changed then the partitioning of elements between source and melt (D and P in equation 1) will change. Thirdly, the concentration of elements in the source rock ($C_0$) could be changed.

Our approach is to take the equivalent model of Neill *et al*. (2015) for the most geochemically depleted samples from the northern Lesser Caucasus and iteratively vary two of these parameters to attempt reproduce the average composition of primitive basalts in the south. Variations in the mineralogy of the melt source are simplified to spinel *versus* garnet peridotite melting. Spinel peridotite modal mineralogy and melting proportions are from Shaw (2005) and Neill *et al*. (2015), respectively, while for the garnet peridotite they are from Thirlwall *et al*. (1994) and Allen *et al*. (2013), respectively (Table 4). Varying the fraction of melting is self-explanatory. Remaining disparities between the model and observed trace element concentrations are likely to be due to differences in the composition of the mantle source. The different stages of melt modelling are shown in Table 4.

REE chemistry is used to obtain a qualitative understanding of the changing conditions of melting between the northern and southern Lesser Caucasus (Fig. 14). In Fig. 14a, two vectors are plotted which show how the composition of the magmas should change with the degree of melting *versus* source mineralogy (presence/absence of garnet) and, or,

changes in source composition. Davidson *et al*. (2013) showed that REE partitioning between clinopyroxene and basaltic magma means that melting curves for peridotite will be very steep on a Dy/Dy* *versus* Dy/Yb plot. The assumption that clinopyroxene is a residual phase is reasonable given the low degrees of melting (3% or less) previously estimated for the northern Lesser Caucasus (Neill *et al*., 2015). Amphibole is also likely to be an important residual phase given the positive correlation between Dy/Dy* and Ti/Ti* (the size of the Ti anomaly in Fig. 8; not shown here). It is unclear from Fig. 14a whether garnet in the mantle source, or a LREE enriched source is responsible for the high Dy/Yb ratio in southern Lesser Caucasus samples. Both should give vectors close to horizontal in Fig. 14a, as both changes will steepen the REE profile rather than changing its curvature (Davidson *et al*., 2013). The southern Lesser Caucasus samples have lower heavy rare earth element (HREE) abundances than samples from the north (Fig. 9). HREE all behave incompatibly during melting of spinel peridotite (Table 4), such that lower degrees of melting as suggested by the lower Dy/Dy* ratio should only increase the concentration of HREE. Therefore, garnet as a residual phase during melting must explain at least some of the increase in Dy/Yb in Fig. 14a. In Fig. 14b, the northern Lesser Caucasus samples sit close to the spinel peridotite melting curve, but the southern Lesser Caucasus samples are intermediate between the spinel and garnet melting curves, suggesting melting of a mixed source involving both garnet and spinel peridotite. This could be a consequence of polybaric melting across the spinel-garnet transition at ~ 75 km depth (Robinson & Wood, 1998), suggesting melting at greater depths in the south.

Returning to the partial melting model, the melt fraction was estimated on the basis that the Nb concentration (Table 4) is not affected by the mineralogy of the source rock, and assuming that its concentration in the source rock is constant along the transect. Utilising this assumption gives 3% melting in the north, *versus* 1% melting in the south (Fig. 15). The proportions of garnet peridotite and spinel peridotite which contribute to the total mantle

source are estimated from the Hf and Yb concentrations. Both elements are assumed to have constant concentrations in the mantle source because HFSE and HREE would be less affected by metasomatic events which could alter the source composition. The best fit to the Hf and Yb data is a magma source which is 65% garnet lherzolite and 35% spinel lherzolite (Fig. 15).

Across the Lesser Caucasus, as lithosphere thickness increases, the degree of melting decreases and melting occurs at greater depths, with garnet as a residual phase for a significant portion of the melting interval. However, the model is still unable to explain the high concentrations of several of the LREE (La, Gd and Dy, Fig. 15- black line), and requires changes in the composition of the mantle source with lithospheric thickness as well.

In order to understand how melting is occurring, it is important to understand where magma is forming with respect to the lithospheric structure. For this, we have used major element thermobarometry to estimate the conditions of last equilibration between magmas and the mantle.

**Pressure and temperature of melting**

In order to calculate these intensive parameters, we use the parameterisations of Plank & Forsyth (2016), based on the major element chemistry of primitive magmas, building on the work of Lee *et al*. (2009). These calculations are for magmas produced from a peridotite mantle source at pressures below 3 GPa (Plank & Forsyth, 2016). The temperature (*T*) dependence of Mg partitioning between olivine and melt (Roeder & Emslie, 1970), and the pressure (*P*) dependence of silica activity in melts co-saturated in olivine and orthopyroxene (Carmichael *et al*., 1970), are exploited to give the equations:

$$T = 1264.5 + 7.85(Mg_4Si_2O_8) + \frac{8545}{Si_4O_8} - 5.96(Al_{16.3}O_8) - \Delta T_{H_2O} - \Delta T_{CO_2}, \quad (2)$$

$$P = \frac{\ln(Si_4O_8) - 4.045 + 0.0114(Fe_4Si_2O_8) + 0.00052(Ca_4Si_2O_8)^2 + 0.0024(Mg_4Si_2O_8)}{-336.3T^{-1} - 0.0007T^{1/2}} \quad (3)$$

All major element oxides are calculated in mol % as described in Lee *et al*. (2009), except that they are calculated on an anhydrous basis. The two terms $\Delta T_{H_2O}$ and $\Delta T_{CO_2}$ account for the lower temperature and higher pressure melting in the presence of volatiles as follows:

$$\Delta T_{H_2O} = 40.4(H_2O) - 2.97(H_2O)^2 + 0.0761(H_2O)^3 \quad (4)$$

$$\Delta T_{CO_2} = \frac{(SiO_2) - 50.3}{0.12(-1.067)} \quad (5)$$

where $H_2O$ and $SiO_2$ are in wt %. In order to use these equations, the composition of the primary melt must be known. Given that no samples from the Lesser Caucasus have #Mg>67, it is clear that all the studied samples have undergone some degree of fractional crystallisation. If only olivine has fractionated, then it is a simple process to add olivine incrementally to the melt until it is in equilibrium with mantle olivine of $Fo_{90}$ (Lee *et al*., 2009). If, however, other phases, such as amphibole or clinopyroxene have also fractionated, then this calculation becomes non-trivial. In a study on the collision-related volcanism of Anatolia, McNab *et al*. (2018) took 8.5 wt % bulk-rock MgO as a reasonable lower limit for magmas which have only fractionated olivine. Only two such samples exist in the Lesser Caucasus, and it is likely they have both been affected by olivine accumulation rather than being truly primitive melts. Instead, the complete sample suite from the Shirak and Lori, and Syunik volcanic highlands (1 and 4 in Fig. 1) is used to project back to the likely composition at 8.5 wt % MgO of two end-member primitive magmas for the Lesser Caucasus. This correction is shown in Supplementary Data B.

In order to calculate the pressures and temperatures of melting, two magma composition parameters must be constrained: $Fe^{3+}/\Sigma Fe$ and water content. The water content of the primary magma has a large effect on the temperature estimate through equation 4

(~25°C/wt %), but a smaller effect on the pressure estimate (~30 MPa/wt %). The presence of hydrous mineral phases in mafic rocks (as opposed to only in more evolved samples), only in the southern Lesser Caucasus (Fig. 5), suggests higher water contents in the south. Based on previous studies of amphibole peridotite xenoliths (Thirwall *et* al., 1994; Ionov & Hofmann, 1995), it is assumed that the mantle source contains between 2 and 10 modal % amphibole, which is assumed to contain 2 wt % $H_2O$, such that the mantle source could have up to 0.2 wt % $H_2O$. Using Ce partition coefficients for water during mantle melting (Dixon *et al*., 2002; Ionov *et al*., 2002; Thirwall *et al*., 1994), and the melting models shown in Table 4, gives 2-7 wt % $H_2O$ for southern Lesser Caucasus primary magmas, and 1-4.6 wt % for the north.

As only ferrous iron substitutes in olivine, a higher $Fe^{3+}/\Sigma Fe$ increases the apparent melt Mg#, and so reduces the amount of olivine addition required to produce the primary magma, the MgO content of the primary magma, and thus the calculated pressure and temperature. The $Fe^{3+}/\Sigma Fe$ ratio varies from a minimum of 0.1 in MORB (Cottrell & Kelley, 2011) to as high as 0.3 in some arc basalts (Brounce *et al*., 2014). Given the ubiquitous arc-type geochemical signatures in Lesser Caucasus volcanic rocks, we take 0.25 as a conservative estimate of the $Fe^{3+}/\Sigma Fe$ ratio (Brounce *et al*., 2014).

It should be noted that equations 2 and 3 will only give meaningful estimates of the pressure and temperature of melting if the mantle source is peridotitic, because the parameterisations assume the melt is saturated in both orthopyroxene and olivine (Plank & Forsyth, 2016). The use of these equations on magmas derived from a pyroxenite source would yield meaningless results. Figure 16 shows that for Lesser Caucasus and NW Iran samples, pyroxenite is not a major component of the mantle source. Pyroxenite partial melts have much higher Ni/MgO ratios. As magmas fractionate, those derived from a peridotite source should evolve along a trajectory below the dashed line in Fig. 16, those from a pyroxenite source would plot above the line.

Based on our water content estimates, southern Lesser Caucasus magmas last equilibrated with the mantle at between 1198 and 1292°C, whereas northern Lesser Caucasus magmas last equilibrated at between 1174 and 1267°C. Given the observation that amphibole is likely to be a residual phase in the mantle source (see previous section), it is likely melting was occurring at temperatures close to the amphibole dehydration solidus, because amphibole is likely to completely breakdown within a few 10s °C of crossing the dehydration solidus (Green & Falloon, 2005; Mandler & Grove, 2016). As such, it is likely that the minimum temperatures of these ranges are the more realistic. Using these temperatures gives pressure estimates of 2.1 GPa (~75 km) in the southern Lesser Caucasus, and 1.2 GPa (~45 km) in the north. These estimates are shown in Fig. 17, along with the position of the amphibole dehydration solidus. Southern Lesser Caucasus magmas are produced deeper, but at similar temperatures to those in the north.

The parameterisations first developed by Lee *et al*. (2009) were designed to expand the applicability of basalt melt geothermobarometry beyond mid-ocean ridge systems to any setting involving the melting of terrestrial peridotite. Both our modelled major element compositions, and the pressure and temperature calculated, fall within the experimental range of the dataset in Lee *et al*. (2009), and to this extent our approach is justified.

However, the presence of metasomatic phases such as amphibole in the mantle source means that the pressures and temperatures calculated here must be interpreted with caution. Alkaline volcanic rocks from monogenetic volcanic fields in Western Mexico, geochemically similar to those from volcanic highlands in the Lesser Caucasus, have very high $Fe^{3+}/\Sigma Fe$ ratios and whole-rock #Mg in excess of the ~72 value normally assumed to be in equilibrium with mantle peridotite (Carmichael *et al*., 1996). The effects of a potential underestimation of both $Fe^{3+}/\Sigma Fe$, and of the amount of olivine addition required to produce the primary magma will tend to counteract each other, where the former would give an overestimation of

temperature, and the latter an underestimate. In the case of Western Mexico, both of these observations are ascribed to the incongruent melting of phlogopite (Carmichael *et al*., 1996), which does not seem to be a major metasomatic phase in the Lesser Caucasus mantle (see Fig. 21 below).

Even if these issues are relevant to the Lesser Caucasus, the constraint provided by the position of the amphibole dehydration solidus shows the temperature estimates provided here to be reasonable, although some of the ~50°C disparity with the dehydration solidus could be explained by these issues. The sensitivities of the pressure estimate to $Fe^{3+}/\Sigma Fe$ (-0.2 GPa/0.1 increase), primary melt Mg# (+0.5 GPa/10% increase) and estimated temperature (+0.1 GPa/100°C) are all small. The pressure estimate is primarily based on silica activity in a system co-saturated in olivine and orthopyroxene. Given the indications from Fig. 16, and reasonably successful trace element modelling of partial melting of a peridotite mantle source, it seems likely that these pressure estimates are robust.

Further constraints on the thickness of the crust are required to interpret these results. Crustal thickness is estimated using the formulations of Hu *et al*. (2017), which links the Sr/Y and $(La/Yb)_N$ ratios of intermediate magmatic rocks from continental collision zones with the crustal thickness. The basis of this technique is the polarising effects different fractionating mineral assemblages have on the Sr/Y and $(La/Yb)_N$ ratios in shallow *versus* deep storage reservoirs. To the nearest 5 km, we estimate crustal thickness as: 45 km in Shirak and Lori, 55 km in Gegham and 60 km in both Vardenis and Syunik.

The depth of melting in the northern Lesser Caucasus is very similar to the ~45 km Moho depth, possibly suggesting the presence of a very thin mantle lithosphere. It is instructive to compare this result with recent estimates of melting conditions in neighbouring Eastern Anatolia from McNab *et al*. (2018). East Anatolian magmas can be split into high K/Nb (>500) and low K/Nb types. Low K/Nb magmas generally have OIB-like geochemistry,

and are considered to be directly derived from melting of the convecting mantle, which is apparently anomalously hot in the region, plotting to the right of the ambient mantle adiabat (Fig. 17), at a much higher temperature than any temperatures modelled for the northern Lesser Caucasus. This can be interpreted as northern Lesser Caucasus magmas being derived from the lithosphere, and not the convecting mantle.

Deeper melting in the south is associated with thicker crust, but magma generation is occurring at much shallower depths than the > 100 km lithosphere-asthenosphere boundary estimated by Priestley *et al*. (2012). The depth of melt equilibration is much deeper than the anhydrous solidus, confirming the need for a volatile-enriched lithospheric mantle root.

These *P-T* conditions of melting can be compared with estimates made for this study of the melting conditions of samples from NW Iran, based on the data of Allen *et al*. (2013). The *P-T* conditions of melting of NW Iran volcanic rocks were estimated using the same $Fe^{3+}/\Sigma Fe$ and water contents as southern Lesser Caucasus magmas (0.25 and 7 wt %, respectively). This is on the basis that the geochemistry of NW Iran magmas is similar to southern Lesser Caucasus magmas (Fig. 8), and both formed in a thicker lithosphere regime. Most of the magmas in NW Iran formed under similar conditions to southern Lesser Caucasus magmas, with a small subsidiary group of samples which formed at shallower depths, similar to northern Lesser Caucasus magmas, possibly representing magmas which re-equilibrated with the mantle at the base of the crust during their ascent to the surface.

The melting depth in both the southern Lesser Caucasus and NW Iran is significantly shallower than the estimated lithospheric thicknesses. One possible explanation for what these melting conditions represent could be a thermal maximum in a back-bent non-linear geothermal gradient (Fig. 17). In recently thickened orogenic lithosphere, this type of kinked profile is probably more realistic than the linear geothermal gradient more typical of a cratonic region (Mather *et al*., 2011).

It is worth noting that these differences in melting conditions probably reflect variations in the location of magma generation today, and are not the product of temporal changes in lithosphere structure. This is because in Fig. 8, the trace element compositions of basalts from each volcanic highland are distinct, with each having a fairly narrow range of trace element compositions, despite all the volcanic highlands spanning an age range > 1 Myr, and with the Gegham and Syunik highlands thought to have very similar timespans of activity (Joannin *et al*., 2010; Lebedev *et al*., 2013).

## Geodynamic implications

Using constraints from geochemistry and the estimated pressures and temperatures of melting, it is possible to develop a model of how melting occurs under the Lesser Caucasus region. It seems clear that a majority of melting is taking place in the lithosphere for two reasons. Firstly, all samples display an arc-type geochemistry. Subduction ceased around 35 Ma (Rolland *et al*., 2012), such that these arc signatures will likely only be preserved in the lithosphere. It is possible that the mantle lithosphere retains phases such as amphibole and rutile, which if equilibrated with the magmas, are sufficient to impart the arc-type geochemical signature (Allen *et al*., 2013). Secondly, both northern and southern Lesser Caucasus magmas appear to be produced at significantly lower temperatures than the low K/Nb magmas of Eastern Anatolia, which are thought to be derived from the convecting mantle (McNab *et al*., 2018), such that the Lesser Caucasus magmas have either re-equilibrated in colder lithosphere or are entirely derived from the lithosphere.

Based on the smooth trend in $^{87}Sr/^{86}Sr$ *versus* $^{143}Nd/^{144}Nd$ in Fig. 11 and the gradational changes in trace element patterns (Fig. 8), it appears that magmas are produced from melting of two source types in varying proportions. If these two source types reflect

geochemical end-members, one would be typified by the northern Lesser Caucasus volcanic rocks, whereas the other end-member would be most clearly seen in NW Iran.

Unfortunately constraints on the lithospheric thickness are very limited for the northern Lesser Caucasus (Fig. 1), with the Priestley *et al*. (2012) model showing only that it is <100 km. Taking a typical conductive geothermal gradient for this lithosphere, melting would be expected to occur close to the lithosphere-asthenosphere boundary. Mantle-melt equilibration close to the base of the crust (Fig. 17) suggests that the lithosphere is very thin. If this were the case it is likely that there would be some melting of the convecting mantle based on elevated mantle $T_p$ in the region (McNab *et al*., 2018). However, such a thin lithosphere would make it difficult to insulate the crust from heating, such that more crustal contamination would be expected. As was noted above, this mantle source type appears also to be present in the southern Lesser Caucasus, where the lithosphere is sufficiently thick to supress melting of anhydrous convecting mantle, but where melting of a hydrous lithospheric source would still be possible. It is likely that this magma type is derived from melting of the base of the lithosphere in response to small-scale convective removal, as suggested by Neill *et al*. (2015). This is shown in Fig. 18a as melt zone 1, with small portions of lithosphere being delaminated. This type of delamination is suggested to occur because a very small amount of water (a few hundred ppm) left over from previous subduction lowers the viscosity of the mantle sufficiently to allow more vigorous convection to render the lithosphere-asthenosphere boundary unstable (Kaislaniemi *et al*., 2014). Small-scale convective removal is preferred over catastrophic large scale delamination because volcanism in the Lesser Caucasus is generally small-scale and sustained, with no evidence of crustal contamination, consistent with a continuous, less invasive process. While this magma type is a mixing component in the southern Lesser Caucasus, it is not seen in NW Iran because the lithosphere is too thick for wet or dry melting at its base (Green & Falloon, 2005; Priestley *et al*., 2012). As the

lithosphere is thickened, the degree of melting in response to convective removal will decrease as the wet peridotite solidus is approached with depth (Fig. 18a), which may help to explain the lower degrees of melting in the south.

The second melting zone is the sole magma source for volcanic rocks in NW Iran (Fig. 18b). Despite very different lithosphere thicknesses, both NW Iran and southern Lesser Caucasus magmas formed under similar conditions within the lithosphere (Fig. 17). It is suggested that continental collision could have led to the formation of a kinked geothermal gradient (Fig. 18c). A linear craton-style geothermal gradient is likely to be unrealistic for orogenic lithosphere (Allen *et al*., 2013). It has been suggested that orogenesis may proceed by underthrusting of mantle lithosphere from the oncoming plate (e.g. Willet *et al*., 1993). In this case under-thrusting of Arabian mantle lithosphere, with its own pre-existing geothermal gradient, may lead to a kinked geothermal gradient with the kink forming along the subduction plane between overlying Eurasian lithosphere and underlying Arabian lithosphere. Upon initial collision, this kink will be very sharp ($t_0$ in Fig. 18b), but over time the gradient will thermally relax ($t_1$) towards a gradient that resembles the one characteristic for cratons ($t_2$). This thermal relaxation would heat the lithosphere just under the kink, which would previously have been cool. Dewatering and melting of this horizon would follow, which is what we argue we see in our *P-T* estimates of magma generation in Fig. 17. Given the lower degrees of melting in the southern Lesser Caucasus, it appears that this mechanism only develops low-degree melts.

To summarise, in the northern Lesser Caucasus magma is generated by small-scale delamination events heating the base of the lithosphere. This process also occurs in the southern Lesser Caucasus, but at greater depths. Magmas generated by this mechanism mix with a second type of magma produced in the mid-lithosphere from thermal relaxation of a kinked geotherm. Further south, in NW Iran, melting of the base of the lithosphere is

suppressed due to the depth being too great even for wet melting. However, melting in the mid-lithosphere continues.

**How does thicker mantle lithosphere influence the composition of the mantle source?**

The gradient in Sr-Nd isotope ratios in Fig. 11, along with a lack of evidence for crustal contamination, requires that there be some variation in the composition of the mantle source. One possibility is that magmas are tapping different lithosphere domains. Northern Lesser Caucasus magmas are exclusively found on Mesozoic arc lithosphere (Fig. 2), whereas southern Lesser Caucasus magmas are on South Armenian Block lithosphere, or else are very close to the suture. However, crossing such lithospheric sutures would likely result in a step-change in isotope ratios, rather than the smooth gradation observed in the Lesser Caucasus. A minority of samples from the Vardenis volcanic highland (Figs 1 and 2) are thought to be on the east (Mesozoic arc) side of the suture, these are shown by a * in Table 3. As Table 3 shows, these samples have Sr-Nd isotope compositions indistinguishable from other Vardenis samples, suggesting the suture zone is not a major dividing line in isotope composition. This suggests that melting zone 2 in the mid-lithosphere has a different composition to melting zone 1 at the base of the lithosphere. In this discussion on the nature of the mantle sources, only the most mafic samples (> 4 wt % MgO, < 54% $SiO_2$) are used in order to try and minimise the effects of fractional crystallisation on trace element contents.

The lower crust is thought to behave as a weak layer during continental collision (Bürgmann & Dresen, 2008). This could lead to some lower crust being incorporated into the mantle lithosphere perhaps during underthrusting of Arabian lithosphere, as has been suggested for numerical models of other collision zones such as the Himalayas (e.g. Toussaint *et al*., 2004; Li *et al*., 2011). This could lead to the addition of lower continental crust (LCC)

to melting zone 2 in the middle of the lithosphere, and hence enrichment of the mantle source of the southern Lesser Caucasus. Incorporation of LCC into the mantle source could result in significant enrichments in all of the most incompatible trace elements, as in Fig. 8e, given the much higher concentrations of most incompatible trace elements in the lower crust relative to the primitive mantle (Rudnick & Gao, 2003; Sun & McDonough, 1989).

The La/Nb ratios of the least enriched samples from the northern Lesser Caucasus and the same ratio estimated for the LCC (Rudnick & Gao, 2003) provides a serendipitous coincidence, with both around 1.6 (Fig. 19). Given that La/Nb is unaffected by melting and crystallisation (i.e. both elements have similar bulk partition coefficients with respect to the melt) regardless of source mineralogy (Ionov *et al*., 2002; Foley, 2008), any variations in the La/Nb ratio should reflect variations in the source La/Nb. If the lower crust was responsible for the source enrichment, La/Nb should be near-constant along the transect. Samples from the southern Lesser Caucasus have much higher La/Nb ranging from 2.5 to 5 (Fig. 19), which cannot be explained by the addition of average LCC.

However, it is worth noting that several estimates of the composition of individual lower crust sections do give higher La/Nb of up to 4.9 (Weaver & Tamey, 1984; Villaseca *et al*., 1999; Jagoutz & Schmidt, 2013), such that the involvement of lower crust in the southern Lesser Caucasus magma source cannot be precluded.

Lithospheric mantle which is significantly shallower than the lithosphere-asthenosphere boundary (melting zone 2) is expected to be colder than the deep lithosphere (melting zone 1) prior to any heating, even if the lithosphere does have a kinked geothermal gradient (Fig. 17). These lower temperatures should stabilise minerals such as amphibole and phlogopite which can retain chemical components derived from mantle metasomatism (Luth, 2003; Frost, 2006; and references therein). In the deep lithosphere, these components would be subject to upward mobilization by fluid release following dehydration at higher pre-

melting temperatures. Under-thrusting of Arabian lithosphere, as suggested in Fig. 18, would also introduce a new lithospheric domain, which could have a different composition (including isotopically) to the Eurasian lithosphere.

If this metasomatic material is responsible for the enrichments in the southern Lesser Caucasus, then it must have a composition capable of producing those most enriched melts. La/Yb and Sr/Y are two ratios which increase most dramatically with latitude as shown in Figs 20a and b. Both of these ratios show excellent correlations with $P_2O_5$ content (Figs 20c and d) within all Lesser Caucasus samples. The La/Yb ratios and $P_2O_5$ contents of the NW Iran samples (interpreted to be pure melting zone 2 magmas) appear as end-members on the Lesser Caucasus mixing line (Fig. 20d), suggesting apatite may be a metasomatic phase in the host rock of melting zone 2 (Fig. 18). This is consistent with the presence of large apatite crystals in some southern Lesser Caucasus samples (up to 2mm across; Fig. 5b). It is also consistent with previous suggestions that metasomatic apatite may be an important phase in the Iranian SCLM (Pang *et al*., 2013). As was shown in Fig. 15, it is difficult to produce such high LREE concentrations (shown by La in Fig. 15) simply by lower degrees of melting or more garnet in the mantle source. Apatite is soluble in melts with a low $SiO_2$ content (Watson, 1980), such that apatite may simply be added to the initial modelled melt composition, as shown by the blue dashed line in Fig. 15, producing a much improved agreement with natural southern Lesser Caucasus samples.

While apatite can explain the enrichment in LREE, it cannot explain the large enrichment in other elements such as Ba, which likely requires wider metasomatic reworking. Two minerals which could explain this enrichment in Ba are amphibole and phlogopite. As Fig. 21 shows, the high Ba/Rb ratio favours amphibole as the major metasomatic phase in the source of both the Lesser Caucasus and NW Iran magmas. However, in both the southern Lesser Caucasus and NW Iran there are a minority of samples for which phlogopite could be

an important metasomatic phase. It is noteworthy that the presence of phlogopite in the mantle source is indicated in a minority of cases for Vardenis, but not Syunik (Fig. 21), given that biotite is only found as a phenocryst phase in mafic samples from Vardenis (see Petrography section). The presence of these metasomatic signatures in the southern Lesser Caucasus and NW Iran is consistent with melting zone 2 being host to apatite, amphibole, and occasionally phlogopite prior to melting.

Sr/Y is a ratio which does not follow a simple mixing pattern. It increases across the Lesser Caucasus, but is actually lower in NW Iran compared to the southern Lesser Caucasus. This ratio probably reflects the involvement of garnet in the mantle source (Defant & Drummond, 1990), which should become dominant at greater depths. In NW Iran, all melting is occurring in the mid-lithosphere, however in the southern Lesser Caucasus magmatism is driven by melting in both the mid-lithosphere and at the base of the lithosphere (Fig. 18). This means that in the southern Lesser Caucasus, the average depth of melting may actually be greater than in NW Iran, despite the thinner lithosphere, leading to the mantle source being more dominated by garnet, increasing the Sr/Y ratio of the resulting magmas.

High Sr/Y ratios have been associated with adakites and the melting of oceanic slabs (Defant & Drummond, 1990). Adakitic signatures have been seen in some volcanic suites from NW Iran (e.g. Ghalamghash *et al*., 2016), suggesting that the Iranian enriched signature could somehow derive from slab melting. These adakites are generally andesites and dacites. The more primitive NW Iran lavas of Allen *et al*. (2013) and the southern Lesser Caucasus lavas have higher Y contents than true adakites, and it is likely the adakite-like compositions of andesites and dacites are derived from fractional crystallisation processes (e.g. Chiaradia *et al*., 2009), rather than slab melting.

Melting zone 2 does appear to have a more enriched composition than melting zone 1, as demonstrated by signatures of the metasomatic minerals apatite and amphibole in magmas

derived from the southern Lesser Caucasus and NW Iran. However, variations between the chemistry of the northern and southern Lesser Caucasus volcanic rocks do not just reflect mixing of source reservoirs, but also changes in the degree of melting (lower degree of melting will increase La/Yb and Sr/Y ratios), and the mineralogy of the melt source (garnet in the melt source of the southern Lesser Caucasus also increases Sr/Y and La/Yb). The multiple parameters controlling the trace element composition of Lesser Caucasus volcanic rocks means that variations between the northern Lesser Caucasus, southern Lesser Caucasus and NW Iran are often non-linear.

## SUMMARY AND CONCLUSIONS

Magmas generated in the thicker lithosphere of the southern Lesser Caucasus have higher incompatible trace element concentrations, higher $^{87}Sr/^{86}Sr$ ratios and lower $^{143}Nd/^{144}Nd$ ratios than volcanic rocks from the northern Lesser Caucasus. A lack of consistent variation between the isotope compositions of basalts and rhyolites and $SiO_2$ suggests crustal contamination is unimportant in generating the enriched geochemistry. The negative Nb-Ta anomalies, and enrichments in large-ion-lithophile elements and LREE are instead likely to be produced by partial melting of a subduction-modified mantle source. This subduction component is uniform across the Lesser Caucasus and is likely inherited from Mesozoic (Tethyan) slab subduction prior to continental collision. The more enriched geochemistry of southern Lesser Caucasus rocks is the result of lower degrees of melting, an increased proportion of garnet in the mantle source, and also a distinct mantle source composition.

The temperatures of melt formation in the mantle are all less than 1200°C, which when compared with the much higher temperatures for magmas formed in the asthenosphere below nearby Eastern Anatolia, suggests magma generation occurs in the lithosphere, which

is also consistent with the ubiquitous subduction signature. Very similar conditions of melt generation in NW Iran and the southern Lesser Caucasus, as well as several similarities in geochemistry, suggest a common magma generation mechanism in the mid-lithosphere, despite very different lithospheric thicknesses. This magma type appears to mix in the southern Lesser Caucasus with magma from a second source, which probably originates at the base of the lithosphere. This latter magma source is the sole site of magma generation in the northern Lesser Caucasus, where melting occurs at the base of a ~50 km thick lithosphere. In the southern Lesser Caucasus melting occurs at ~75 km depth, significantly shallower than the estimated 120 km thickness of the lithosphere. Melting in the mid-lithosphere occurs due to relaxation of a kinked geothermal gradient, whereas melting at the base of the lithosphere is the result of small-scale delamination events. This latter melting mechanism only proceeds until the point where the lithosphere becomes too thick to melt at its base, even if the mantle peridotite is hydrated. The enriched composition of the mid-lithospheric mantle source could be derived from the incorporation of weak lower crust during collision. However, several signatures of the metasomatic minerals amphibole, apatite and occasionally phlogopite suggest that the enriched nature of the mantle source in the mid-lithosphere is derived from the increased retention of metasomatic components in hydrous minerals prior to the post-collisional magmatism.

Interestingly, it appears that a melt source exists at somewhat less than 100 km depth regardless of the lithospheric thickness across the Anatolian-Armenian-Iranian plateau. This is consistent with the geophysical observations of Maggi & Priestley (2005), which show a low shear wave velocity at around 100 km depth below the entire plateau. Further work on understanding the interplay between lithospheric thickness and melt generation in continental collision zones would benefit from detailed tomographic work in the critical region of the Lesser Caucasus to help us better understand how the thickness of the lithosphere varies along

this mountain range. Investigations of the petrogenesis of primitive magmatic rocks from NW Iran, could elucidate whether thermal relaxation of a kinked geothermal gradient is a viable mechanism to generate magma in the mid-lithosphere. Studies of stable fluid-sensitive isotopes systems such as O and B would help decipher the nature and role of inherited subduction components in the generation of collision-related magmas.


## FUNDING

This work was supported as part of Patrick Sugden's PhD "Collision-related volcanoes in Armenia" which is funded by the Natural Environment Research Council (NERC), as part of the Leeds-York *Spheres* doctoral training programme. Financial support for more than a decade of annual fieldwork sessions for IPS was kindly provided by the Carnegie Institution for Science, Smithsonian Institution-NMNH, Armenian Academy of Sciences and the University of Leeds.

## ACKNOWLEDGEMENTS

We would like to thank the late Sergei Karapetyan, late Arkadi Karakhanian, and also Ruben Jrbashyan (all from the Armenian institute of Geological Sciences) for their initial fieldwork efforts on constructing the earlier versions of the now completed and georeferenced geological map of the Syunik Volcanic Highland (our Fig. 4). Without their critical guidance in the field, this study would have been impossible. IPS is grateful to the late Jim Luhr (Smithsonian-NMNH) and Rick Carlson (Carnegie Institution-DTM) for their help in the field and for obtaining the elemental and Sr and Nd isotope dataset for the Gegham Volcanic Highland samples. Harri Wyn Williams prepared the thin sections, while Richard Walshaw set up and helped with SEM analysis at Leeds University. Iain Neill, Dan Morgan, Chuck

Connor and Samuele Agostini provided insightful advice and comments on various stages of this research. The authors would like to thank the Editor John Gamble, as well as Stephen Daly, Dejan Prelević and Mehmet Keskin for their very helpful reviews which considerably improved the clarity of the manuscript.



## REFERENCES

Al-Lazki, A. I. (2003). Tomographic Pn velocity and anisotropy structure beneath the Anatolian plateau (eastern Turkey) and the surrounding regions. *Geophysical Research Letters* **30**, 4–7.

Allen, M. B., Kheirkhah, M., Neill, I., Emami, M. H. & McLeod, C. L. (2013). Generation of arc and within-plate chemical signatures in collision zone magmatism: Quaternary lavas from kurdistan province, Iran. *Journal of Petrology* **54**, 887–911.

Angus, D. A., Wilson, D. C., Sandvol, E. & Ni, J. F. (2006). Lithospheric structure of the Arabian and Eurasian collision zone in eastern Turkey from S-wave receiver functions. *Geophysical Journal International* **166**, 1335-1346.

Baghdasaryan, G.P. & Ghukasyan, R.Kh., (1985). Geochronology of magmatic, metamorphic and ore formations of Armenian SSR. *Publication of the Academy of Sciences of Armenian Soviet Socialist Republic* (in Russian).

Brounce, M. N., Kelley, K. A. & Cottrell, E. (2014). Variations in Fe3+/∑ Fe of Mariana Arc Basalts and Mantle Wedge f O2. *Journal of Petrology* **55**, 2513-2536.

Bürgmann, R. & Dresen, G. (2008). Rheology of the lower crust and upper mantle: Evidence from rock mechanics, geodesy, and field observations. *Annual Review of Earth and Planetary Sciences* **36**, 531-567.

Carmichael, I. S. E., Nicholls, J. T. & Smith, A. L. (1970). Silica activity in igneous rocks. *American Mineralogist* **55**, 246-263.

Carmichael, I. S. E., Lange, R. A. & Luhr, J. F. (1996). Quaternary minettes and associated volcanic rocks of Mascota, western Mexico: a consequence of plate extension above a subduction modified mantle wedge. *Contributions to Mineralogy and Petrology* **124**, 302-333.

Chernyshev, I.V., Lebedev, V.A., Arakleyants, M.M., Jrbashyan, R.T. & Ghukasyan, Y.G. (2002). Geochronology of the Aragats volcanic centre, Armenia: evidence from K/Ar dating. *Doklady Earth Sciences* **384**, 393–398 (in Russian).

Chiaradia, M., Müntener, O., Beate, B. & Fontignie, D. (2009). Adakite-like volcanism of Ecuador: lower crust magmatic evolution and recycling. *Contributions to Mineralogy and Petrology* **158**, 563–588.

Connor, C., Connor, L., Halama, R., Meliksetian, K. & Savov, I. (2011). Volcanic Hazard Assessment of the Armenia Nuclear Power Plant Site: Final Report, 1–274.

Cottrell, E. & Kelley, K. A. (2011). The oxidation state of Fe in MORB glasses and the oxygen fugacity of the upper mantle. *Earth and Planetary Science Letters* **305**, 270-282.

Cox, K. G., Bell, J. D. & Pankhurst, R. J. (1979). *The Classification of Igneous Rocks*. Allen & Unwin UK.

Davidson, J., Turner, S. & Plank, T. (2013). Dy/Dy*: variations arising from mantle sources and petrogenetic processes. *Journal of Petrology* **54**, 525-537.

Defant, M. J., & Drummond, M. S. (1990). Derivation of some modern arc magmas by melting of young subducted lithosphere. *Nature* **347**, 662-665.

Dixon, J. E., Leist, L., Langmuir, C. & Schilling, J. G. (2002). Recycled dehydrated lithosphere observed in plume-influenced mid-ocean-ridge basalt. *Nature* **420**, 385-389.

Faccenna, C., Becker, T. W., Jolivet, L. & Keskin, M. (2013). Mantle convection in the Middle East: Reconciling Afar upwelling, Arabia indentation and Aegean trench rollback. *Earth and Planetary Science Letters* **375**, 254–269.

Frost, D.J. (2006). The stability of hydrous mantle phases. In: Keppler H. & Smyth J.R. (eds). *Water in Nominally Anhydrous Minerals. Reviews in Mineralogy*, **62**, pp 243–271.

Furman, T. & Graham, D. (1999). Erosion of lithospheric mantle beneath the East African Rift system: geochemical evidence from the Kivu volcanic province. *Lithos* **48**, 237-262.

Galoyan, G., Rolland, Y., Sosson, M., Corsini, M. & Melkonyan, R., (2007). Evidence for superposed MORB, oceanic plateau and volcanic arc series in the Lesser Caucasus (Stepanavan, Armenia). *Comptes Rendus Geosciences* **339**, 482–492.

Galoyan, G., Rolland, Y., Sosson,M., Corsini, M., Billo, S., Verati, C. & Melkonyan, R. (2009). Geology, geochemistry and Ar/Ar dating of Sevan ophiolites (Lesser Caucasus, Armenia): evidence for Jurassic back-arc opening and hot spot event between the South Armenian Block and Eurasia. *Journal of Asian Earth Sciences* **34**, 135–153.

Garbe-Schönberg, C. D. (1993). Simultaneous determination of thirty-seven trace elements in twenty-eight international rock standards by ICP-MS. *Geostandard Newsletter* **17**, 81–97.

Göğüş, O. H. & Pysklywec, R. N. (2008). Mantle lithosphere delamination driving plateau uplift and synconvergent extension in eastern Anatolia. *Geology* **36**, 723-726.

Gök, R., Mellors, R. J., Sandvol, E., Pasyanos, M., Hauk, T., Takedatsu, R. & Javakishvirli, Z. (2011). Lithospheric velocity structure of the Anatolian plateau - Caucasus - Caspian region. *Journal of Geophysical Research: Solid Earth,* **116**, 1–14.

Green, D. H. & Falloon, T. J. (2005). Primary magmas at mid-ocean ridges, 'hotspots', and other intraplate settings: Constraints on mantle potential temperature. In: Foulger, G. R., Natland, J. H., Presnall, D. C. & Anderson, D. L. (eds) *Plates, Plumes and Paradigms.* Geological Society of America, Special Papers **388**, 217-248.

Hässig, M., Rolland, Y., Sahakyan, L., Sosson, M., Galoyan, G., Avagyan, A., Bosch, D. & Müller, C. (2015). Multi-stage metamorphism in the South Armenian Block during the Late Jurassic to Early Cretaceous: tectonics over South-dipping subduction of Paleotethys. *Journal of Asian Earth Science* **102**, 4–23.

Hofmann, A. W. (2003). Sampling mantle heterogeneity through oceanic basalts: isotopes and trace elements. In: Carlson, R. W. (ed) *Treatise on geochemistry*, **2**, pp 61-102.

Hosseinpour, M., Williams, S., Seton, M., Barnett-Moore, N. & Müller, R. D. (2016). Tectonic evolution of Western Tethys from Jurassic to present day: coupling geological and geophysical data with seismic tomography models. *International Geology Review* **58**, 1616-1645.

Hu, F., Ducea, M. N., Liu, S. & Chapman, J. B. (2017). Quantifying Crustal Thickness in Continental Collisional Belts: Global Perspective and a Geologic Application. *Scientific reports* **7**, 7058.

Ionov, D. A. & Hofmann, A. W. (1995). Nb□ Ta-rich mantle amphiboles and micas: Implications for subduction-related metasomatic trace element fractionations. *Earth and Planetary Science Letters* **131**, 341-356.

Ionov, D.A., Bodinier, J.L., Mukasa, S.B. & Zanetti, A. (2002). Mechanisms and sources of mantle metasomatism: major and trace element compositions of peridotite xenoliths from Spitsbergen in the context of numerical modelling. *Journal of Petrology* **43**, 2219–2259.

Jacobsen, S. B. & Wasserburg, G. J. (1980). Sm-Nd isotopic evolution of chondrites. *Earth and Planetary Science Letters* **50**, 139-155.

Jagoutz, O. & Schmidt, M. W. (2013). The composition of the foundered complement to the continental crust and a re-evaluation of fluxes in arcs. *Earth and Planetary Science Letters* **371**, 177-190.

Joannin, S., Cornée, J. J., Münch, P., Fornari, M., Vasiliev, I., Krijgsman, W. & Chataigner, C. (2010). Early Pleistocene climate cycles in continental deposits of the Lesser Caucasus of Armenia inferred from palynology, magnetostratigraphy, and 40Ar/39Ar dating. *Earth and Planetary Science Letters* **291**, 149-158.

Jrbashian, R.T., Kazarian, G.A., Karapetian, S.G., Meliksetian, Kh.B., Mnatsakanian, A. & Shirinian, K.G., (1996). Meso-Cenozoic basaltic volcanism in the northeastern part of Armenian Highland. *Letters to the Armenian Academy of Sciences: Earth Sciences* **49**, 19–32 (in Russian).

Kaislaniemi, L., Van Hunen, J., Allen, M. B. & Neill, I. (2014). Sublithospheric small-scale convection—a mechanism for collision zone magmatism. *Geology*, **42**, 291-294.

Karakhanian, A., Djrbashian, R., Trifonov, V., Philip, H., Arakelian, S., & Avagian, A. (2002). Holocene-historical volcanism and active faults as natural risk factors for Armenia and adjacent countries. *Journal of Volcanology and Geothermal Research* **113**, 319-344.

Karaoğlan, F., Parlak, O., Robertson, A., Thöni, M., Klötzli, U., Koller, F. & Okay, A.İ. (2013). Evidence of Eocene high-temperature/high-pressure metamorphism of ophiolitic rocks and granitoid intrusion related to Neotethyan subduction processes (Doğanşehir area, SE Anatolia). *Geological Society Special Publication* **372**, 249–272.

Karaoğlan, F., Parlak, O., Hejl, E., Neubauer, F. & Klötzli, U. (2016). The temporal evolution of the active margin along the South-east Anatolian Orogenic Belt (SE Turkey): evidence from U–Pb, Ar–Ar and fission track chronology. *Gondwana Research* **33**, 190–208.

Karapetian, S. G., Jrbashian, R. T. & Mnatsakanian, A. K. (2001). Late collision rhyolitic volcanism in the north-eastern part of the Armenian highland. *Journal of Volcanology and Geothermal Research* **112**, 189–220.

Kelemen, P. B., Hanghøj, K. & Greene, A. R. (2003). One View of the Geochemistry of Subduction-related Magmatic Arcs, with an Emphasis on Primitive Andesite and Lower Crust. In: Holland, H. D. & Turekian, K. K. (eds) *Treatise on Geochemistry*, **3**. Elsevier, pp 593-658.

Keskin, M., Pearce, J. A. & Mitchell, J. G. (1998). Volcano-stratigraphy and geochemistry of collision-related volcanism on the Erzurum-Kars Plateau, northeastern Turkey. *Journal of Volcanology and Geothermal Research* **85**, 355–404.

Keskin, M. (2003). Magma generation by slab steepening and breakoff beneath a subduction-accretion complex: An alternative model for collision-related volcanism in Eastern Anatolia, Turkey. *Geophysical Research Letters* **30**, 7–10.

Keskin, M., Pearce, J. A., Kempton, P. D. & Greenwood, P. (2006). Magma-crust interactions and magma plumbing in a postcollisional setting: geochemical evidence from the Erzurum-Kars volcanic plateau, eastern Turkey. In: Postcollisional tectonics and magmatism in the Mediterranean region and Asia (Y. Dilek & S. Pavlides eds.). *Special Papers-Geological Society of America* **409**, pp. 475-505.

Keskin, M. (2007). Eastern Anatolia: a hot spot in a collision zone without a mantle plume. *Geological Society of America, Special Publication* **2430**, 1–40.

Kharazyan, E.Kh. (1983). Geology of Recent Volcanism of North-west Part of Armenian SSR (Basins of Rivers Dzoraget and Akhuryan). (Unpublished PhD thesis), *ArmGeologia*, Yerevan (55 pp.).

Kharazyan, E.Kh. (2005). Geological map of Armenia. Ministry of Nature Protection of Republic of Armenia (1 sheet).

Koulakov, I., Zabelina, I., Amanatashvili, I. & Meskhia, V. (2012). Nature of orogenesis and volcanism in the Caucasus region based on results of regional tomography. *Solid Earth* **3**, 327–337.

Le Bas, M., Le Maitre, R., Streckeisen, A. & Zanettin, B. (1986). A chemical classification of volcanic rocks based on the total alkali–silica diagram. *Journal of Petrology* **27**, 745–750.

Lebedev, V. A., Chernyshev, I. V., Shatagin, K. N., Bubnov, S. N. & Yakushev, A. I. (2013). The Quaternary volcanic rocks of the Geghama highland, Lesser Caucasus, Armenia: Geochronology, isotopic Sr-Nd characteristics, and origin. *Journal of Volcanology and Seismology* **7**, 204-229.

Lechmann, A., Burg, J. P., Ulmer, P., Guillong, M. & Faridi, M. (2018). Metasomatized mantle as the source of Mid-Miocene-Quaternary volcanism in NW-Iranian Azerbaijan: Geochronological and geochemical evidence. *Lithos* **304,** 311-328.

Lee, C. T. A., Luffi, P., Plank, T., Dalton, H. & Leeman, W. P. (2009). Constraints on the depths and temperatures of basaltic magma generation on Earth and other terrestrial planets using new thermobarometers for mafic magmas. *Earth and Planetary Science Letters* **279**, 20-33.

Le Maitre, R. W., Bateman, P., Dudek, A., Keller, J., Lameyre, J., Le Bas, M., Sabine, P., Schmid, R., Sorensen, H. & Streckeisen, A. (1989). *A Classification of Igneous Rocks and Glossary of Terms: Recommendations of the International Union of Geological Sciences Subcommission on the Systematics of Igneous Rocks*. Blackwell Scientific UK.

Li, Z. H., Xu, Z. Q. & Gerya, T. V. (2011). Flat versus steep subduction: Contrasting modes for the formation and exhumation of high-to ultrahigh-pressure rocks in continental collision zones. *Earth and Planetary Science Letters* **301**, 65-77.

Luth, R.W. (2003). Mantle volatiles – distribution and consequences. In: The Mantle and Core (R.W. Carlson, ed.). *Treatise in Geochemistry*, **2**. Elsevier-Pergamon, pp. 319–361.

Maggi, A. & Priestley, K. (2005). Surface waveform tomography of the Turkish-Iranian plateau. *Geophysical Journal International* **160**, 1068-1080.

Mandler, B. E. & Grove, T. L. (2016). Controls on the stability and composition of amphibole in the Earth's mantle. *Contributions to Mineralogy and Petrology* **171**, 68.

Mather, K. A., Pearson, D. G., McKenzie, D., Kjarsgaard, B. A. & Priestley, K. (2011). Constraints on the depth and thermal history of cratonic lithosphere from peridotite xenoliths, xenocrysts and seismology. *Lithos* **125**, 729-742.

McKenzie, D. & O'Nions, R. K. (1991). Partial melt distributions from inversion of rare earth element concentrations. *Journal of Petrology* **32**, 1021-1091.

McKenzie, D. & Priestley, K. (2008). The influence of lithospheric thickness variations on continental evolution. *Lithos* **102**, 1-11.

McNab, F., Ball, P. W., Hoggard, M. J. & White, N. J. (2018). Neogene uplift and magmatism of Anatolia: Insights from drainage analysis and basaltic geochemistry. *Geochemistry, Geophysics, Geosystems* **19**, 1-39.

Mederer, J., Moritz, R., Ulianov, A. & Chiaradia, M. (2013). Middle Jurassic to Cenozoic evolution of arc magmatism during Neotethys subduction and arc-continent collision in the Kapan Zone, southern Armenia. *Lithos* **177**, 61–78.

Meliksetian, K. (2013). Pliocene–Quaternary volcanism of the Syunik upland. *Archäologie in Armenien* **2**, 247-258.

Neill, I., Meliksetian, K., Allen, M. B., Navarsardyan, G. & Karapetyan, S. (2013). Pliocene-Quaternary volcanic rocks of NW Armenia: Magmatism and lithospheric dynamics within an active orogenic plateau. *Lithos* **180–181**, 200–215.

Neill, I., Meliksetian, K., Allen, M. B., Navasardyan, G. & Kuiper, K. (2015). Petrogenesis of mafic collision zone magmatism: The Armenian sector of the Turkish–Iranian Plateau. *Chemical Geology* **403**, 24–41.

Ollivier, V., Nahapetyan, S., Roiron, P., Gabrielyan, I., Gasparyan, B., Chataigner, C. & Munch, P. (2010). Quaternary volcano-lacustrine patterns and palaeobotanical data in southern Armenia. *Quaternary International* **223**, 312-326.

Oyan, V., Keskin, M., Lebedev, V. A., Chugaev, A. V., Sharkov, E. V. & Ünal, E. (2017). Petrology and Geochemistry of the Quaternary Mafic Volcanism to the NE of Lake Van, Eastern Anatolian Collision Zone, Turkey. *Journal of Petrology* **58**, 1701-1728.

Ozdemir, Y., Karaoğlu, O., Tolluoğlu, A. U. & Gülec¸, N. (2006). Volcanostratigraphy and petrogenesis of the Nemrut stratovolcano (East Anatolian High Plateau): The most recent post-collisional volcanism in Turkey. *Chemical Geology* **226**, 189–211.

Pang, K. N., Chung, S. L., Zarrinkoub, M. H., Lin, Y. C., Lee, H. Y., Lo, C. H. & Khatib, M. M. (2013). Iranian ultrapotassic volcanism at~ 11 Ma signifies the initiation of post-collisional magmatism in the Arabia–Eurasia collision zone. *Terra Nova*, **25**, 405-413.

Pearce, J.A., (1983). *Role of the sub-continental lithosphere in magma genesis at active continental margins*. In Hawkesworth C.J. & Norry, M.J. eds., *Continental Basalts and Mantle Xenoliths.* Shiva Press, 230-249.

Pearce, J. A., Bender, J. F., De Long, S. E., Kidd, W. S. F., Low, P. J., Guner, Y., Saroglu, F., Yilmaz, Y. & Mitchell, J. G. (1990). Genesis of collision volcanism in Eastern Anatolia, Turkey. *Journal of Volcanology and Geothermal Research* **44**, 189–229.

Plank, T. & Forsyth, D. W. (2016). Thermal structure and melting conditions in the mantle beneath the Basin and Range province from seismology and petrology. *Geochemistry, Geophysics, Geosystems* **17**, 1312-1338.

Prelević, D., Foley, S. F., Romer, R. & Conticelli, S. (2008). Mediterranean Tertiary lamproites derived from multiple source components in postcollisional dynamics. *Geochimica et Cosmochimica Acta* **72**, 2125-2156.

Prelević, D., Akal, C., Romer, R. L., Mertz-Kraus, R. & Helvacı, C. (2015). Magmatic response to slab tearing: constraints from the Afyon Alkaline Volcanic Complex, Western Turkey. *Journal of Petrology* **56**, 527-562.

Priestley, K. & McKenzie, D. (2006). The thermal structure of the lithosphere from shear wave velocities. *Earth and Planetary Science Letters* **244**, 285-301.

Priestley, K., McKenzie, D., Barron, J., Tatar, M. & Debayle, E. (2012). The Zagros Core: deformation of the continental lithospheric mantle. *Geochemistry, Geophysics, Geosystems* **13**, 1-21.

Priestley, K. & McKenzie, D. (2013). The relationship between shear wave velocity, temperature, attenuation and viscosity in the shallow part of the mantle. *Earth and Planetary Science Letters* **381**, 78-91.

Robinson, J.A.C. & Wood, B.J. (1998). The depth of the spinel to garnet transition at the peridotite solidus. *Earth & Planetary Science Letters* **164**, 277–284.

Roeder, P. L. & Emslie, R. F. (1970). Olivine–liquid equilibrium. *Contributions to Mineralogy and Petrology* **29**, 275–289.

Rolland, Y., Billo, S., Corsini, M., Sosson, M. & Galoyan, G. (2009). Blueschists of the Amassia–Stepanavan Suture Zone (Armenia): linking Tethys subduction history from E-Turkey to W-Iran. *International Journal of Earth Sciences* **98**, 533–550.

Rolland, Y., Galoyan, G., Sosson, M., Melkonian, R. & Avagyan, A. (2010). The Armenian ophiolites: insights for Jurassic back-arc formation, Lower Cretaceous hot-spot magmatism, and Upper Cretaceous obduction over the South Armenian Block. *Geological Society of London, Special Publication* **340**, 353–382.

Rolland, Y., Perincek, D., Kaymakci, N., Sosson, M., Barrier, E. & Avagyan, A. (2012). Evidence for ~80–75Ma subduction jump during Anatolide-Tauride-Armenian block accretion and ~48 Ma Arabia-Eurasia collision in Lesser Caucasus-East Anatolia. *Journal of Geodynamics* **56–57**, 76–85.

Rolland, Y., Hässig, M., Bosch, D.,Meijers, M. J. M., Sosson, M., Bruguier, O., Adamia, Sh. & Sadradze, N. (2016). A review of the plate convergence history of the East Anatolia-Transcaucasus region during the Variscan: insights from the Georgian basement and its connection to the Eastern Pontides. *Journal of Geodynamics* **96**, 131–145.

Rolland, Y. (2017). Caucasus collisional history : Review of data from East Anatolia to West Iran. *Gondwana Research* **49**, 130–146.

Rollinson, H.R. (1993). *Using Geochemical Data*. Routledge, UK.

Rudnick, R. L. & Gao, S. (2003). Composition of the continental crust. In: Holland, H. D. & Turekian, K. K. (eds) *Treatise on Geochemistry*, **3**. Elsevier, pp 659-723.

Şen, P. A., Temel, A. & Gourgaud, A. (2004). Petrogenetic modelling of Quaternary post-collisional volcanism: a case study of central and eastern Anatolia. *Geological Magazine* **141**, 81-98.

Şengör, A.M.C. (1984). The Cimmeride Orogenic system and the tectonics of Eurasia. *Geological Society of America Special Papers* **195**, 181-241.

Şengör, A. M. C., Özeren, S., Genç, T. & Zor, E. (2003). East Anatolian high plateau as a mantle-supported, north-south shortened domal structure. *Geophysical Research Letters* **30,** 8.1-8.4.

Şengör, A. M. C., Sinan, M., Keskin, M., Sak, M., De, A. & Kayan, İ. (2008). Eastern Turkish high plateau as a small Turkic-type orogen : Implications for post-collisional crust-forming processes in Turkic-type orogens. *Earth-Science Reviews* **90**, 1–48.

Shaw, D.M. (2005). *Trace Elements in Magmas, a Theoretical Treatment*. Cambridge University Press UK.

Sheth, H., Meliksetian, K., Gevorgyan, H., Israyelyan, A. & Navasardyan, G. (2015). Intracanyon basalt lavas of the Debed River (northern Armenia ), part of a Pliocene – Pleistocene continental flood basalt province in the South Caucasus. *Journal of Volcanology and Geothermal Research* **295**, 1–15.

Skolbeltsyn, G., Mellors, R., Gök, R., Turkelli, N., Yetirmishli, G. & Sandvol, E. (2014). Upper mantle S wave velocity structure of the East Anatolian-Caucasus region. *Tectonics* **33**, 207–221.

Sobolev, A. V., Hofmann, A. W., Sobolev, S. V. & Nikogosian, I. K. (2005). An olivine-free mantle source of Hawaiian shield basalts. *Nature* **434**, 590-597.

Sosson, M., Rolland, Y., Danelian, T., Muller, C., Melkonyan, R., Adamia, S., Kangarli, T., Avagyan, A. & Galoyan, G. (2010). Subductions, obduction and collision in the Lesser Caucasus (Armenia, Azerbaijan, Georgia), new insights. In Sosson, M. *et al*. (eds) *Sedimentary Basin Tectonics from the Black Sea and Caucasus to the Arabian Platform. Geological Society, London, Special Publication* **340**, 329–352.

Stampfli, G.M., Hochard, C., Vérard, C. & Wilhem, C. (2013). The formation of Pangea. *Tectonophysics* **593**, 1–19.

Sun, S. S. & McDonough, W. F. (1989). Chemical and isotopic systematics of oceanic basalts: implications for mantle composition and processes. In: Saunders, A. D. & Norry, M. J. (eds) *Magmatism in the Ocean Basins. Geological Society, London, Special Publications* **42**, 313-345.

Thirlwall, M. F., Upton, B. G. J. & Jenkins, C. (1994). Interaction between continental lithosphere and the Iceland plume: Sr-Nd-Pb isotope geochemistry of Tertiary basalts, NE Greenland. *Journal of Petrology* **35**, 839-879.

Topuz, G., Göçmengil, G., Rolland, Y., Çelik, Ö.F., Zack, T. & Schmitt, A.K. (2013a). Jurassic accretionary complex and ophiolite from northeast Turkey: no evidence for the Cimmerian continent. *Geology* **41**, 255–258.

Topuz, G., Çelık, Ö.F., Şengör, A.M.C., Altintaş, İ.E., Zack, T., Rolland, Y. & Barth,M. (2013b). Jurassic ophiolite formation and emplacement as backstop to a subduction-accretion complex in northeast Turkey, the Refahıye ophiolite, and relation to the Balkan ophiolites. *American Journal of Science* **313**, 1054–1087.

Topuz, G., Okay, A.I., Altherr, R., Schwarz, W.H., Sunal, G. & Altinkaynak, L. (2014). Triassic warm subduction in northeast Turkey: evidence from the Agvanis metamorphic rocks. *Island Arc* **23***,* 181–205.

Toussaint, G., Burov, E. & Avouac, J. P. (2004). Tectonic evolution of a continental collision zone: A thermomechanical numerical model. *Tectonics* **23**, 1-24.

Turner, S. J., Langmuir, C. H., Dungan, M. A. & Escrig, S. (2017). The importance of mantle wedge heterogeneity to subduction zone magmatism and the origin of EM1. *Earth and Planetary Science Letters* **472**, 216–228.

Villaseca, C., Orejana, D., Paterson, B. A., Billstrom, K. & Pérez-Soba, C. (2007). Metaluminous pyroxene-bearing granulite xenoliths from the lower continental crust in central Spain: their role in the genesis of Hercynian I-type granites. *European Journal of Mineralogy* **19**, 463-477.

Walsh, J. N., Buckley F. & Barker J. (1981). The simultaneous determination of the rare-earth elements in rocks using inductively coupled plasma source spectrometry. *Chemical Geology* **33**, 141–153.

Watson, E. B. (1980). Apatite and phosphorus in mantle source regions: an experimental study of apatite/melt equilibria at pressures to 25 kbar. *Earth and Planetary Science Letters* **51**, 322-335.

Weaver, B. L. & Tarney, J. (1984). Empirical approach to estimating the composition of the continental crust. *Nature* **310**, 575-577.

Weis, D., Kieffer, B., Maerschalk, C., Barling, J., de Jong, J., Williams, G. A., Hanano, D., Pretorius, W., Mattielli, N., Scoates, J. S., Goolaerts, A., Friedman, R. M. & Mahoney, J. B. (2006). High-precision isotopic characterization of USGS reference materials by TIMS and MC-ICP-MS. *Geochemistry, Geophysics, Geosystems* **7**, 1-30.

Willett, S., Beaumont, C. & Fullsack, P. (1993). Mechanical model for the tectonics of doubly vergent compressional orogens. *Geology* **21**, 371-374.

Yilmaz, A., Adamia, S., Chabukiani, A., Chkhotua, T., Erdoğan, K., Tuzcu, S. & Karabiyikoğlu, M. (2000). Structural correlation of the southern Transcaucasus (Georgia)-eastern Pontides (Turkey). In Bozkurt, E., Winchester, J. A. & Piper, J. D. A. (eds) *Tectonics and Magmatism in Turkey and the Surrounding Area. Geological Society, London, Special Publications* **173**, 171–182.

Zor, E. (2008). Tomographic evidence of slab detachment beneath eastern Turkey and the Caucasus. *Geophysical Journal International* **175**, 1273–1282.

## FIGURE CAPTIONS

**Figure 1:** Terrane map of the Caucasus region with inset showing the location of the Caucasus mountains. The major tectonic blocks are labelled, which from north to south are: Greater Caucasus, Kura Basin, Pontides-Lesser Caucasus (LCA)-Alborz Mesozoic-early Cenozoic arc, Taurides-Anatolides-South Armenian Block (SAB)-Cimmeria microcontinent terranes, East Anatolian Accretionary Complex (EAAC), Bitlis Mountains and the Arabian foreland. Terrane boundaries are after Neill *et al*. (2015). Red triangles denote the locations of major composite volcanoes. The locations of volcanic highlands which are used for the geochemical comparison which forms the focus of this study are shown by the coloured fields. These are labelled as 1- Shirak and Lori (Neill *et al*., 2013, 2015); 2- Gegham (Savov, unpublished data); 3- Vardenis; and 4- Syunik. New data for this study are from volcanic highlands 3 and 4. These volcanic highlands are close to parallel with major tectonic boundaries in the collision zone. Volcanic rocks from NW Iran referred to in the text are from the region labelled at the bottom of the map. Contours of lithospheric thickness from Priestley

*et al*. (2012) are shown in red, numbers give lithospheric thickness in km. The "Zagros Core" refers to the region of maximum lithosphere thickness in the collision zone.

**Figure 2:** Geological map of the major geological units of the Lesser Caucasus mountains within the territory of Armenia. After Neill *et al*. (2015), Kharazyan (2005) and Mederer *et al*. (2013). The volcanic highlands which form the focus of this study are labelled 1-4: 1- Shirak and Lori; 2- Gegham; 3- Vardenis; 4- Syunik. The bold black line shows the Pambak-Sevan-Syunik strike-slip fault zone.

**Figure 3:** Illustration of the progressive closure of the oceanic domains which separated Arabia from Eurasia during the Mesozoic, after Rolland (2017). SAB- South Armenian Block, SAB-BP- South Armenian Block- Bitlis Poturge terrane. The movement of the Bitlis Poturge terrane from Arabia to the South Armenian Block is not shown in these figures but occurs between panels 1 and 2.

**Figure 4:** Geological age map of the Syunik volcanic highland (field 4 in Figs 1 and 2), based on the work of Sergei Karapetyan, Ruben Jrbashyan and Gevorg Navasardyan of the Institute of Geological sciences at the Armenian National Academy of Sciences. Red dashes- monogenetic volcanic centres. Red and white dashes- crater rims of Ishkhanasar and Tskhouk stratovolcanoes. Faint red lines- active faults. Bold red line shows the main road. A PDF version of this map is provided as Supplementary Data C.

**Figure 5:** Representative back-scattered electron images (a-c) and photomicrographs (d-f) of collision-related volcanic rocks in the southern Lesser Caucasus. (a) Unaltered amphibole

(amph) phenocryst in trachybasaltic andesite scoria from Syunik. Groundmass composed of clinopyroxene, plagioclase and oxides. (b) Large apatite (Ap) phenocryst >1mm in diameter, with oxide inclusions in trachybasaltic andesite lava, Syunik. (c) Large amphibole phenocryst with overgrowing plagioclase (plag) grains in trachybasaltic andesite lava from Vardenis. The rim of the amphibole is broken down into oxides and clinopyroxene. (d) Crossed polars (XPL) image of olivine (Ol) phenocrysts in trachybasalt lava from Syunik. (e) XPL image of plagioclase phenocryst in trachybasaltic andesite lava with sharp compositional boundary between the core and rim (in extinction) of this crystal. (f) XPL image of clinopyroxene (cpx) glomerocryst in trachyandesite sample from Vardenis.

**Figure 6:** Total alkalis *vs* silica classification diagram for volcanic rocks from the Lesser Caucasus mountain chain. Classification boundaries are from Le Bas *et al*. (1986), Le Maitre *et al*. (1989) and Cox *et al*. (1979). Data for Syunik and Vardenis are from this study, while Shirak and Lori data are from Neill *et al*. (2013, 2015), in this and all subsequent figures. Gegham data are from Savov *et al*., (unpublished data). Abbreviations for classification fields are as follows: B, basalt; BA, basaltic andesite; A, andesite; D, dacite; R, rhyolite; TB, trachybasalt; TBA, trachybasaltic andesite; TA, trachyandesite; Tr, trachyte; Te, tephrite/basanite; PTe, phonotephrite.

**Figure 7:** Selected major and trace elements plotted *versus* $SiO_2$. (a) $K_2O$, (b) MgO, (c) $P_2O_5$, (d) Y, (e) Ta, (f) La. All major elements are recalculated to 100% on an anhydrous basis. Symbols and data sources are as in Fig. 6.

**Figure 8:** MORB-normalised trace element patterns of mafic end-member samples for the Shirak and Lori (a), Gegham (b), Vardenis (c), and Syunik (d) volcanic highlands, which correspond to regions 1 to 4 in Fig. 1, respectively. The selected samples are the three samples with the highest MgO content (wt %) in each volcanic highland. Data sources are as in Fig. 6. For comparison, the total range of 'basalts' (< 52% $SiO_2$) from the Syunik volcanic highland is shown in (a) and (b) as the pale green field. The total range of Shirak and Lori basalts is shown as a gold field in (c) and (d). (d) also shows the composition of a Syunik rhyolite (diamonds) and bulk continental crust (stars) for Rb, K and Sr, in order to demonstrate whether these rhyolites are likely to be formed by assimilation and, or, melting of continental crust. Composition of the continental crust from Rudnick & Gao, 2003. The total compositional variability is illustrated in (e), where averages from the geographic extremes (Shirak in the north and Syunik in the south) are compared. Also shown here is a sample from Kurdistan, NW Iran from Allen *et al*. (2013), formed from melting in a region of very thick lithosphere. Normalisation factors from Sun & McDonough (1989). The average composition of Continental Arc basalt is from Kelemen *et al*. (2003).

**Figure 9:** Chondrite normalised REE profiles for Plio-Pleistocene mafic volcanic rocks from the Lesser Caucasus for Shirak and Lori (a), Gegham (b), Vardenis (c) and Syunik (d) volcanic highlands. The total compositional variability is illustrated in (e) where samples from Syunik and Shirak are compared. Normalisation factors from Sun & McDonough (1989). Data sources as in Fig. 6.

**Figure 10:** Th/Yb *vs* Ta/Yb variations in the volcanic rocks of the Lesser Caucasus. Mantle source array and enrichment vectors after Pearce (1983). Lesser Caucasus data sources as in

Fig. 6. NW Iran data from Allen *et al*. (2013). Fractional crystallisation (FC) vector: from basalt to andesite uses a 50% amphibole + 50% clinopyroxene assemblage and basaltic melt partition coefficients; from andesite to rhyolite uses a 50% plagioclase + 50% amphibole assemblage and andesite melt partition coefficients. The vector has a starting composition as the most mafic sample. Partition coefficients for Ta are: clinopyroxene-basalt = 0.017; amphibole-basalt = 0.05; amphibole-andesite = 0.21; plagioclase-andesite = 0.03. For Th: clinopyroxene-basalt = 0.007; amphibole-basalt = 0.05; amphibole-andesite = 0.16; plagioclase-andesite = 0.01. For Yb: clinopyroxene-basalt = 0.28; amphibole-basalt = 0.59; amphibole-andesite = 1.25; plagioclase-andesite = 1.25. All partition coefficients are from the GERM database (earthref.org/GERM/). The average compositions of Mesozoic arc rocks from the Kapan zone arc rocks are from Mederer *et al*. (2013). The grey box labelled BCC is the composition of bulk continental crust from Rudnick & Gao (2003).

**Figure 11:** εNd *vs* $^{87}Sr/^{86}Sr$ for volcanic rocks from the Lesser Caucasus. Bulk Earth value and mantle array after Rollinson (1993). NW Iran data are from Allen *et al*. (2013) - this region has very thick lithosphere, estimated to be > 200 km by Priestley *et al*. (2012). Mixing line shown between depleted MORB mantle (DMM) and Tethyan Flysch (Prelevic *et al*., 2008): DMM [Sr] = 21 ppm, [Nd] = 1.35 ppm, $^{87}Sr/^{86}Sr = 0.7028$, $^{143}Nd/^{144}Nd = 0.5131$; Tethyan Flysch [Sr] = 349.2 ppm, [Nd] = 25.9 ppm, $^{87}Sr/^{86}Sr = 0.7112$, $^{143}Nd/^{144}Nd = 0.512107$.

**Figure 12:** (a) $^{87}Sr/^{86}Sr$ *vs* $SiO_2$ (wt %) for all samples across the Lesser Caucasus. Fractional crystallisation is denoted by a horizontal arrow labelled “FC”. The dashed line labelled $^{87}Rb$ decay refers to the effect of post-crystallisation radioactive decay in rocks with very high

Rb/Sr ratios (see text for discussion). The crustal xenolith was collected in association with sample 1-4A-08 in the Syunik volcanic highland. It has a granitic texture. (b) $^{143}Nd/^{144}Nd$ *vs* $SiO_2$ (wt %).

**Figure 13:** The latitudinal variation in the ratios Ba/La (a), Ce/Pb (b), Sr/Nd (c) and Nb/U (d) of mafic volcanic rocks along the Lesser Caucasus mountain chain. These ratios are nearly invariant in MORB and OIB (shaded fields), but arc basalts show substantial variability in these ratios (CAB- continental arc basalt, with arrows showing the ranges across several arcs from Kelemen *et al*. (2003)). As such, they are a proxy for slab input, and show a uniform input across the Lesser Caucasus. After Turner *et al*. (2017).

**Figure 14:** (a) Dy/Dy* *vs* Dy/Yb after Davidson *et al*. (2013). The two arrows depict the expected vectors from changing the fraction of melting or source mineralogy/composition. The vector for a lower fraction of melting after Davidson *et al*. (2013), Figure 4, based on melting of an olivine-pyroxene-amphibole dominated mantle source. The presence of garnet in the magma source should follow a horizontal vector after Davidson *et al*. (2013), Figure 5. (b) Dy/Yb *vs* La/Yb, melting curves based on the modal mineralogies, melting modes, and partition coefficients given in Table 5.

**Figure 15:** N-MORB normalised concentrations of Nb, La, Zr, Hf, Gd, Dy and Yb for the average of mafic samples from Syunik volcanic highland (green line) and several non-modal batch melting models which attempt to explain these trace element concentrations. Melting models: spinel peridotite at 3% melting (yellow dashed line), 1% melting of spinel peridotite (dashed black line), 1% melting of garnet peridotite (black solid line) and 1% melting of a

source composed of 65% garnet peridotite and 35% spinel peridotite (dash-dot line). The blue dashed line represents a magma derived from the same 65% garnet peridotite source, with 4% apatite dissolved in the melt. Apatite composition is for magmatic apatite from Western Turkey in Prelević *et al*. (2015).

**Figure 16:** Ni/MgO *vs* $SiO_2$ in primitive Lesser Caucasus and NW Iran bulk-rock samples (<54% $SiO_2$, > 4% MgO), after Allen *et al*. (2013). Pyroxenite melting should generate compositions above the bold red dashed line (Sobolev *et al*., 2005). Primary melts of peridotite and pyroxenite (from Hawaii), after Sobolev *et al*. (2005). FC- fractional crystallisation. Syunik, Shirak and Lori and NW Iran data shown with the same symbols as in other figures.

**Figure 17:** Depth *vs* temperature of melting for the northern Lesser Caucasus and southern Lesser Caucasus. Also shown are the anhydrous peridotite solidus (1100°C+3.5°C/km) after Plank & Forsyth (2016), the wet solidus (amphibole present) after Green & Falloon (2005), samples from East Anatolia with low K/Nb (red circles) from McNab *et al*. (2018). The pressures and temperatures of melting of NW Iran magmas were calculated for this study assuming $Fe^{3+}/\Sigma Fe$ of 0.25 and melt water contents of 7 wt%, as were used for the southern Lesser Caucasus estimate. See text for discussion.

**Figure 18:** (a): Geodynamic model of magmatism showing the lithosphere and upper mantle across the Lesser Caucasus. Crustal thickness is estimated on the basis of formulations relating the Sr/Y and $(La/Yb)_N$ ratios in intermediate volcanic rocks to Moho depth (Hu *et al*., 2017). Data filtering follows the approach outlined in Hu *et al*. (2017). Each volcanic

highland has a range of Moho depth estimates of around 20 km. For both the Sr/Y and $(La/Yb)_N$ the median value for each volcanic highland is taken and then the two values are averaged to give an estimate of crustal thickness. Lithosphere thickness estimates are from Priestley *et al*. (2012). It is noted that they only estimate thicknesses where the lithosphere is >100 km, so the lithospheric thickness in the NW is schematic after Neill *et al*. (2015). Melting at the wet peridotite solidus lower depth limit is on the basis of upwelling convecting mantle at 1300-1400°C $T_p$, which would lead to the wet solidus being crossed at ~ 140 km depth (Green & Falloon, 2005). Also shown are the two melting zones (labelled 1 and 2) which are discussed in the text. Melting zone 1 is along the base of the lithosphere, and is suggested to be in response to small-scale convective removal of the lithosphere. Melting zone 2 is in the mid-lithosphere. (b) Sketch of the lithospheric structure of NW Iran and the location of melting in the mid-lithosphere (c) schematic illustration of the thermal relaxation of a kinked geothermal gradient leading to melting in the mid-lithosphere from initial under-plating at time $t_0$, through thermal evolution at time $t_1$, to establishing a cratonic geotherm by time $t_2$.

**Figure 19:** La/Nb *vs* latitude for primitive volcanic rocks in the Lesser Caucasus. The least enriched Shirak and Lori samples have a La/Nb ratio of ~1.6. Fraction of melting and garnet *vs* spinel lherzolite melting have a limited effect on this ratio. Lower continental crust (LCC) has a La/Nb ratio with a similar value of around 1.6 (Rudnick & Gao, 2003). Therefore if LCC is enriching the melt source, the La/Nb ratio should be close to invariant.

**Figure 20:** Sr/Y and La/Yb show strong variations between the northern and southern Lesser Caucasus as shown in (a) and (b). Both of these ratios show strong correlations with $P_2O_5$ (wt

%) (c and d), r=0.89 in both cases. NW Iran data in (c) and (d) represent melting in a region of very thick lithosphere (data from Allen *et al*., 2013).

Figure 21: Rb/Sr *vs* Ba/Rb for Lesser Caucasus and NW Iran samples, after Furman & Graham (1999). See text for discussion.

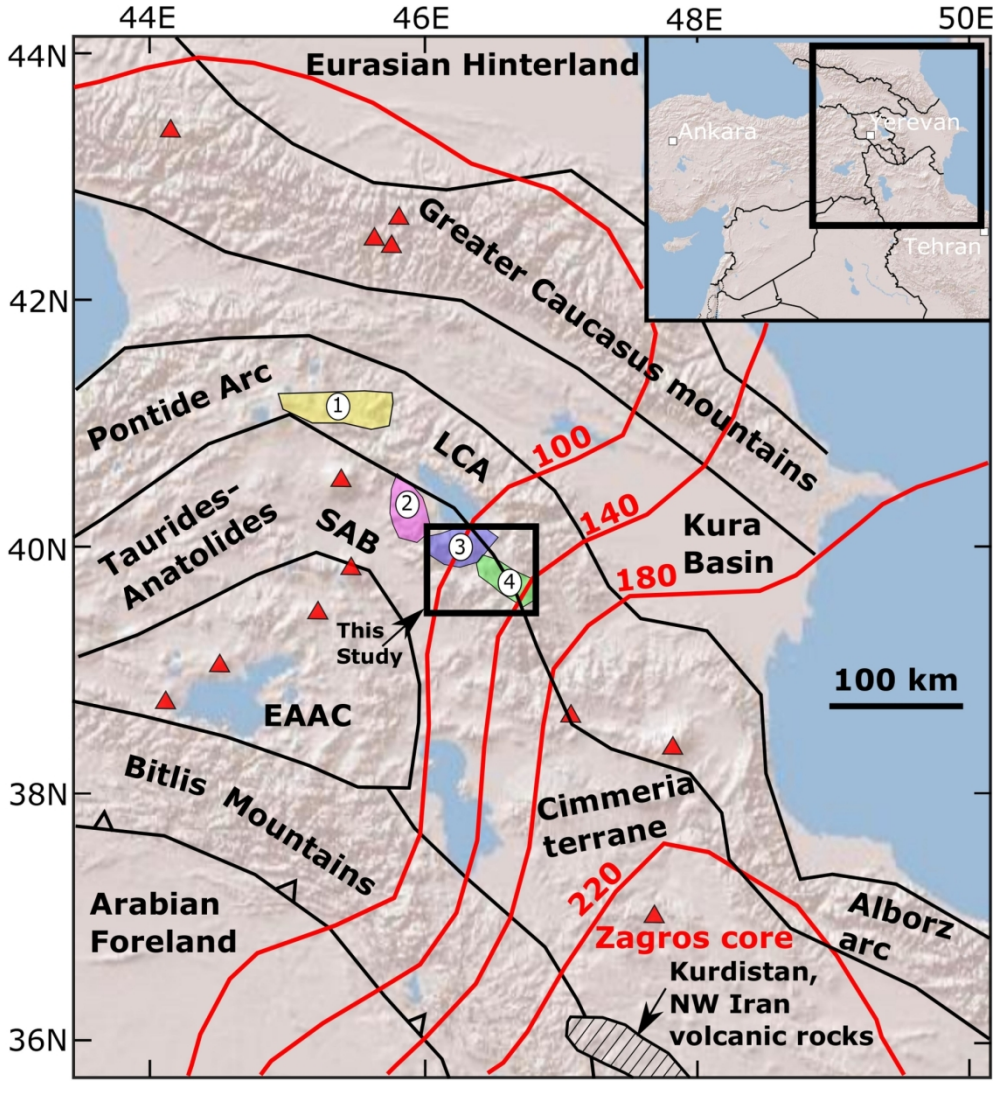


Figure 1

164x177mm (300 x 300 DPI)

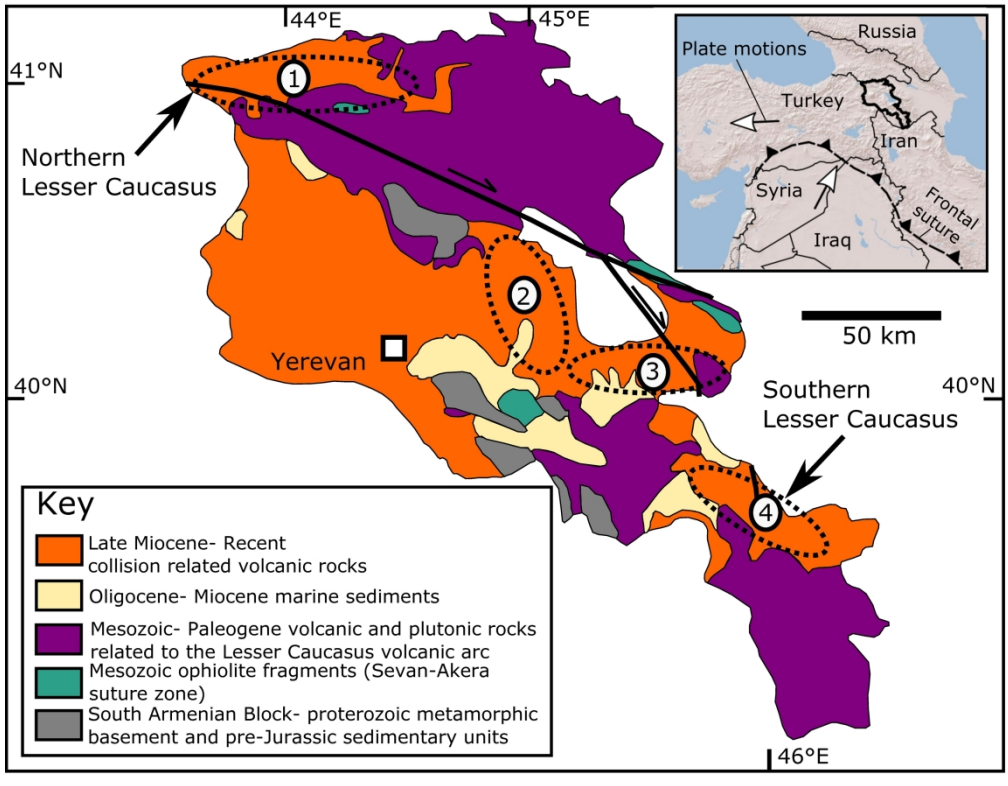


Figure 2

269x209mm (300 x 300 DPI)

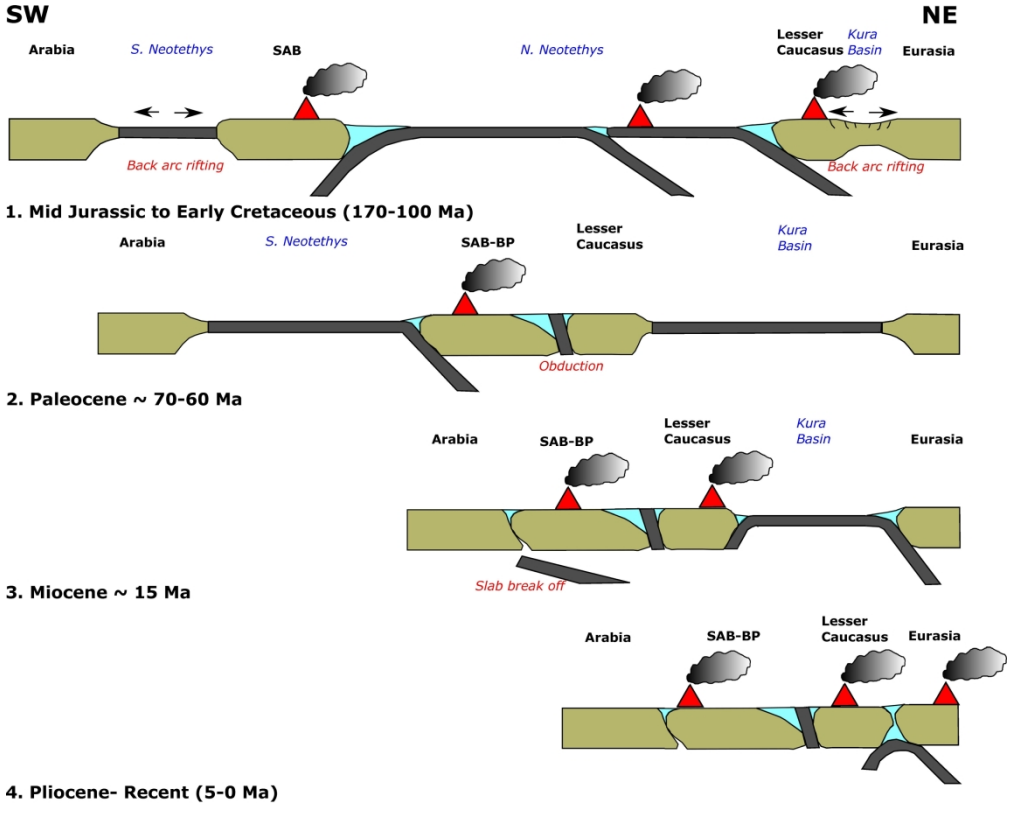


Figure 3

260x207mm (300 x 300 DPI)

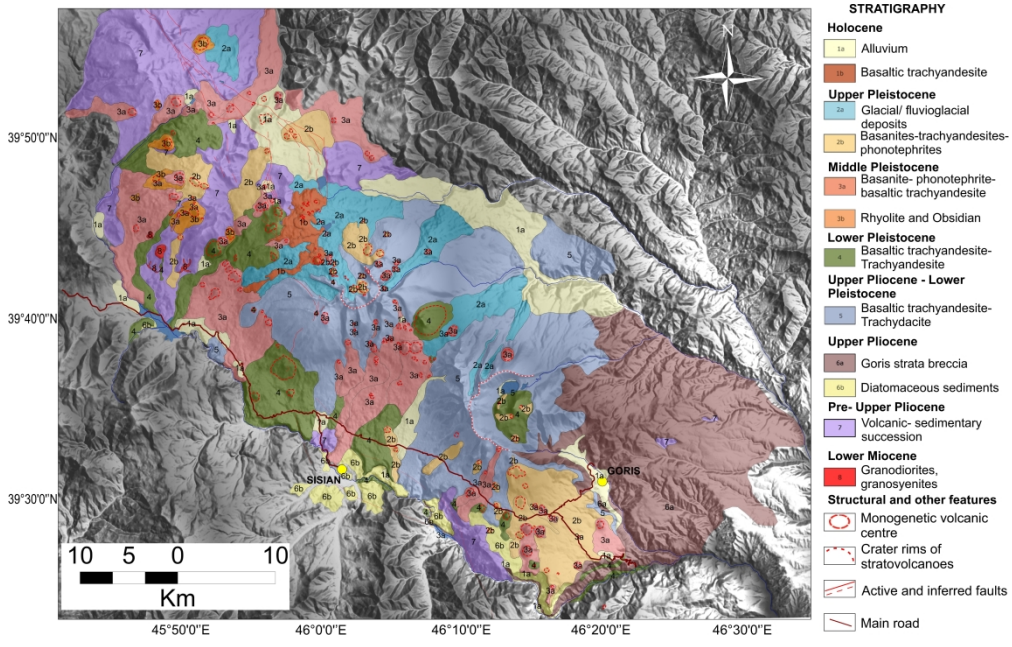


Figure 4

555x349mm (300 x 300 DPI)

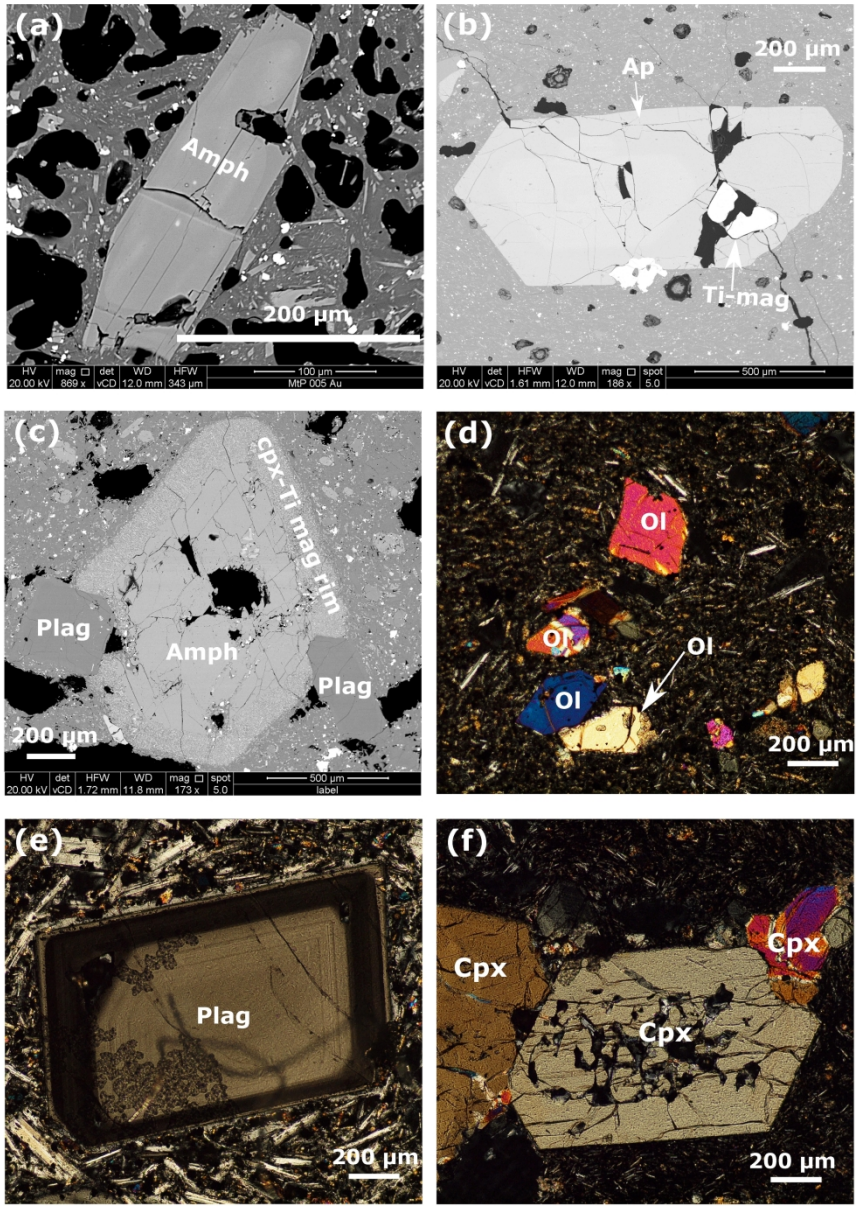


Figure 5

262x369mm (300 x 300 DPI)

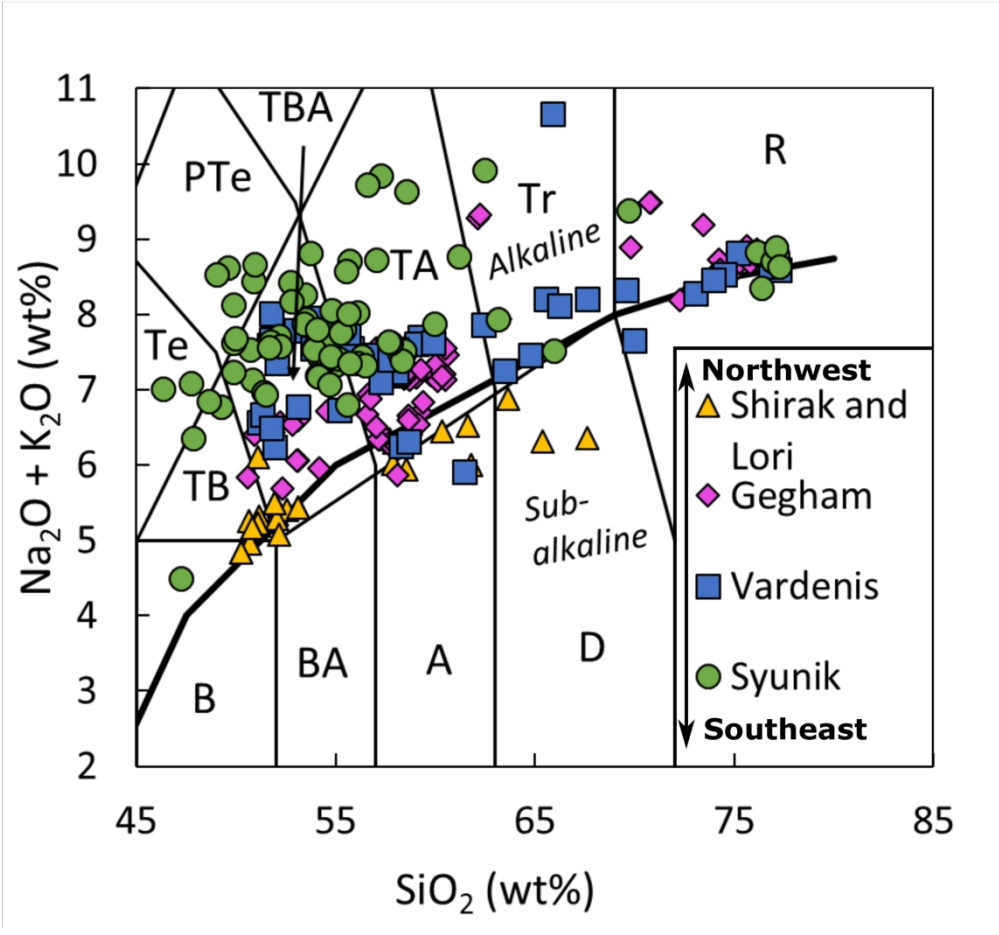


Figure 6

192x178mm (300 x 300 DPI)

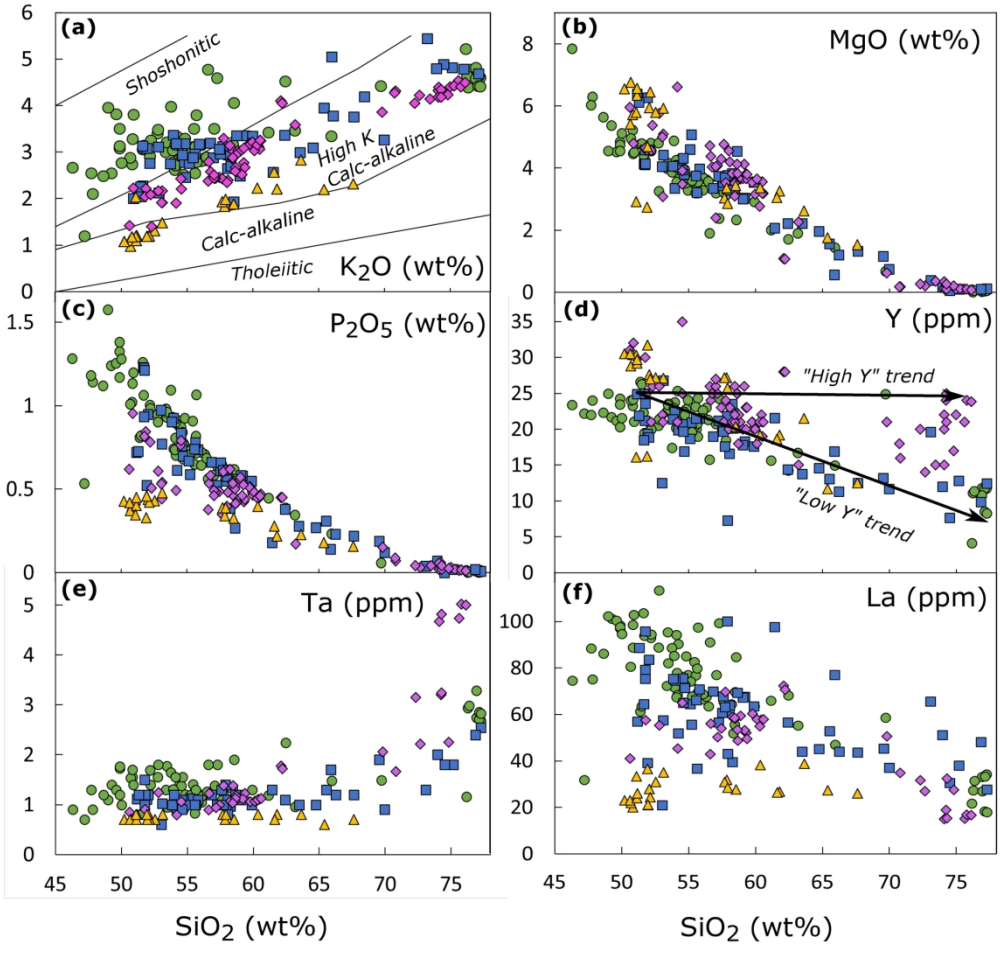


Figure 7

197x185mm (300 x 300 DPI)

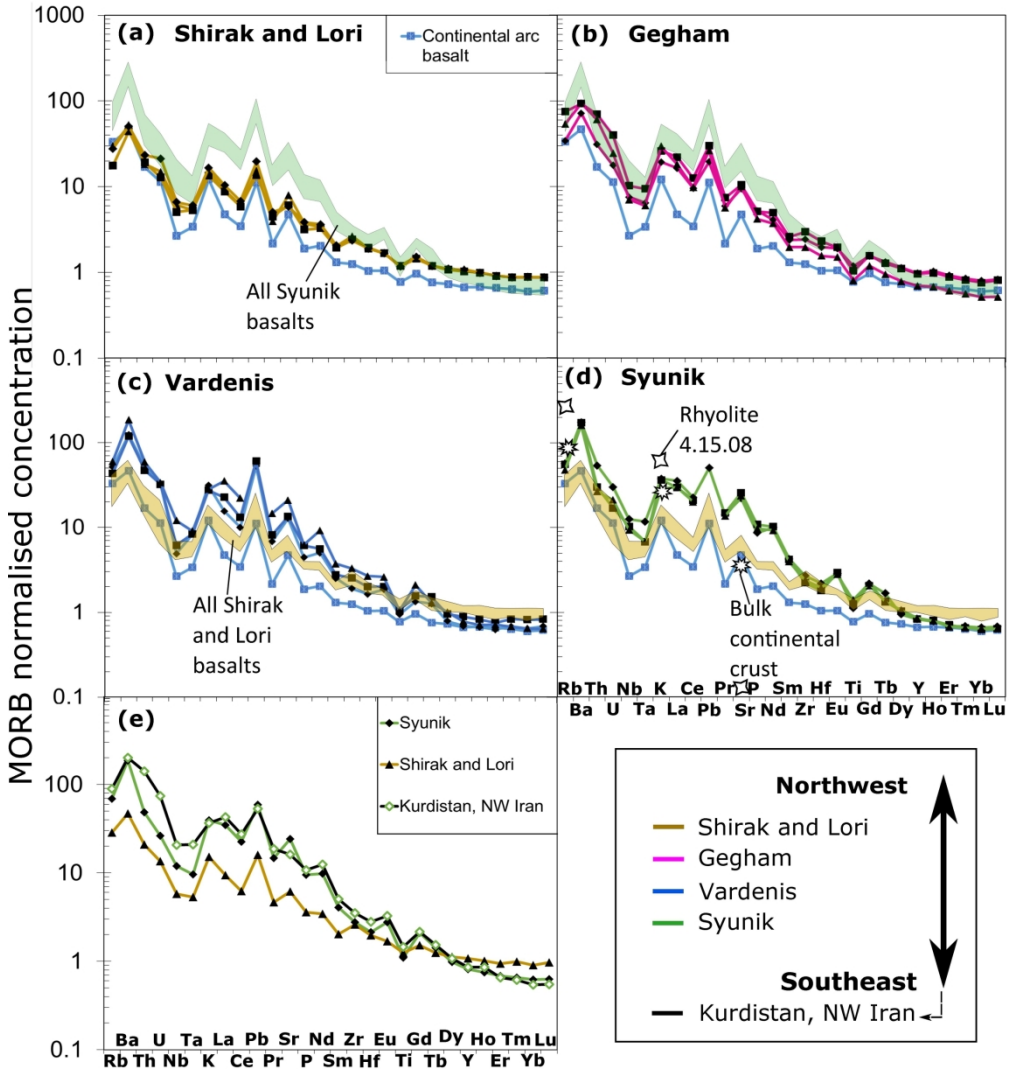


Figure 8

218x233mm (300 x 300 DPI)

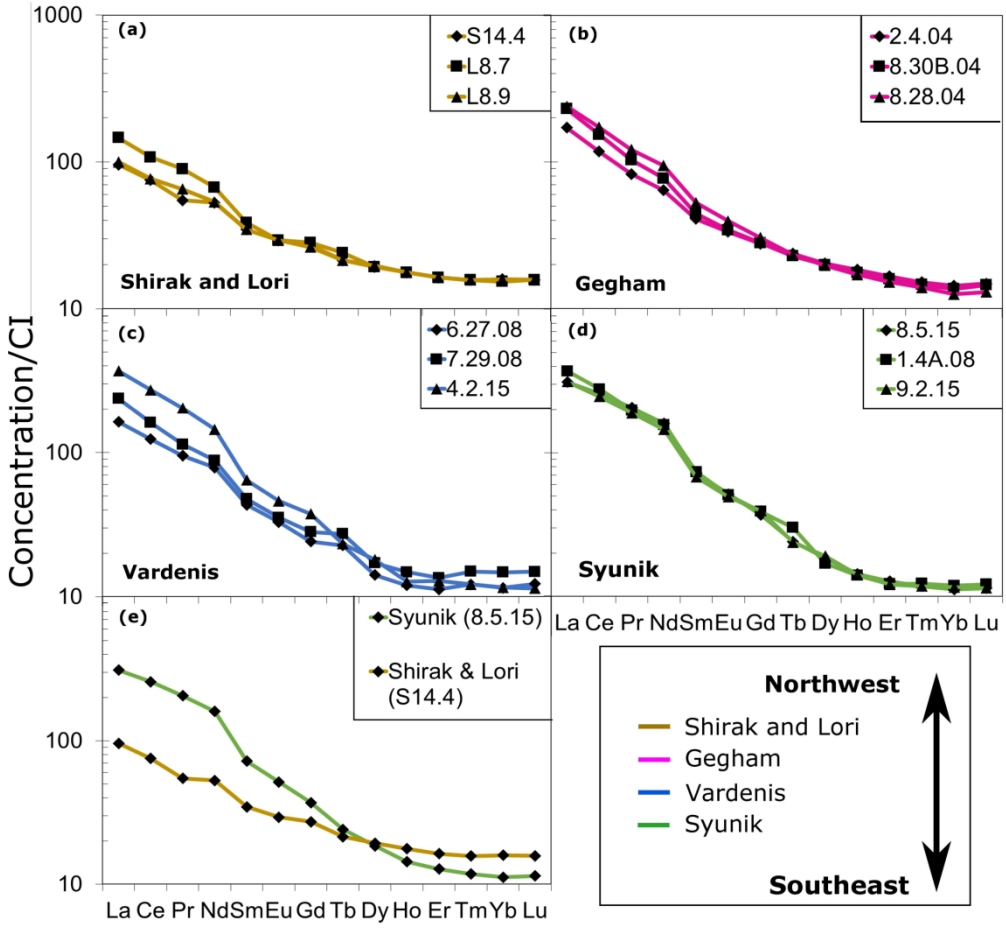


Figure 9

184x170mm (300 x 300 DPI)

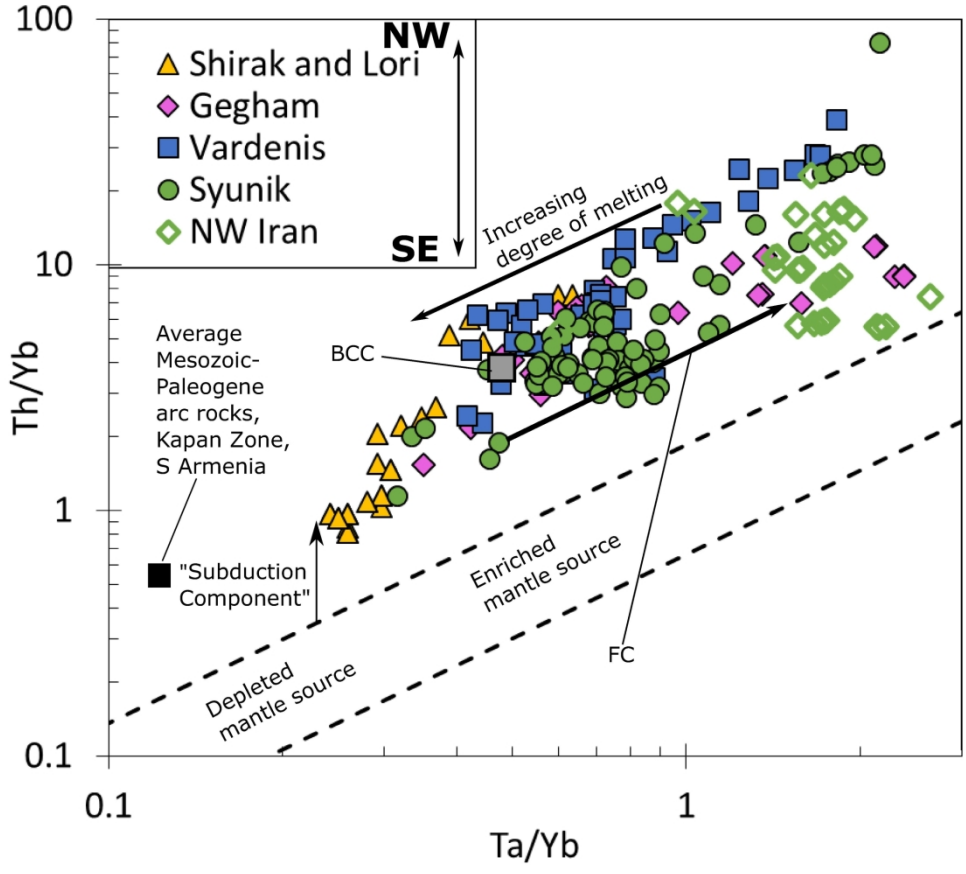


Figure 10

199x178mm (300 x 300 DPI)

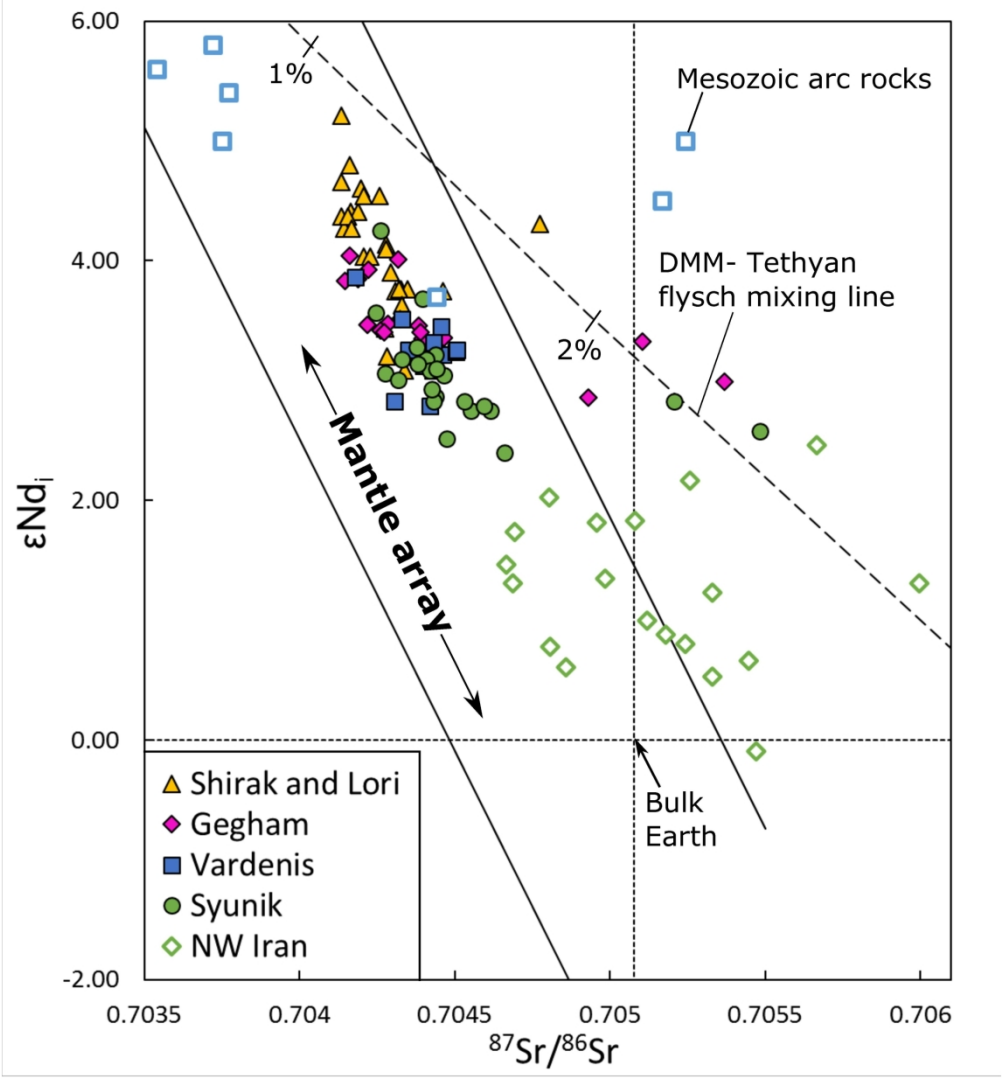


Figure 11

182x196mm (300 x 300 DPI)

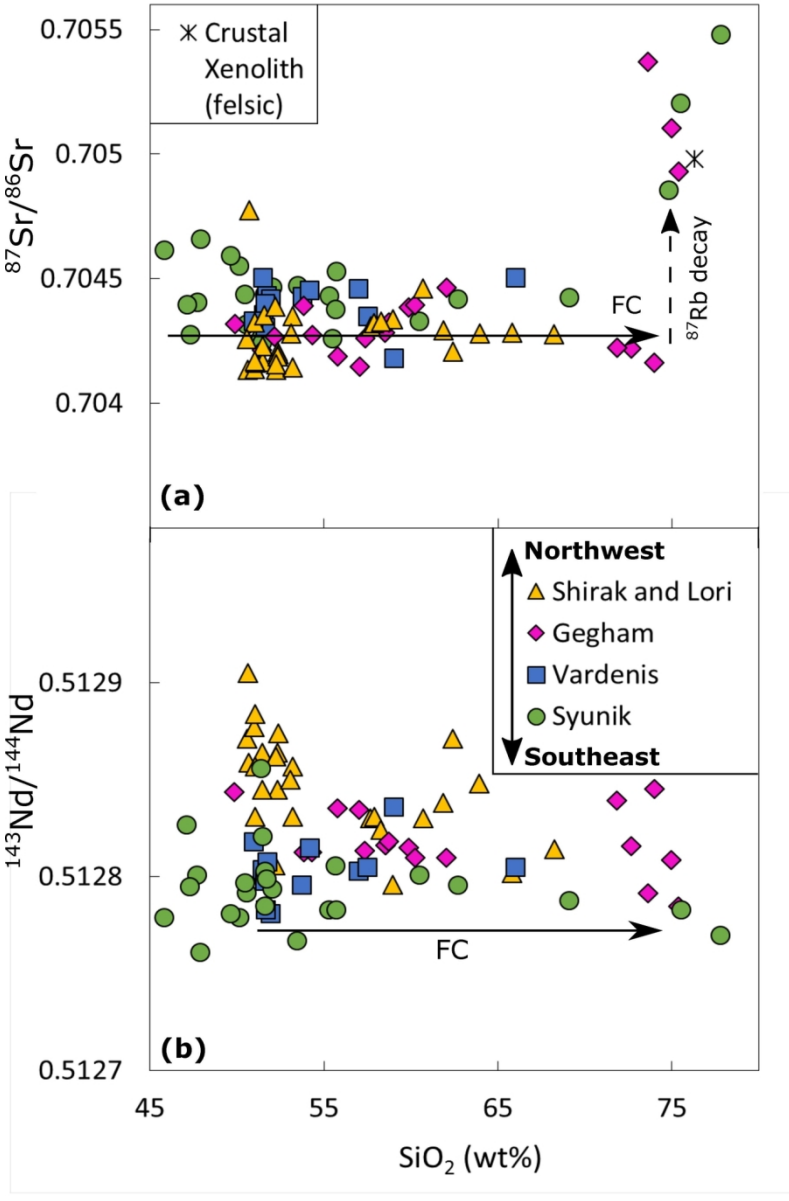


Figure 12

116x176mm (300 x 300 DPI)

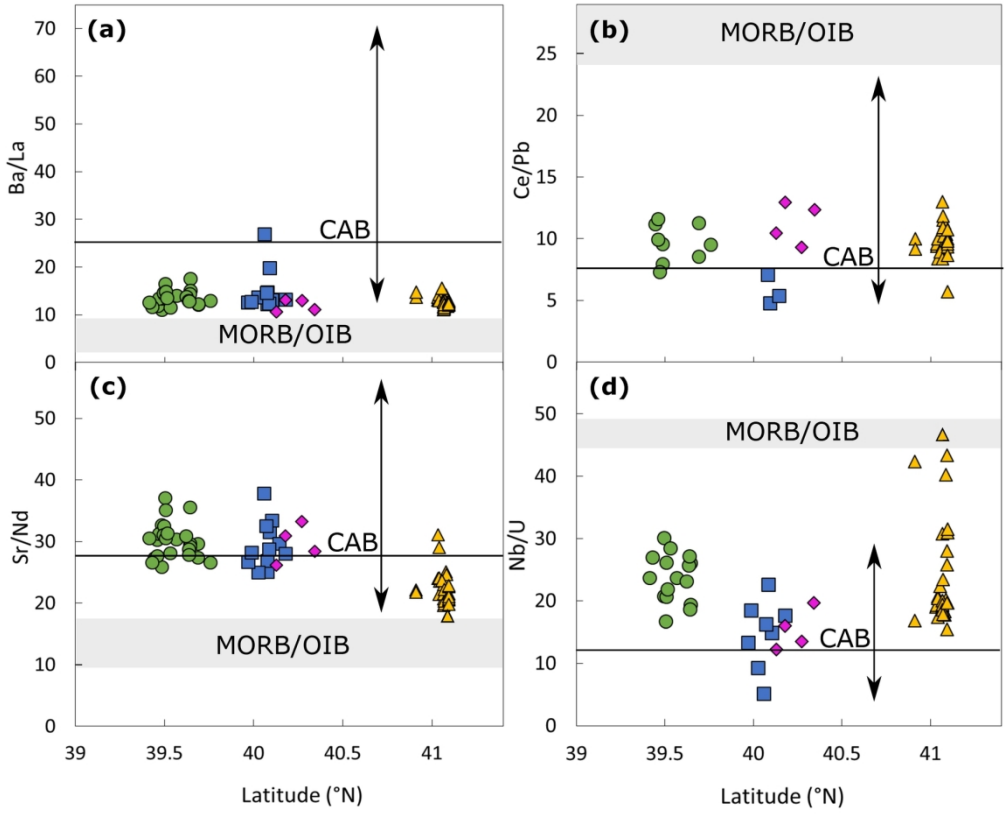


Figure 13

160x130mm (300 x 300 DPI)

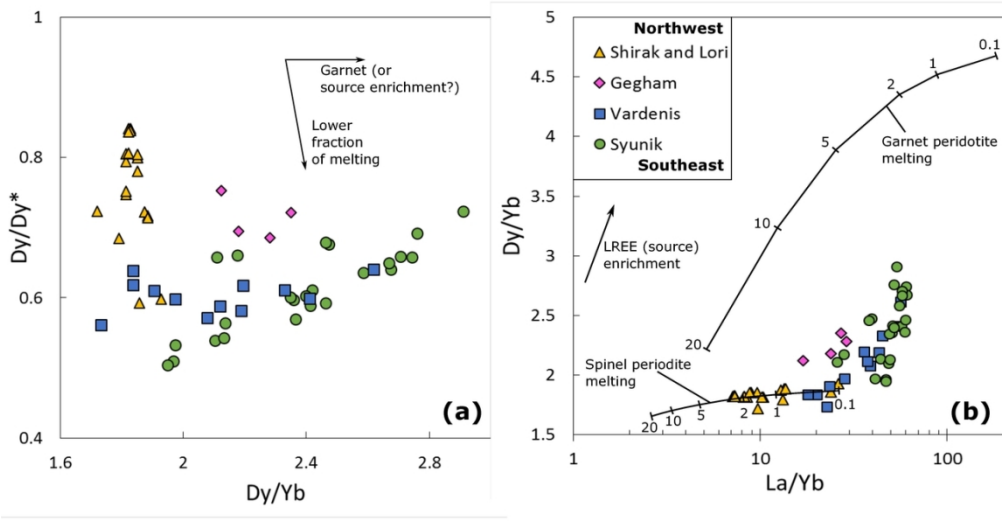


Figure 14

110x58mm (300 x 300 DPI)

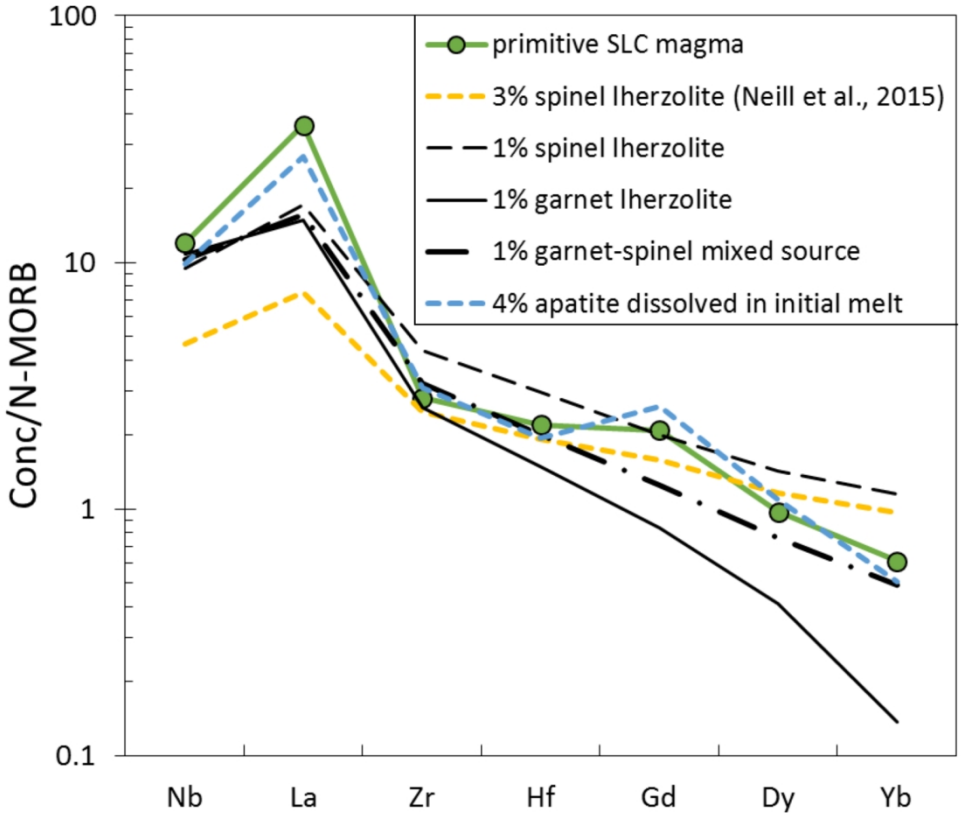


Figure 15

153x138mm (300 x 300 DPI)

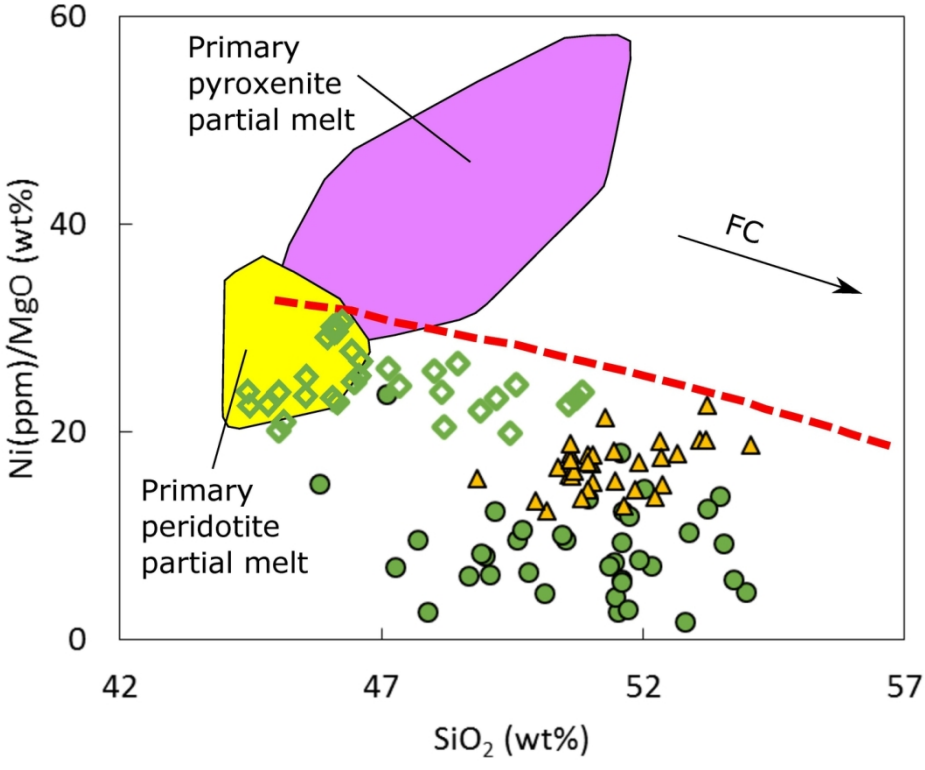


Figure 16

135x107mm (300 x 300 DPI)

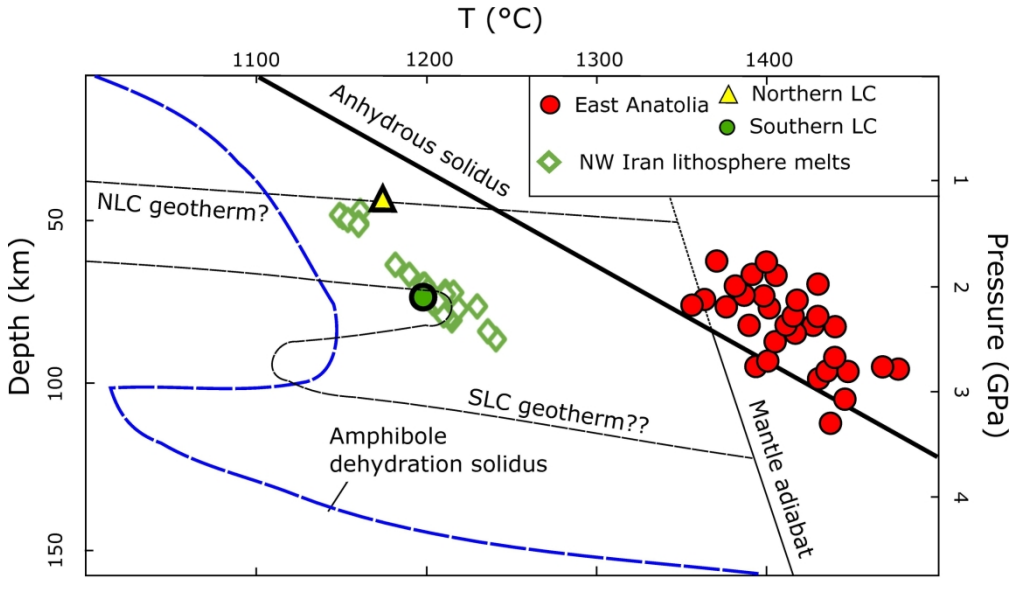


Figure 17

205x117mm (300 x 300 DPI)

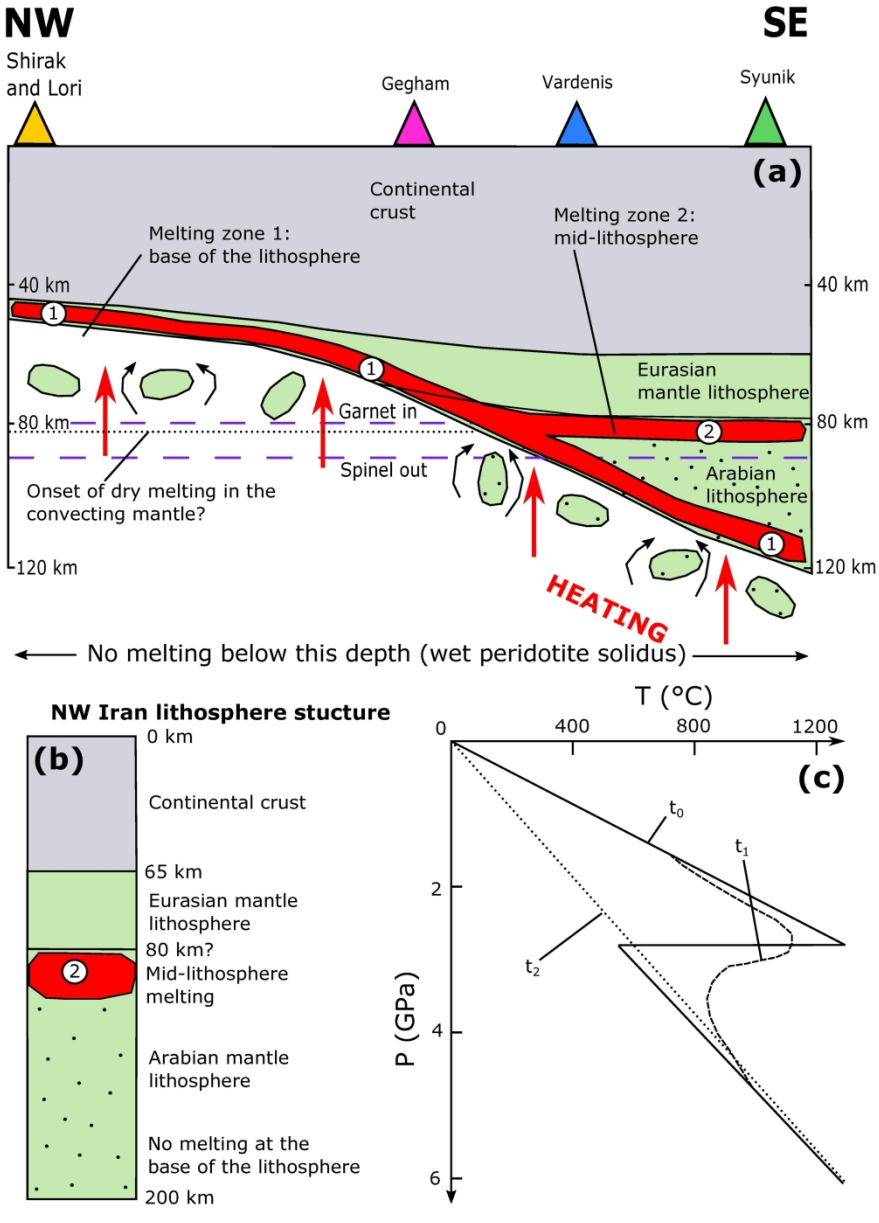


Figure 18

229x316mm (300 x 300 DPI)

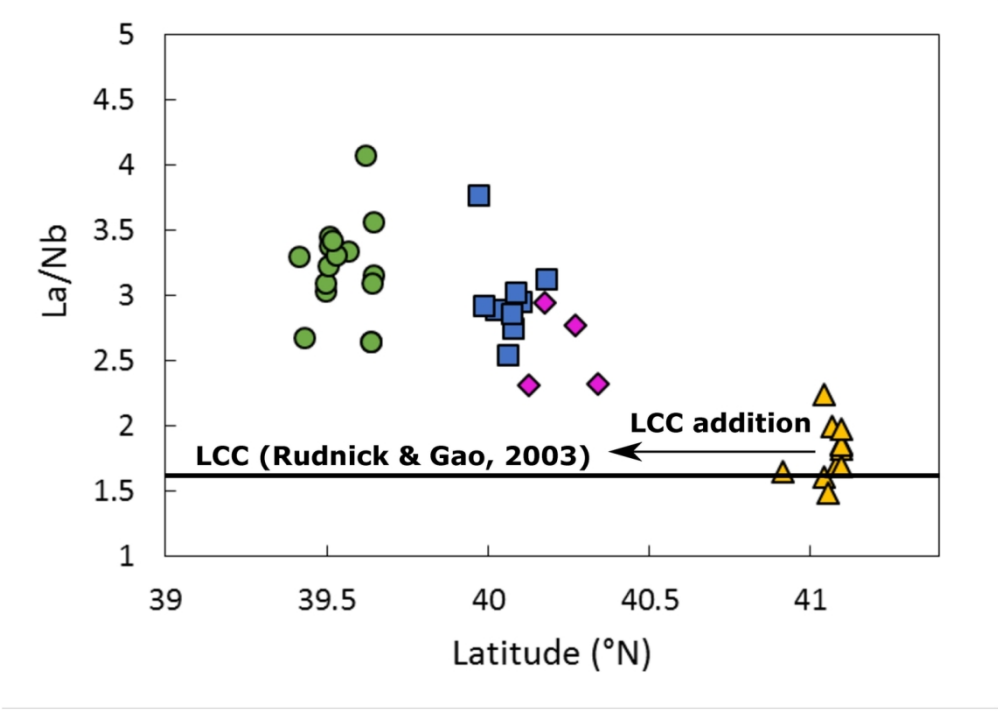


Figure 19

135x96mm (300 x 300 DPI)

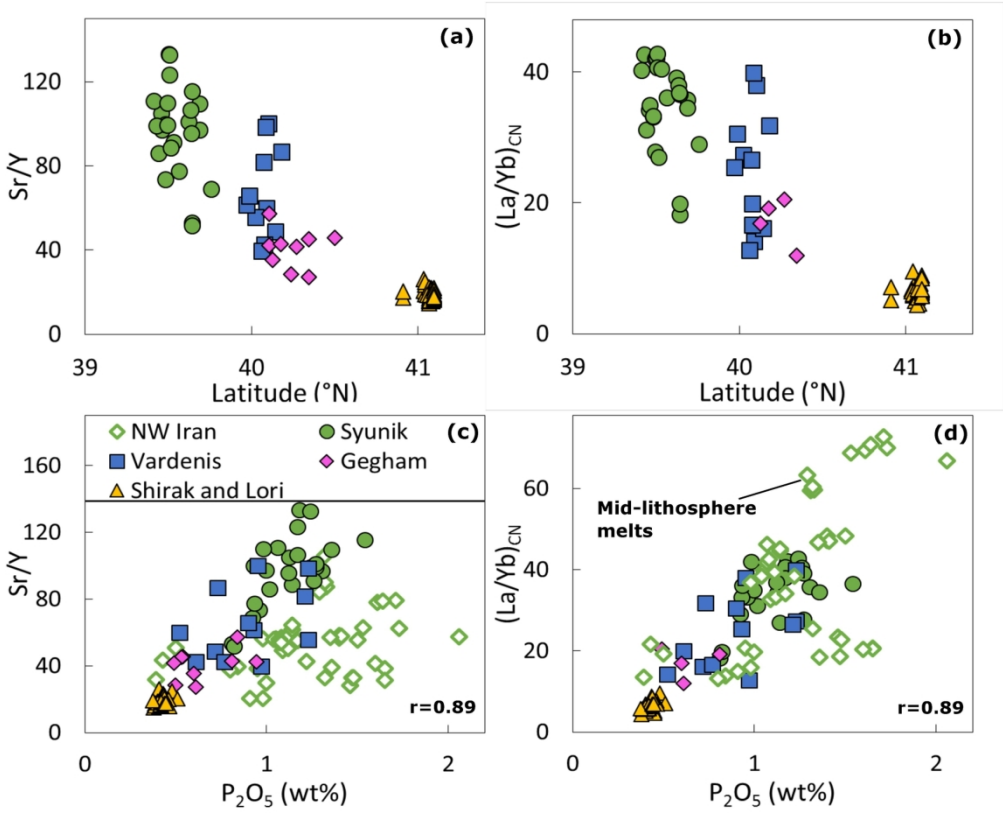


Figure 20

157x128mm (300 x 300 DPI)

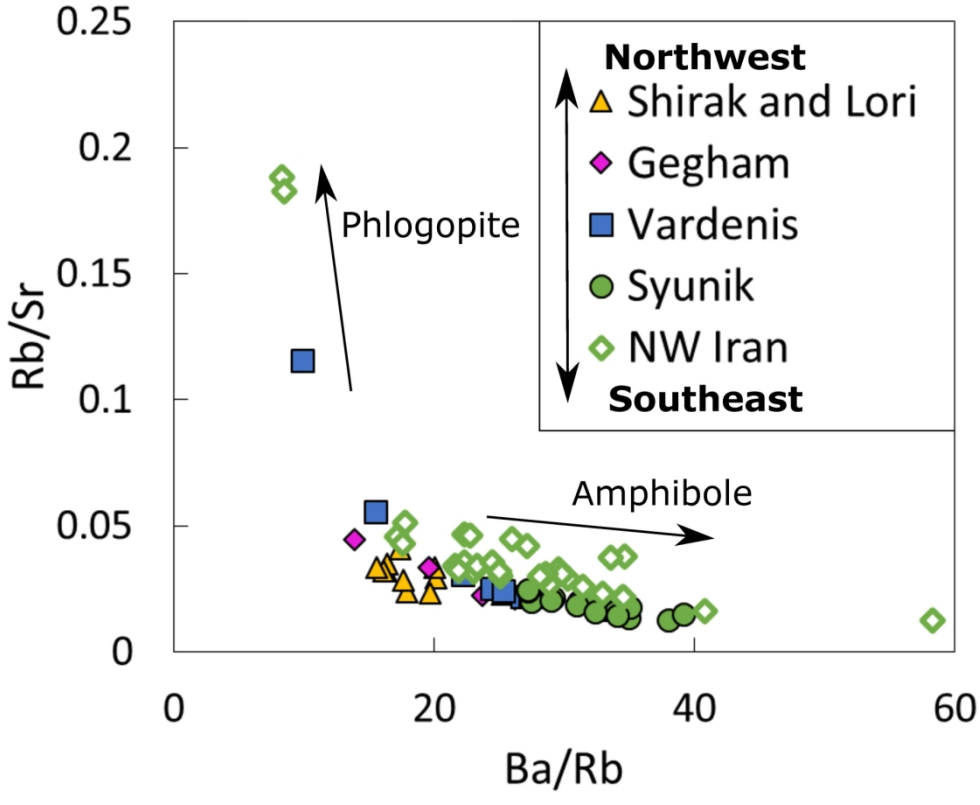


Figure 21

167x136mm (300 x 300 DPI)

**Table 1: Major and Trace Element compositions of mafic volcanic rocks from the Vardenis and**

| Volcanic field | Vardenis | Vardenis | Vardenis | Vardenis | Vardenis | Vardenis | Vardenis | Vardenis | Vardenis |
|---|---|---|---|---|---|---|---|---|---|
| Sample | 6.27.08 | 7.29.08 | 7.30.08 | 7.32.08 | 2.1.12 | 1.1.13 | 1.2.13 | 3.2.13 | 3.3.13 |
| Erup. type | Lava | Lava | Bomb | Lava | Lava | Lava | Lava | Lava | Lava |
| Latitude | 40.0905 | 40.14205 | 40.0768 | 40.07712 | 40.10283 | 40.02458 | 40.08497 | 40.05927 | 40.07163 |
| Longitude | 45.414 | 45.6192 | 45.51587 | 45.5256 | 45.39072 | 45.83628 | 45.83638 | 45.79923 | 45.78805 |
| Elevation (m) | 2257 | 2101 | 2340 | 2280 | 2188 | 2347 | 2375 | 2538 | 2539 |
| Lab analysis[1] | RH | RH | ACME | RH | ACME | ACME | ACME | ACME | ACME |
| $SiO_2$ | 51.62 | 50.94 | 53.96 | 52.87 | 52.17 | 51.71 | 51.93 | 52.81 | 51.60 |
| $TiO_2$ | 1.20 | 1.34 | 1.01 | 1.23 | 1.11 | 1.39 | 1.38 | 1.29 | 1.37 |
| $Al_2O_3$ | 16.31 | 16.37 | 16.47 | 16.93 | 17.40 | 17.31 | 17.39 | 16.42 | 17.23 |
| $Fe_2O_3$ (tot)[2] | 9.61 | 9.69 | 6.82 | 9.49 | 7.77 | 8.34 | 8.39 | 7.87 | 8.25 |
| MnO | 0.13 | 0.14 | 0.12 | 0.14 | 0.13 | 0.13 | 0.13 | 0.14 | 0.13 |
| MgO | 6.23 | 6.36 | 4.08 | 4.40 | 4.60 | 4.15 | 4.12 | 4.03 | 4.12 |
| CaO | 8.54 | 8.43 | 7.97 | 7.93 | 8.27 | 7.34 | 7.32 | 7.49 | 7.34 |
| $Na_2O$ | 3.93 | 4.54 | 4.36 | 4.61 | 4.62 | 4.52 | 4.61 | 4.65 | 4.85 |
| $K_2O$ | 2.27 | 2.00 | 3.37 | 2.13 | 2.76 | 3.08 | 3.08 | 3.11 | 3.13 |
| $P_2O_5$ | 0.52 | 0.72 | 0.61 | 0.77 | 0.95 | 1.23 | 1.23 | 0.97 | 1.21 |
| Total | 98.45 | 99.56 | 99.49 | 99.56 | 100.25 | 100.09 | 100.34 | 99.62 | 99.66 |
| LOI | | | 0.59 | | 0.35 | 0.75 | 0.61 | 0.7 | 0.27 |
| #Mg | 56.2 | 56.5 | 54.2 | 47.9 | 54.0 | 49.6 | 49.3 | 50.4 | 49.7 |
| Ni | 77.6 | 86.8 | 18.8 | 45.9 | 32.8 | 12 | 32 | 7.1 | 23.1 |
| La | 39 | 57 | 52 | 58 | 84 | 64 | 96 | 21 | 79 |
| Ce | 76 | 99 | 91 | 102 | 148 | 112 | 180 | 35 | 151 |
| Pr | 9.0 | 10.8 | 9.9 | 11.0 | 16.3 | 12.1 | 20.6 | 3.7 | 16.8 |
| Nd | 37 | 41 | 34 | 42 | 57 | 41 | 73 | 13 | 59 |
| Sm | 6.6 | 7.3 | 5.5 | 7.6 | 8.0 | 6.4 | 10.0 | 2.5 | 8.9 |
| Eu | 1.9 | 2.1 | 1.5 | 2.1 | 2.2 | 1.7 | 2.6 | 0.8 | 2.4 |
| Gd | 5.0 | 5.8 | 4.5 | 5.9 | 6.1 | 5.0 | 7.4 | 2.5 | 6.7 |
| Tb | 0.8 | 1.0 | 0.6 | 1.0 | 0.7 | 0.7 | 0.8 | 0.4 | 0.8 |
| Dy | 3.6 | 4.3 | 3.7 | 4.7 | 3.8 | 3.5 | 4.5 | 2.1 | 4.5 |
| Ho | 0.7 | 0.8 | 0.7 | 0.9 | 0.7 | 0.6 | 0.7 | 0.4 | 0.8 |
| Er | 1.9 | 2.2 | 2.0 | 2.3 | 1.7 | 1.8 | 1.9 | 1.3 | 2.3 |
| Tm | 0.3 | 0.4 | 0.3 | 0.4 | 0.3 | 0.3 | 0.3 | 0.2 | 0.3 |
| Yb | 2.0 | 2.5 | 1.9 | 2.4 | 1.6 | 1.7 | 1.7 | 1.2 | 2.1 |
| Lu | 0.3 | 0.4 | 0.3 | 0.4 | 0.3 | 0.3 | 0.3 | 0.2 | 0.3 |
| Ba | 778 | 754 | 768 | 707 | 1098 | 881 | 1184 | 563 | 1162 |
| Hf | 3.4 | 4.1 | 4.4 | 4.1 | 4.3 | 4.5 | 4.6 | 2.8 | 4.4 |
| Nb | | | 18.9 | | 28.3 | 22.2 | 31.6 | 8.2 | 27.6 |
| Rb | | | 67.7 | | 41.1 | 56.9 | 35.4 | 57.3 | 42.5 |
| Sr | 1161 | 1217 | 845 | 1142 | 1890 | 1026 | 2084 | 495 | 1932 |
| Pb | 15.9 | 18.23 | | 14.43 | | | | | |
| Ta | 1.1 | 1.1 | 0.9 | 1.0 | 1.2 | 1.2 | 1.5 | 0.6 | 1.2 |
| Th | 6.3 | 5.7 | 11.8 | 5.9 | 9.4 | 9.4 | 5.9 | 6.6 | 6.9 |
| U | 1.5 | 1.5 | 3.3 | 1.2 | 1.9 | 2.4 | 1.4 | 1.6 | 1.7 |
| Zr | 141 | 188 | 187 | 187 | 195 | 209 | 213 | 114 | 210 |
| Y | 19.4 | 24.9 | 19.9 | 26.8 | 18.9 | 18.5 | 21.2 | 12.5 | 23.6 |

**Syunik volcanic fields in the Southern Lesser Caucasus.**

**[1]Laboratory where samples were analysed: ACME- ACME labs, Bureau Veritas minerals, Vancouver, Canada; RH- Royal Holloway University, UK.**

**[2] Royal Holloway major element data report Fe as FeO*, which was recalculated to $Fe_2O_3$ (tot) by dividing by a factor of 0.89981. Totals are the original totals prior to $Fe_2O_3$ (tot) recalculation.**

| Volcanic Field | Vardenis | Vardenis | Vardenis | Syunik | Syunik | Syunik | Syunik | Syunik | Syunik |
|---|---|---|---|---|---|---|---|---|---|
| Sample | 4.02.15 | 5.06.15 | 6.03.15 | 1.4A.08 | 2.6.08 | 2.7.08 | 2.8.08 | 2.9.08 | 2.10.08 |
| Eruptive type | Lava | Lava | Lava | Scoria | Bomb | Bomb | Lava | Bomb | Lava |
| Latitude | 40.17904 | 39.96908 | 39.98746 | 39.44133 | 39.48285 | 39.4587 | 39.4601 | 39.48452 | 39.46787 |
| Longitude | 45.6186 | 45.68293 | 45.61326 | 46.08888 | 46.2693 | 46.24037 | 46.26768 | 46.2177 | 46.25762 |
| Elevation (m) | 1956 | 2872 | 3454 | 1876 | 1969 | 1849 | 1958 | 2107 | 1956 |
| Lab analysis[1] | ACME | ACME | ACME | RH | RH | RH | RH | RH | RH |
| $SiO_2$ | 51.51 | 51.47 | 53.73 | 50.52 | 53.23 | 50.44 | 51.74 | 51.58 | 47.08 |
| $TiO_2$ | 1.33 | 1.52 | 1.08 | 1.43 | 1.12 | 1.32 | 1.14 | 1.07 | 1.31 |
| $Al_2O_3$ | 16.77 | 16.47 | 17.09 | 16.31 | 17.11 | 16.82 | 16.26 | 16.49 | 14.39 |
| $Fe_2O_3$ tot[2] | 8.57 | 8.60 | 7.60 | 9.97 | 8.65 | 9.31 | 8.75 | 8.46 | 11.45 |
| MnO | 0.14 | 0.14 | 0.13 | 0.14 | 0.13 | 0.14 | 0.13 | 0.13 | 0.15 |
| MgO | 6.15 | 4.56 | 4.06 | 5.20 | 4.15 | 4.44 | 4.77 | 4.71 | 11.65 |
| CaO | 8.33 | 8.59 | 7.24 | 8.74 | 6.87 | 8.16 | 8.61 | 7.03 | 9.83 |
| $Na_2O$ | 4.66 | 4.20 | 4.79 | 4.36 | 5.03 | 5.12 | 4.76 | 4.90 | 3.29 |
| $K_2O$ | 2.04 | 2.26 | 2.75 | 2.73 | 3.20 | 3.25 | 2.89 | 3.33 | 1.19 |
| $P_2O_5$ | 0.73 | 0.93 | 0.90 | 1.02 | 0.96 | 1.12 | 1.00 | 0.93 | 0.53 |
| Total | 100.41 | 99.46 | 99.78 | 99.40 | 99.59 | 99.20 | 99.17 | 97.78 | 99.74 |
| LOI | 0.06 | 0.62 | 0.27 | | | | | | |
| #Mg | 58.7 | 51.2 | 51.4 | 50.8 | 48.8 | 48.6 | 51.9 | 52.5 | 66.8 |
| Ni | 16.3 | 18.8 | 23.7 | 49.9 | 52.4 | 45.0 | 56.7 | 85.1 | 275.5 |
| La | 89 | 75 | 75 | 89 | 95 | 99 | 93 | 89 | 32 |
| Ce | 167 | 138 | 132 | 170 | 172 | 193 | 175 | 159 | 66 |
| Pr | 19.4 | 15.7 | 14.5 | 18.8 | 18.0 | 21.4 | 18.7 | 16.8 | 8.3 |
| Nd | 68 | 58 | 50 | 73 | 67 | 84 | 72 | 63 | 34 |
| Sm | 9.9 | 8.6 | 8.0 | 11.3 | 10.3 | 12.7 | 11.1 | 9.5 | 6.5 |
| Eu | 2.7 | 2.4 | 2.0 | 2.9 | 2.7 | 3.3 | 2.9 | 2.6 | 1.8 |
| Gd | 7.7 | 7.1 | 5.8 | 8.0 | 7.5 | 8.7 | 7.7 | 7.0 | 4.9 |
| Tb | 0.9 | 0.8 | 0.7 | 1.1 | 1.0 | 1.2 | 1.1 | 1.0 | 0.9 |
| Dy | 4.6 | 4.6 | 3.8 | 4.3 | 4.0 | 4.3 | 4.0 | 3.7 | 4.0 |
| Ho | 0.7 | 0.9 | 0.7 | 0.8 | 0.7 | 0.8 | 0.7 | 0.7 | 0.8 |
| Er | 2.1 | 2.4 | 2.0 | 2.0 | 2.0 | 2.0 | 1.9 | 1.8 | 2.1 |
| Tm | 0.3 | 0.3 | 0.3 | 0.3 | 0.3 | 0.3 | 0.3 | 0.3 | 0.4 |
| Yb | 2.0 | 2.1 | 1.8 | 2.0 | 2.0 | 2.0 | 1.9 | 1.9 | 2.2 |
| Lu | 0.3 | 0.3 | 0.3 | 0.3 | 0.3 | 0.3 | 0.3 | 0.3 | 0.4 |
| Ba | 1171 | 947 | 962 | 1109 | 1057 | 1220 | 1107 | 1192 | 430 |
| Hf | 5.5 | 4.5 | 4.3 | 4.5 | 5.1 | 4.9 | 5.4 | 4.7 | 3.0 |
| Nb | 28.3 | 20.0 | 25.8 | | | | | | |
| Rb | 47.9 | 37.4 | 43.4 | | | | | | |
| Sr | 1899 | 1537 | 1411 | 2003 | 1722 | 2531 | 1998 | 2050 | 1073 |
| Pb | | | | 15.2 | 18.0 | 16.7 | 17.5 | 19.9 | 9.0 |
| Ta | 1.2 | 1.0 | 1.0 | 1.6 | 1.8 | 1.7 | 1.7 | 1.6 | 0.7 |
| Th | 7.1 | 6.9 | 7.1 | 6.5 | 8.2 | 6.8 | 8.4 | 7.8 | 2.6 |
| U | 1.6 | 1.5 | 1.4 | 1.4 | 1.7 | 1.5 | 1.5 | 1.7 | 0.7 |
| Zr | 245 | 202 | 215 | 199 | 234 | 224 | 246 | 220 | 126 |
| Y | 21.9 | 25.0 | 21.4 | 23.3 | 23.4 | 24.1 | 20.6 | 20.5 | 22.2 |

**Table 1 continued.**

**Table 1 continued.**

| Volcanic Field | Syunik | Syunik | Syunik | Syunik | Syunik | Syunik | Syunik | Syunik | Syunik |
|---|---|---|---|---|---|---|---|---|---|
| Sample | 5.21.08 | 6.24.08 | 6.25.08 | 4.16.10 | 8.02.15 | 8.03.15 | 8.04.15 | 8.05.15 | 8.06.15 |
| Eruptive type | Lava | Scoria | Bomb | Lava | Bomb | Bomb | Lava | Bomb | Lava |
| Latitude | 39.75548 | 39.68745 | 39.68745 | 39.56577 | 39.42896 | 39.4141 | 39.49615 | 39.49431 | 39.50412 |
| Longitude | 45.85745 | 45.91403 | 45.91403 | 46.21687 | 46.27307 | 46.28308 | 46.24583 | 46.24621 | 46.20926 |
| Elevation (m) | 2871 | 2514 | 2514 | 2731 | 1896 | 1603 | 2168 | 2185 | 2237 |
| Lab analysis[1] | RH | RH | RH | RH | ACME | ACME | ACME | ACME | ACME |
| $SiO_2$ | 53.46 | 48.97 | 48.91 | 53.53 | 49.16 | 51.58 | 52.01 | 45.80 | 50.11 |
| $TiO_2$ | 1.05 | 1.56 | 1.60 | 1.13 | 1.43 | 1.21 | 1.12 | 1.58 | 1.14 |
| $Al_2O_3$ | 16.41 | 16.28 | 16.37 | 17.08 | 16.91 | 16.65 | 16.68 | 14.92 | 15.92 |
| $Fe_2O_3$ tot[2] | 8.62 | 10.06 | 10.14 | 8.48 | 9.03 | 7.66 | 7.26 | 9.56 | 7.28 |
| MnO | 0.13 | 0.14 | 0.14 | 0.12 | 0.14 | 0.13 | 0.13 | 0.16 | 0.13 |
| MgO | 4.84 | 4.77 | 4.66 | 4.02 | 5.37 | 4.29 | 4.54 | 7.77 | 4.44 |
| CaO | 7.12 | 8.63 | 8.81 | 7.71 | 8.66 | 8.01 | 7.23 | 10.02 | 8.60 |
| $Na_2O$ | 4.45 | 4.47 | 4.02 | 4.75 | 4.23 | 4.48 | 4.31 | 4.30 | 4.78 |
| $K_2O$ | 3.02 | 3.03 | 3.07 | 3.20 | 2.54 | 3.14 | 3.24 | 2.64 | 3.75 |
| $P_2O_5$ | 0.92 | 1.30 | 1.36 | 0.93 | 1.24 | 1.06 | 0.98 | 1.27 | 1.18 |
| Total | 99.15 | 98.19 | 98.05 | 100.10 | 99.83 | 99.76 | 99.60 | 98.90 | 98.42 |
| LOI | | | | | 0.98 | 1.41 | 1.92 | 0.73 | 0.88 |
| #Mg | 52.7 | 48.4 | 47.6 | 48.4 | 54.1 | 52.6 | 55.3 | 61.7 | 54.7 |
| Ni | 66.9 | 38.3 | 38.6 | 37.5 | 66.3 | 25 | 66.3 | 117.1 | 19.9 |
| La | 85 | 97 | 98 | 82 | 101 | 94 | 94 | 75 | 103 |
| Ce | 150 | 194 | 198 | 152 | 197 | 175 | 177 | 158 | 190 |
| Pr | 15.9 | 21.8 | 22.1 | 16.0 | 23.1 | 20.0 | 19.6 | 19.6 | 21.3 |
| Nd | 60 | 86 | 87 | 60 | 81 | 71 | 68 | 75 | 76 |
| Sm | 9.4 | 13.2 | 13.5 | 9.0 | 11.7 | 9.7 | 9.5 | 11.0 | 10.4 |
| Eu | 2.4 | 3.3 | 3.4 | 2.4 | 3.1 | 2.6 | 2.5 | 3.0 | 2.8 |
| Gd | 7.0 | 8.9 | 9.3 | 6.5 | 8.0 | 6.8 | 6.6 | 7.6 | 7.4 |
| Tb | 1.1 | 1.2 | 1.3 | 0.8 | 0.9 | 0.8 | 0.7 | 0.9 | 0.9 |
| Dy | 4.1 | 4.5 | 4.7 | 3.9 | 4.6 | 4.0 | 3.8 | 4.7 | 4.3 |
| Ho | 0.8 | 0.8 | 0.8 | 0.8 | 0.7 | 0.7 | 0.7 | 0.8 | 0.7 |
| Er | 2.0 | 2.1 | 2.1 | 2.1 | 1.9 | 1.7 | 1.8 | 2.1 | 1.9 |
| Tm | 0.3 | 0.3 | 0.3 | 0.3 | 0.3 | 0.3 | 0.3 | 0.3 | 0.3 |
| Yb | 2.1 | 1.9 | 2.0 | 1.6 | 1.7 | 1.7 | 1.6 | 1.9 | 1.7 |
| Lu | 0.4 | 0.3 | 0.3 | 0.2 | 0.3 | 0.2 | 0.3 | 0.3 | 0.3 |
| Ba | 1102 | 1176 | 1211 | 1152 | 1181 | 1180 | 1363 | 1093 | 1705 |
| Hf | 4.3 | 4.7 | 4.6 | 4.3 | 4.5 | 4.5 | 4.6 | 3.7 | 4.7 |
| Nb | | | | 24.5 | 37.8 | 28.4 | 31.1 | 24.1 | 31.8 |
| Rb | | | | 37.0 | 34.9 | 43.0 | 46.7 | 31.3 | 53.3 |
| Sr | 1585 | 2358 | 2576 | 1827 | 2150 | 2161 | 2198 | 2325 | 2812 |
| Pb | 15.7 | 17.2 | 23.2 | | | | | | |
| Ta | 1.3 | 1.7 | 1.8 | 0.9 | 1.4 | 1.2 | 1.4 | 0.9 | 1.4 |
| Th | 8.3 | 6.1 | 6.0 | 5.5 | 6.6 | 6.6 | 7.9 | 3.6 | 7.8 |
| U | 1.4 | 1.4 | 1.3 | 1.0 | 1.4 | 1.2 | 1.5 | 0.8 | 1.9 |
| Zr | 192 | 198 | 198 | 201 | 204 | 217 | 244 | 166 | 236 |
| Y | 23.0 | 24.3 | 23.5 | 23.6 | 21.7 | 19.5 | 20.0 | 23.4 | 21.1 |

| Volcanic Field | Syunik | Syunik | Syunik | Syunik | Syunik | Syunik | Syunik | Syunik | Syunik |
|---|---|---|---|---|---|---|---|---|---|
| Sample | 8.07.15 | 9.01.15 | 9.02.15 | 10.01.15 | 10.02.15 | 10.03.15 | 11.02.15 | 11.3.15 | 11.04.15 |
| Eruptive type | Bomb | Plug | Bomb | Bomb | Lava | Scoria | Lava | Scoria | Lava |
| Latitude | 39.50771 | 39.53042 | 39.51419 | 39.64401 | 39.64359 | 39.6413 | 39.62041 | 39.63605 | 39.63671 |
| Longitude | 46.20948 | 46.22106 | 46.23795 | 46.102 | 46.10184 | 46.10138 | 46.02615 | 46.03841 | 46.04296 |
| Elevation (m) | 2314 | 2738 | 2608 | 2811 | 2693 | 2614 | 2321 | 2536 | 2542 |
| Lab analysis[1] | ACME | ACME | ACME | ACME | ACME | ACME | ACME | ACME | ACME |
| $SiO_2$ | 49.81 | 51.60 | 47.68 | 47.89 | 51.35 | 51.44 | 49.60 | 47.27 | 48.67 |
| $TiO_2$ | 1.37 | 1.22 | 1.78 | 1.26 | 1.48 | 1.46 | 1.25 | 1.80 | 1.73 |
| $Al_2O_3$ | 16.80 | 17.40 | 15.80 | 15.58 | 16.93 | 16.91 | 16.87 | 15.49 | 15.86 |
| $Fe_2O_3$ tot[2] | 8.15 | 8.20 | 10.07 | 8.14 | 8.96 | 8.92 | 8.49 | 10.07 | 9.77 |
| MnO | 0.13 | 0.13 | 0.15 | 0.14 | 0.14 | 0.14 | 0.14 | 0.15 | 0.14 |
| MgO | 4.55 | 4.42 | 6.28 | 4.45 | 4.78 | 4.79 | 5.09 | 5.97 | 5.65 |
| CaO | 8.29 | 7.51 | 9.54 | 9.64 | 8.23 | 8.07 | 8.48 | 9.87 | 9.69 |
| $Na_2O$ | 4.62 | 4.50 | 4.24 | 4.47 | 4.85 | 4.81 | 4.87 | 4.50 | 4.37 |
| $K_2O$ | 3.50 | 3.06 | 2.10 | 3.87 | 2.11 | 2.13 | 2.75 | 2.52 | 2.49 |
| $P_2O_5$ | 1.17 | 1.26 | 1.14 | 1.54 | 0.81 | 0.82 | 1.27 | 1.17 | 1.12 |
| Total | 98.91 | 99.94 | 99.68 | 97.74 | 99.93 | 99.9 | 99.19 | 99.04 | 100.06 |
| LOI | 1.07 | 0.49 | 0.77 | 0.55 | 0.18 | 0.29 | 0.22 | 0.08 | 0.44 |
| #Mg | 52.8 | 51.6 | 55.3 | 52.0 | 51.4 | 51.5 | 54.3 | 54.0 | 53.4 |
| Ni | 29.6 | 41.6 | 60.8 | 12.1 | 34 | 35.8 | 49 | 41.7 | 35 |
| La | 98 | 104 | 75 | 102 | 61 | 64 | 95 | 88 | 86 |
| Ce | 193 | 189 | 151 | 195 | 115 | 114 | 175 | 187 | 175 |
| Pr | 22.7 | 21.2 | 18.0 | 22.9 | 12.9 | 13.0 | 20.3 | 22.3 | 20.9 |
| Nd | 82 | 72 | 68 | 81 | 48 | 47 | 71 | 82 | 77 |
| Sm | 11.7 | 10.1 | 10.4 | 11.6 | 8.0 | 7.6 | 10.0 | 11.7 | 10.7 |
| Eu | 3.0 | 2.7 | 2.9 | 3.1 | 2.3 | 2.4 | 2.7 | 3.1 | 2.9 |
| Gd | 7.6 | 7.7 | 8.1 | 8.6 | 6.9 | 7.1 | 7.1 | 8.6 | 7.8 |
| Tb | 0.9 | 0.9 | 0.9 | 0.9 | 0.8 | 0.9 | 0.8 | 0.9 | 0.9 |
| Dy | 4.6 | 4.8 | 4.9 | 4.8 | 5.0 | 4.9 | 4.4 | 4.8 | 4.6 |
| Ho | 0.7 | 0.7 | 0.8 | 0.8 | 0.9 | 0.9 | 0.7 | 0.7 | 0.8 |
| Er | 1.9 | 2.1 | 2.0 | 2.1 | 2.6 | 2.5 | 1.8 | 2.0 | 1.9 |
| Tm | 0.3 | 0.3 | 0.3 | 0.3 | 0.4 | 0.4 | 0.3 | 0.3 | 0.3 |
| Yb | 1.7 | 1.8 | 2.0 | 2.0 | 2.4 | 2.3 | 1.7 | 1.7 | 1.7 |
| Lu | 0.2 | 0.3 | 0.3 | 0.3 | 0.4 | 0.4 | 0.2 | 0.2 | 0.3 |
| Ba | 1446 | 1201 | 1022 | 1795 | 924 | 915 | 1301 | 1151 | 1105 |
| Hf | 4.6 | 4.3 | 4.0 | 4.5 | 5.1 | 4.8 | 3.9 | 3.9 | 4.0 |
| Nb | 28.8 | 31.3 | 21.9 | 28.7 | 19.4 | 20.5 | 23.2 | 33.4 | 32.6 |
| Rb | 44.2 | 41.5 | 26.9 | 51.2 | 34.0 | 33.7 | 33.2 | 33.8 | 34.1 |
| Sr | 2504 | 2032 | 2128 | 2889 | 1413 | 1363 | 2185 | 2348 | 2131 |
| Pb | | | | | | | | | |
| Ta | 1.2 | 1.2 | 0.9 | 1.1 | 0.8 | 0.8 | 1.0 | 1.3 | 1.2 |
| Th | 5.1 | 6.0 | 3.2 | 7.1 | 4.8 | 4.9 | 5.5 | 5.5 | 5.8 |
| U | 1.1 | 1.1 | 1.0 | 1.1 | 1.0 | 1.1 | 1.0 | 1.3 | 1.2 |
| Zr | 210 | 218 | 177 | 202 | 240 | 235 | 169 | 190 | 186 |
| Y | 20.3 | 22.3 | 24.0 | 25.0 | 26.6 | 26.3 | 21.6 | 22.0 | 22.3 |

**Table 1 continued.**

**Table 2: Phenocryst and groundmass minerals for volcanic rocks from the southern Lesser Caucasus. Volcanic field abbreviations: V- Vardenis; S- Syunik. Mineral abbreviations: ol- olivine; cpx- clinopyroxene; plag- plagioclase; ox- Fe-Ti oxide; kspar- potassium feldspar; qtz- quartz; amph- amphibole; bio- gfgfgf biotite; ap- apatite. Mineral texture abbreviations: xen- xenocrystic; pseud- pseudomorphic. Rock names: B, basalt; R, rhyolite; TB, trachybasalt; TBA, trachybasaltic andesite; TA, trachyandesite; Tr, trachyte; Te, tephrite/basanite; PTe, phonotephrite.**

| Sample | Field | Volcano/place | Eruptive type | Rock name | #Mg | Phenocrysts | Groundmass |
|---|---|---|---|---|---|---|---|
| 6.27.08. | V | Khrbekner | Lava | TBA | 56.2 | ol, cpx, plag | plag, cpx, ox, |
| 4.1.12 | V | Tsovak pyroclastic flow | Pumice | R | 17.3 | kspar, plag, qtz | glass |
| 5.1.13 | V | Smbatasar | Lava | TA | 50.9 | cpx, plag, amph | plag, ox, cpx |
| 5.1.15 | V | Geghagar tuff | Ignimbrite | R | 44.5 | kspar, plag, phlog, qtz | glass |
| 5.3.15 | V | Porak | Lava | TA | 53.9 | cpx, plag | plag, cpx, ox |
| 5.4.15 | V | Zhiligyol | Lava | TA | 51.1 | cpx, qtz (xen) | plag, glass, ox, cpx |
| 5.5.15 | V | Vent W. of Zhiligyol | Plug | R | 17.6 | kspar, plag, bio, qtz | altered |
| 5.9.15 | V | Lake Al-Lich | Plug | Tr | 29.5 | plag, phlog, kspar, cpx | kspar, qtz, ox, cpx |
| 6.3.15 | V | Torgomayr | Lava | TBA | 51.4 | Cpx | plag, bio, ox |
| 7.2.15 | V | Dome E. of Trdatanist | Plug | R | 25.4 | kspar, qtz, plag, bio | altered |
| 7.4.15 | V | S. slopes of V upland | Lava | TA | 54.8 | cpx, amph (pseud), plag | plag, cpx, ox, glass |
| 7.5.15 | V | S. slopes of V upland | Lava | TBA | 54.0 | cpx, plag, amph | plag, cpx, ox, ol |
| 1.4C.08 | S | Garusar | Scoria | TBA | 50.8 | cpx, amph | plag, cpx, ox |
| 2.5.08 | S | Shinuayr | Bomb | TBA | 50.5 | cpx, amph, ol | glass, plag, ox, cpx |
| 2.6.08 | S | Morutumb | Bomb | TBA | 48.8 | cpx, amph, ol, ap | plag, glass, cpx, ox |
| 2.7.08 | S | Yerakov Blur | Bomb | PTe | 48.6 | amph, cpx | glass, plag, ox, cpx |
| 2.9.08 | S | Pokr Chobanasar | Bomb | TBA | 52.5 | cpx, amph, ol | plag, cpx, ox |
| 2.10.08 | S | Barurtumb | Lava | B | 66.8 | ol, cpx | plag, cpx, ox |
| 5.21.08 | S | Berd | Lava | TBA | 52.7 | ol, cpx | plag, ox |
| 6.24.08 | S | Tekblur | Scoria | PTe | 48.4 | Cpx | glass, plag |
| 3.10.10 | S | Unit 7 | Lava | Tr | 42.5 | plag, cpx, amph (pseud) | plag, ox, cpx |
| 3.11.10 | S | Unit 7 | Lava | TA | 46.5 | cpx, amph (pseud) | plag, ox, cpx |
| 4.19.10 | S | Ishkhanasar | Lava | TA | 44.5 | plag, amph | Plag |
| 5.5.12 | S | Tshkhouk | Lava | TA | 50.0 | cpx, plag, ox | plag, ox, cpx |
| 8.2.15 | S | Khozazblur | Bomb | TB | 54.1 | cpx, ol | plag, cpx, ox |
| 8.3.15 | S | Verjiblur | Bomb | TBA | 52.6 | cpx, amph | plag, cpx, ap |
| 8.7.15 | S | Marakhlasar | Scoria | PTe | 52.8 | amph, cpx | glass, plag |
| 9.1.15 | S | Spiovblur | Plug | TBA | 51.6 | cpx, amph, plag, ol, ap | plag, cpx, ox |
| 9.2.15 | S | Chobanasar | Bomb | TB | 55.3 | cpx, ol, amph (pseud) | plag, cpx, ox |
| 10.2.15 | S | Kyorpasar | Lava | TBA | 51.4 | Aphyric | plag, cpx, ol, ox |
| 10.3.15 | S | Mets Yerkvoryak | Scoria | TBA | 51.5 | plag, ol, cpx, ox | glass |
| 10.6.15 | S | Mets Yerkoryak | Scoria | TBA | 51.6 | Cpx | glass, plag, cpx, ox |
| 11.1.15 | S | Quarry, Shaqi village | Lava | TBA | 46.3 | plag, cpx | plag, cpx, ox |
| 11.3.15 | S | Sherepasar | Scoria | Te | 54.0 | cpx, ol, amph | plag, glass, cpx, ox |

**Table 3: Sr-Nd isotope compositions for Pleistocene lavas from the southern LC. Rock types use the same abbreviations as Fig. 6 and Table 2. All Sr ratios are normalised to NIST SRM 987, and all Nd ratios are normalised to La Jolla corrected BHVO-I (see Methods). Epsilon values are calculated for the present day using $(^{143}Nd/^{144}Nd)_{CHUR}$ = 0.512638 for Chondritic Earth (Jacobson & Wasserburg, 1980). Samples marked with an asterix are from the east side of the Sevan-Akera suture- see text for discussion**

| | Rock type | $^{87}Sr/^{86}Sr$ | ± 2σ (x10$^{-6}$) | $^{143}Nd/^{144}Nd$ | ± 2σ (x10$^{-6}$) | εNd |
|---|---|---|---|---|---|---|
| ***Vardenis*** | | | | | | |
| 4.2.15* | TBA | 0.704356 | 10 | 0.512802 | 12 | 3.20 |
| 5.3.15* | | 0.704461 | 8 | 0.512803 | 10 | 3.22 |
| 5.6.15 | TBA | 0.704505 | 12 | 0.512789 | 10 | 3.24 |
| 5.9.15 | Tr | 0.704506 | 12 | 0.512805 | 10 | 3.26 |
| 6.3.15 | | 0.704429 | 8 | 0.512796 | 10 | 3.08 |
| 1.1.13* | TBA | 0.704432 | 10 | 0.512808 | 10 | 3.32 |
| 1.2.13* | TBA | 0.704420 | 8 | 0.512781 | 6 | 2.79 |
| 3.3.13* | TBA | 0.704399 | 12 | 0.512798 | 10 | 3.12 |
| 5.1.13 | | 0.704351 | 8 | 0.512805 | 6 | 3.26 |
| 5.2.13 | | 0.704181 | 8 | 0.512836 | 10 | 3.86 |
| 6.2.13 | TBA | 0.704455 | 8 | 0.512815 | 8 | 3.45 |
| 6.27.08 | TBA | 0.704307 | 12 | 0.512783 | 12 | 2.83 |
| 7.29.08 | TBA | 0.70433 | 8 | 0.512799 | 14 | 3.51 |
| ***Syunik*** | | | | | | |
| 8.3.15 | TBA | 0.704438 | 8 | 0.512785 | 8 | 2.87 |
| 8.4.15 | TBA | 0.704466 | 8 | 0.512794 | 9 | 3.04 |
| 8.5.15 | Te | 0.704615 | 8 | 0.512779 | 10 | 2.75 |
| 8.6.15 | PTe | 0.704553 | 10 | 0.512779 | 12 | 2.75 |
| 9.1.15 | TBA | 0.704439 | 10 | 0.512803 | 8 | 3.22 |
| 9.2.15 | TB | 0.704407 | 14 | 0.512801 | 8 | 3.18 |
| 10.1.15 | PTe | 0.704660 | 10 | 0.512761 | 10 | 2.40 |
| 10.2.15 | TBA | 0.704262 | 10 | 0.512856 | 10 | 4.25 |
| 10.3.15 | TBA | 0.704245 | 10 | 0.512821 | 10 | 3.57 |
| 11.1.15 | TA | 0.704378 | 10 | 0.512806 | 8 | 3.28 |
| 11.2.15 | PTe | 0.704595 | 12 | 0.512781 | 11 | 2.79 |
| 11.3.15 | Te | 0.704277 | 12 | 0.512795 | 5 | 3.06 |
| 5.5.12 | TA | 0.704432 | 10 | 0.512783 | 10 | 2.83 |
| 2.3.10 | R | 0.704425 | 8 | 0.512788 | 8 | 2.93 |
| 3.10.10 | Tr | 0.704419 | 8 | 0.512796 | 4 | 3.08 |
| 3.11.10 | TA | 0.704530 | 10 | 0.512783 | 4 | 2.83 |
| 4.19.10. | TA | 0.704330 | 8 | 0.512801 | 12 | 3.18 |
| 1.4A.08 | TBA | 0.704317 | 6 | 0.512792 | 10 | 3.00 |
| 1.4B.08. (xenolith) | G | 0.704981 | 32 | 0.512797 | 12 | 3.10 |
| 2.7.08. | PTe | 0.704440 | 10 | 0.512797 | 7 | 3.10 |
| 2.8.08. | TBA | 0.704381 | 10 | 0.512799 | 10 | 3.14 |
| 2.10.08. | B | 0.704396 | 14 | 0.512827 | 12 | 3.69 |
| 4.15A.08. | R | 0.705207 | 6 | 0.512783 | 8 | 2.83 |
| 4.18A.08. | R | 0.704857 | 8 | | | |
| 5.20A.08 | R | 0.705482 | 14 | 0.512770 | 14 | 2.57 |
| 5.21.08. | TBA | 0.704475 | 9 | 0.512767 | 10 | 2.52 |
| 6.26.08. | TA | 0.704273 | 8 | | | |

**Table 4: Parameters used for non-modal batch melt modelling. The source modes for spinel and garnet peridotite are from Shaw (2005) and Thirwall *et al*. (1994) respectively. Melt modes are from Neill *et al*. (2015) and Allen *et al*. (2013). The starting composition of the mantle source is the same as that used in Neill *et al*. (2015). Partition coefficients are from Ionov *et al*. (2002), except for those for garnet which comes from McKenzie & O'Nions (1991) and Green *et al*. (2000). The most primitive Syunik sample used for comparison is 8-5-15. OL- olivine; OPX- orthopyroxene; CPX- clinopyroxene; AMPH- amphibole; SP- spinel; GRNT- garnet.**

| Lithology | | OL | OPX | CPX | AMPH | SP | GRNT | Sum |
|---|---|---|---|---|---|---|---|---|
| **Spinel peridotite** | Source mode | 0.794 | 0.123 | 0.03 | 0.042 | 0.011 | 0 | 1 |
| | Melt mode | 0.15 | 0.15 | 0.22 | 0.42 | 0.06 | 0 | 1 |
| **Garnet peridotite** | Source mode | 0.569 | 0.212 | 0.077 | 0.026 | 0 | 0.116 | 1 |
| | Melt mode | 0.05 | 0.19 | 0.28 | 0.06 | 0 | 0.42 | 1 |
| | | **La** | **Gd** | **Dy** | **Yb** | **Zr** | **Hf** | **Nb** |
| Starting composition | | 0.5869 | 0.321 | 0.317 | 0.202 | 7 | 0.172 | 0.3635 |
| **Kd values** | | **La** | **Gd** | **Dy** | **Yb** | **Zr** | **Hf** | **Nb** |
| Olivine | | 0.0001 | 0.00076 | 0.0014 | 0.00364 | 0.004 | 0.006 | 0.0002 |
| Orthopyroxene | | 0.0002 | 0.0128 | 0.0261 | 0.0986 | 0.005 | 0.01 | 0.0005 |
| Clinopyroxene | | 0.054 | 0.4 | 0.442 | 0.427 | 0.13 | 0.2 | 0.0077 |
| Amphibole | | 0.086 | 0.64 | 0.707 | 0.683 | 0.156 | 0.24 | 0.2 |
| Spinel | | 0.0004 | 0.00042 | 0.0004 | 0.00053 | 0.005 | 0.01 | 0.001 |
| Garnet | | 0.01 | 0.498 | 1.06 | 4.03 | 0.12 | 0.23 | 0.00054 |
| **Melting models** | | **La** | **Gd** | **Dy** | **Yb** | **Zr** | **Hf** | **Nb** |
| 1. 3% melting spinel lherzolite (Neill et al, 2015) | Initial | 17.3 | 5.3 | 4.9 | 2.7 | 169.0 | 3.6 | 10.0 |
| | After 8% fractionation | 18.8 | 5.8 | 5.3 | 2.9 | 183.6 | 3.9 | 10.9 |
| 2. 1% melting spinel lherzolite | Initial | 39.5 | 6.8 | 5.9 | 3.2 | 299.9 | 5.6 | 20.2 |
| | After 8% fractionation | 42.9 | 7.3 | 6.5 | 3.5 | 325.9 | 6.1 | 21.9 |
| 3. 1% melting garnet lherzolite | Initial | 34.0 | 2.8 | 1.7 | 0.4 | 175.3 | 2.8 | 23.1 |
| | After 8% fractionation | 37.0 | 3.1 | 1.9 | 0.4 | 190.5 | 3.1 | 25.1 |
| 4. 1% melting of 65% garnet lherzolite, 35% spinel lherzolite | Initial | 35.9 | 4.2 | 3.2 | 1.4 | 218.9 | 3.8 | 22.1 |
| | After 8% fractionation | 39.1 | 4.6 | 3.5 | 1.5 | 237.9 | 4.1 | 24.0 |
| Most primitive Syunik sample for comparison | | 74.8 | 7.6 | 4.7 | 1.9 | 166.0 | 3.7 | 24.0 |